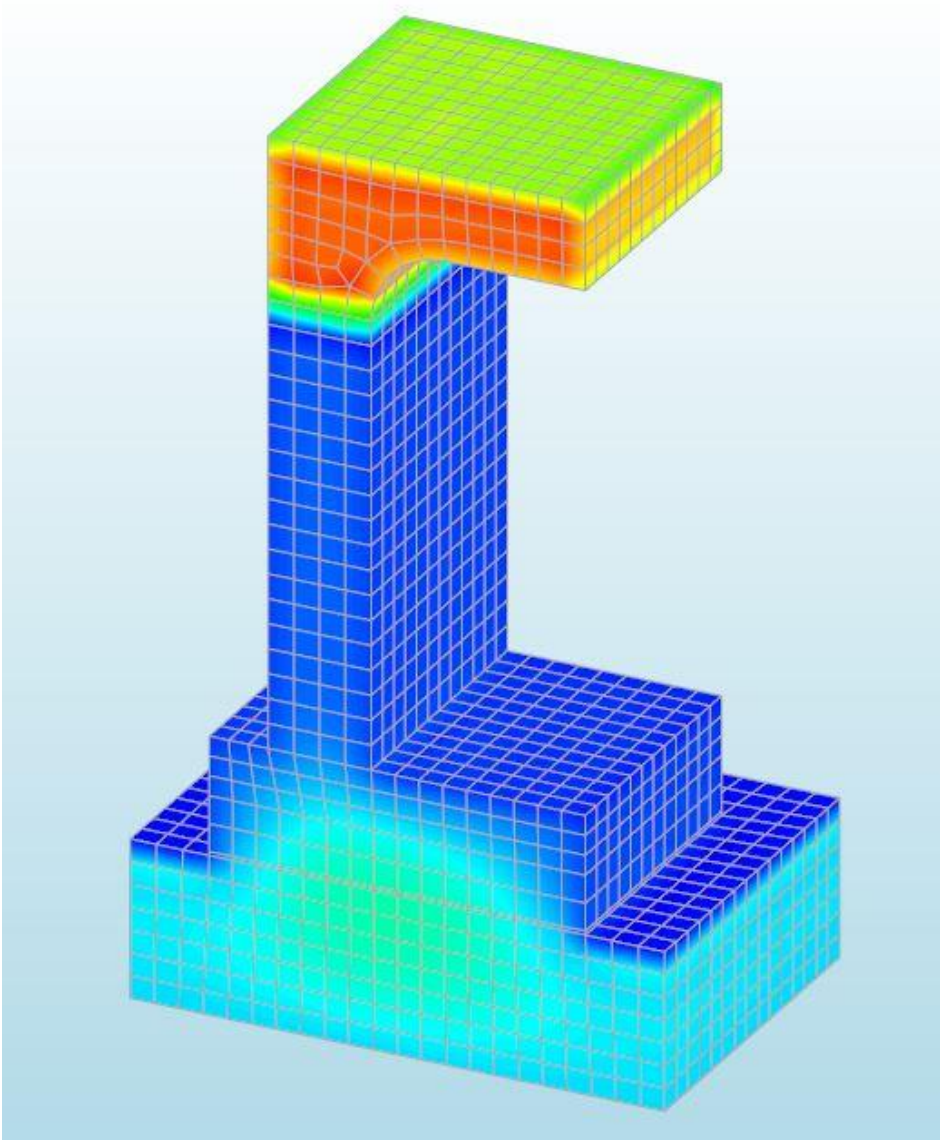

Early-Age Thermal Cracking in Concrete

A FE-Modelling Approach

Master's Thesis in the Master's Programme in Structural Engineering and Building Technology

FRANCISCO DIAZ
RIKARD JOHANSSON

Department of Civil and Environmental Engineering
Division of Structural Engineering
Concrete Structures
CHALMERS UNIVERSITY OF TECHNOLOGY
Gothenburg, Sweden 2016
Master's Thesis BOMX02-16-64

MASTER'S THESIS BOMX02-16-64

Early-Age Thermal Cracking in Concrete:
A FE-Modelling approach

Master's Thesis in the Master's Programme in Structural Engineering and Building Technology

FRANCISCO DIAZ

RIKARD JOHANSSON

Department of Civil and Environmental Engineering
Division of Structural Engineering
Concrete Structures
CHALMERS UNIVERSITY OF TECHNOLOGY
Göteborg, Sweden 2016

Early-Age Thermal Cracking in Concrete

A FE-Modelling approach

Master's Thesis in the Master's Programme Structural Engineering and Building Technology

FRANCISCO DIAZ

RIKARD JOHANSSON

Examensarbete BOMX02-16-64/ Institutionen för bygg- och miljöteknik,
Chalmers tekniska högskola 2016

Department of Civil and Environmental Engineering
Division of Structural Engineering
Concrete Structures
Chalmers University of Technology
SE-412 96 Göteborg
Sweden
Telephone: + 46 (0)31-772 1000

Cover:
Thermal profile of the Mock-up element after cast of the roof slab.
Department of Civil and Environmental Engineering, Göteborg, Sweden, 2016

Early-Age Thermal Cracking in Concrete

Master's thesis in the Master's Programme in Structural Engineering and Building Technology

FRANCISCO DIAZ
RIKARD JOHANSSON
Department of Civil and Environmental Engineering
Division of Structural Engineering
Concrete Structures
Chalmers University of Technology

ABSTRACT

The usage of high strength concrete and the construction of massive structures has created the need for a more detailed design focused on crack control. Regarding this the first hours after casting have a great influence in the crack generation and should be studied carefully.

This concern has arisen in the construction of Marieholm tunnel which will be built in the bottom of the river Göta in Gothenburg, Sweden. It is a submerged tunnel which will be cast in a dry dock before being immersed and connected on the river bottom. As cracking is not allowed for submerged elements, this required a study of early age cracking and the mechanisms that influence it. A full scale mock-up cast was previously done in Göteborg to measure temperature development which served as a basis for this master thesis.

The purpose of this master thesis was to distinguish de most influential mechanisms that affect thermal cracking, through a literature review, and design a FE-based model that considers them. It was also a goal to create this model with a 3D software and compare it with 2D software used nowadays. After a discussion on software options DIANA 10 was selected for the task.

The model implemented the main mechanisms established in the literature review, namely autogenous shrinkage, thermal dilation, creep and restraint. The results showed a good agreement with the real measurements in temperature gauges and plausible stress/strain results.

The usage of a 3D model provided a more complex but complete approach to the task. This enabled considering factors that are disregarded with the usage of simplified 2D models and can permit for a more optimized structure in the design face.

Key words: Early-age cracking, thermal dilation, autogenous shrinkage, creep, FE-Software, adiabatic heat development.

Contents

Preface

This master thesis has been carried during January-June in 2016 and the work will act as a basis for a future doctoral thesis. The project has been done at the Department of Structural Engineering, Concrete Structures, Chalmers University of Technology (Sweden) in collaboration with Thomas Concrete Group.

The thesis has been carried out with Rasmus Rempling as examiner and Ingemar Löfgren as a supervisor, who we thank for their support and feedback along this project. We would also like to send special thanks to Ignasi Fernández Pérez for his help regarding FE-modelling in DIANA and to Alexandre Mathern for his support with Contest.

Göteborg June 2016

Francisco Diaz
Rikard Johansson

Notations

Roman upper case letters

Ã	Normalized affinity
C	Volumetric heat capacity
E	Young's modulus
E	Elastic stiffness tensor
E_∞	Young's modulus for $\xi_0 = \xi_\infty$
E_A	Activation energy
E_{ac}	Creep activation energy
E_c	Young's modulus of elasticity for concrete
E_{ef}	Young's modulus of elasticity for concrete, effective value
H_u	Maximum value of heat production rate
K	System stiffness matrix
L	Latent heat of hydration
R	Degree of restraint
R	Gas constant, 8….
T	Thermodynamic temperature
T	Temperature
T_0	Thermodynamic temperature at 20°C, 273K
T_2	Temperature at time t_2
T_3	Temperature at time t_3

Roman lower case letters

c_A	Arrhenius constant
f	Nodal forces
f_c	Uniaxial compressive strength
k_{bc}^i	Stiffness of spring
$k_{bc,\infty}^i$	Final stiffness matrix
f_{ck}	Characteristic cylinder strength of concrete at 28 days
k	Thermal conductivity
t	Time
t_2	Time until zero stress
t_3	Time when crack risk should be checked
q_ξ	Degree of reaction dependent heat production
q_T	Temperature dependent heat production
u	vector of unknown variables (displacements and rotations)

Greek lower case letters

$\tilde{\sigma}_{sp}^{i}$	Effective stress in the spring
$\tilde{\sigma}_{ds}^{i}$	Effective stress in the damper
$\dot{\tilde{\sigma}}$	Total effective stress
ε_{bc}^{i}	Basic creep strain
η_{bc}^{i}	Damper viscosity
τ_{bc}^{i}	Ratio between damper viscosity and spring stiffness
α	Thermal dilation coefficient
β	Factor depending on the concrete type
β_{as}	Parameters which consider time
$\dot{\varepsilon}_{ca}$	Shrinkage strains
$\dot{\varepsilon}$	Total strain
ε_{as}	Shrinkage strain
$\dot{\varepsilon}_{as}$	Shrinkage strains
$\dot{\varepsilon}_{au}$	Shrinkage strains
$\dot{\varepsilon}_{bc}$	Basic creep strains
$\dot{\varepsilon}_{el}$	Elastic strains
ε_{T}	Thermal strain
$\dot{\varepsilon}_{th}$	Thermal variation strains
ε_{tot}	Total strain
ν	Poisson's ratio
ξ	Degree of hydration
$\dot{\xi}$	Heat of hydration
$\tilde{\sigma}$	Effective stress
φ	Creep coefficient
X_{AEM}	Aging coefficient for young concrete

1 Introduction

1.1 Background

Concrete is a well know building material that is used all over the world. As a construction material, it has many properties that are desired for many different types of structures; high forming abilities, good structural properties and a high durability among others. This, together with the fact that the components used in the material are considered to be cheap and easily accessible, has made it the most used construction material for both land- and sea-based structures.

The Marieholm tunnel is a construction project in Gothenburg where a new tunnel will be built. This tunnel will be constructed in three large reinforced concrete sections, which will be cast in a dry dock before they are immersed and connected on the river bottom. For this type of structure there is often a demand that no thermal cracks should appear in the concrete during the construction phase. To ensure that this requirement is fulfilled, there is a need of being able to analyze the structure, from a thermal cracking risk perspective, with a computer based software.

Concrete has several advantageous qualities, but the material is also complex and several challenges have been identified during the last 80 years. One of these issues is the volume instability, which affects concrete structures that are prevented from moving freely, either by reinforcement or being connected to other already existent structures. The volume instability, in the early-age, is mainly caused by temperature dilation and autogenous shrinkage effects, and there are several parameters that affect these two mechanisms. The consequence of these two mechanisms is often denoted early-age thermal cracking. During the hardening phase the hydration process generates heat. The amount of heat generated is greatly affected by the type and amount of cement as well as the w/c-ratio. High strength concretes with a low w/c-ratio are therefore more sensitive to this type of cracking due to the high cement content which generates high temperatures (Bjøntegaard 2011). Cracking increases the permeability of the concrete and makes it less durable since it increases the risk of damaging processes, such us chloride ingress or reinforcement corrosion, taking place (Ji 2008).

The amount of heat being released during the hydration process can be reduced by replacing part of the cement with mineral additives. These additives create a higher resistance to early age thermal cracking by decreasing the amount of heat that is generated during the hydration, increasing the ultimate strength and decreasing the pore size which lower the concrete's permeability (Ji 2008). Another way to control the temperature in the concrete is to cool its components, or use cooling pipes. In combination with these practical measures, an accurate design and prediction of cracking in early stages would allow for a better usage of the material.

One type of structure that is sensitive when it comes to this type of cracking is submerged tunnels. Cracking in the tunnel segments should be avoided in order to achieve a low permeability and ensure that the structure fulfills the demands on service life. In order to predict the risk of early age thermal cracking in an accurate way, there is a need to further develop the modelling of the mechanisms involved in this type of problem by using a FEM-software.

1.2 Purpose

The purpose of this project was to investigate the potential of using a 3D finite element model software to predict early age thermal cracking in concrete. The modelling focused on implementing the critical parameters: thermal dilation, shrinkage, creep and restraint. The specific objectives investigated were:

- Develop a finite element model that allows predicting the cracking in concrete due to thermal dilation, shrinkage, creep and restraint.
- Asses the accuracy of the model and its limitations, as well as possible improvements and future search in the field.
- Verify the model by comparing the results from with the measurements made at a mock-up
- Discuss the results through a comparison with results from the 2D software, Contest PRO.

1.3 Limitations

A mock-up of a tunnel segment has been cast in Gothenburg where several temperatures have been measured at different points within the segment. The given temperature profiles are real measured values which are influenced by several parameters; such as exterior temperature, radiation, convection etc. that affect the temperatures inside the tunnel segment. In order to simplify the modelling, only the real outside temperatures and convection values were implemented.

There are several mechanisms involved in thermal cracking and not all of them are known in depth due to their complexity. Some of these were considered, but in a simplified way, as it is common in related state of the art research. An example of this is creep. This mechanism should be different if the element is subjected to tension or compression. As a result, this is not included in the model since there aren't any reliable ways of measuring this through experimentation, and it is a field for future studies.

Relative humidity has an effect on several of the included parameters and it would have been more accurate to consider a relative humidity that was time dependent, but it would also drastically increase the complexity of the model. Therefore, the relative humidity is assumed to be constant and this assumption enable the usage of a coupled temperature-age analysis of the thermal cracking.

Limitations in the software are described in more detail in chapter 7.

1.4 Method

The project initially involved a literature review regarding theoretical methods used to predict thermal variations in concrete as well as a study of the 2D models that are used today in order to build up knowledge within the subject. Thus examining the state-of-the-art scientific research concerning crack development in concrete in early stages and identifying the main parameters that influence this process and that should be integrated in the model.

In order to predict the crack development in the concrete a non-linear 3D finite element analysis was done in DIANA 10. Basic examples were used to grow experience into

this field and to study the effect and implementation of each critical parameter. The combined knowledge from the literature study and examples was then used to create the final model of the tunnel segment and implement the critical parameters.

In order to verify the model, the temperature results from the mock-up were used together with temperatures, stresses and strains calculated with the 2D software Contest PRO.

1.5 General layout

In Chapter 2, a theoretical background regarding thermal cracking in concrete is introduced. Starting with a literature review that offers an insight on the advancements achieved in this subject along the last century as well as the milestones in the area. Then the critical mechanisms involved in thermal cracking are presented showing its impact and the variables they depend on.

Chapter 3, presents a basic model of how thermal cracking is calculated and also a FE adapted model based on a hydration degree with individual formulation for the main mechanisms involved in the process. Finally, the main calculation flow in DIANA 10 is introduced.

In Chapter 4, the different software options were analysed with an overview on its limitations as well as a discussion on the final choice made.

Chapter 5 contains information on the input for the problem. From the definition of the Marieholm tunnel to the temperature data measured from the full scale mock-up, together with the chemical components of the concrete that is used in HYMOSTRUC in order to estimate the development of material properties.

Chapter 6 presents the used 3D FEM-model in DIANA, with a step by step approach where the main elements are described, namely the geometry, boundaries, material model and analysis type used.

Chapter 7, shows a discussion on the model limitations, choices made in the modelling process with a discussion about them and possible ways of action to overcome these limitations.

Chapter 8, illustrates the results obtained in the analysis temperature profile, stresses, shrinkage strains and thermal strains, and a sensitivity analysis to show the influence of element size.

Along Chapter 9 a discussion of the results is made, comparing the results from 2D software to the results obtained in DIANA, and analysing how different factors influence the final result both in stresses and temperature profile.

Chapter 10, provides the conclusions obtained throughout this master thesis project as well as different ideas that can give a lead for further studies.

2 Literature Review

2.1 Introduction

The reason why early age thermal cracking occurs is due to the volume instability of concrete. Upon mixing, the concrete behaves almost like a liquid but after a few hours hydration causes the concrete to harden and as time progresses it acts more and more as a solid. The hydration process itself is a chemical reaction between the water and the cement, which consumes water and liberates heat due the exothermic reaction. The volume change that occurs due to this temperature raise is denoted thermal dilation. The shrinkage that occurs due to the fact that the concrete consumes water and self-desiccates is called autogenous shrinkage. These two are the driving mechanisms of concrete´s early-age volume instability (Ji 2008).

However, these two phenomena alone are not the only reason behind the cracking of concrete in early age stages. A specimen of plain concrete that is cast without any restraints will be able to expand and shrink freely without introducing any stresses in it. The problem with cracks occurs since in practice there is always some kind of restraint that partially or totally prevents the volume changes from taking place. Moreover plain concrete is rarely used, in most cases there is also a certain amount of reinforcement embedded in the structure. The reinforcement then acts as an internal restraint, which prevents partially the previously mentioned deformations. It is also often the case that the concrete is casted and connected to already existing adjacent structures which act as external restraint. These various restraints will produce stresses within the material that can be either compressive, tensile or a combination of the two of them (Emborg 1989). The sizes of these stresses are of great importance in order to evaluate if the concrete will be subjected to thermal cracking at early ages or not, see Figure 2.1. These restraints are treated more in depth in Section 2.6.

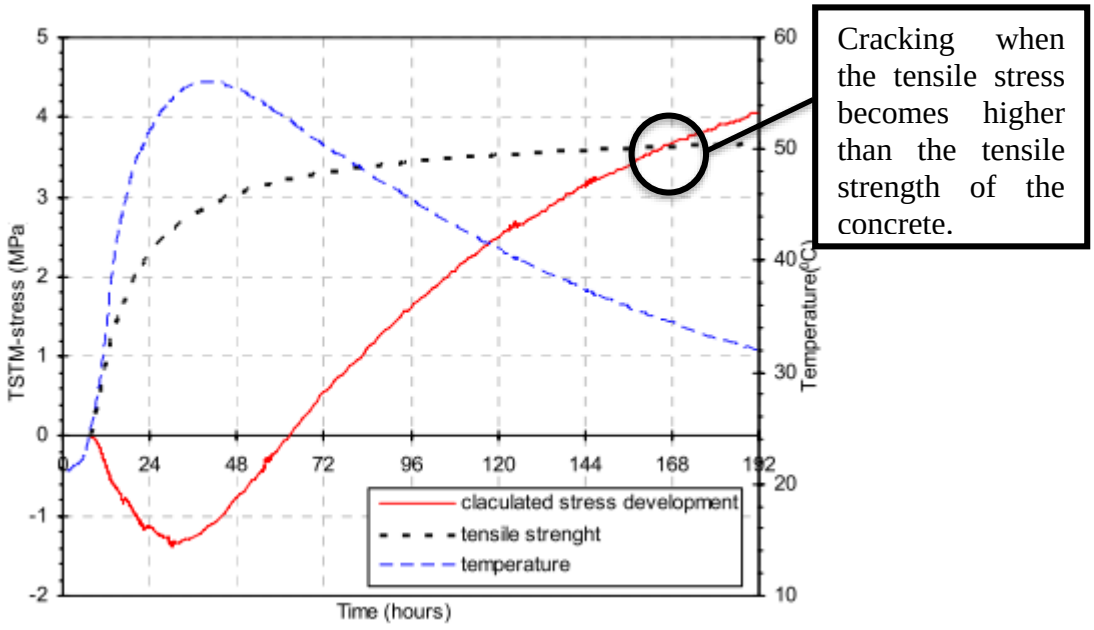

Figure 2.1 Strength and stress growth measured in a temperature stress testing machine (TSTM)(Ji 2008).

2.2 Historical overview

Thermal cracking issues for concrete structures are a major topic within civil engineering research. The modern research started with the construction of massive structures like dams, and in particular the Hoover dam (1931-1936) in the United States (Riding 2007). Norway started building dams around 1900 and in 1930 the Norwegian Engineering Association decided to do an assessment on the current status of these dams. The engineers identified several critical parameters such as drying shrinkage and internal temperature differences that were considered as some of the mechanisms involved in crack generation (Bjøntegaard 2011).

Another important parameter which affects the thermal cracking tendencies in concrete structures was also discovered in the 1930's, the external restraint. This was found to be the origin of one thermal crack type, called through cracks. Although it wasn't until the 1970's that different approaches to adress the problem were developed, such as the formulae to relate the cracking risk to the tensile stress capacity (Bernarder 1973) and (Bamford 2007). These studies were based on the temperature difference within the section or between sections cast at different times, which cannot be extrapolated to every case as the concrete properties dependence on maturity was not considered (Emborg 1989) and (Bernarder & Emborg 1994).

Le Châtelier discovered autogenous shrinkage, and its main component the chemical shrinkage, in the early 1900. The first definition of this type of shrinkage was that it is the readjustment of a system in order to counteract the effect of a change applied in its concentration. This was later reformulated by Lynham who described it as "the shrinkage produced when all the concrete is hydrated, all water is used up or all movement of water is rendered impossible" (Lynam 1934).

Until the 1980s the research on cracking and restraint issues was based on measured temperature or its estimation, having graphic solutions and hand-calculation as the predominant way of dealing with the issue (Bjøntegaard 2011). The usage of computer based technology to deal with these mechanisms started with the development of computerized curing technologies beginning in 1975 with Freiesleben Hansen's one-dimensional "Maturity Computer". This version was upgraded to handle 2D in 1992 including also a stress calculation module (Bjøntegaard 2011).

In the last 20 years quite a lot of research has been done in Norway, Sweden and all around the world concerning early-age cracks in concrete. This is due to the increase in the usage of high strength concrete and the exponential usage of massive infrastructures of different kinds which make into a necessity the development of accurate models that can simulate the conditions that this structures undergo.

2.3 Shrinkage

As mentioned before one of the driving mechanisms of early-age cracking is shrinkage, a macroscopic volume reduction due to the water movement, either through its loss via evaporation (drying shrinkage) or internal reactions (autogenous shrinkage). This often generates compressive stresses that translate into a shortening of the concrete elements.

Shrinkage can be divided in two different phases according to the concrete age: early-age and long term as can be seen in Figure 2.2. Early age is usually defined as the first 24h after casting when the concrete's mechanical properties are developing and the material is gaining resistances after setting. The time after this is addressed as long term, and is usually what is considered in structural analysis while the first 24 hours are often not analyzed in detail, since the early age shrinkage involves a lot of variables difficult to model and which are interdependent. As mentioned by (Holt 2001), an accurate study requires a coupled temperature and stress analysis.

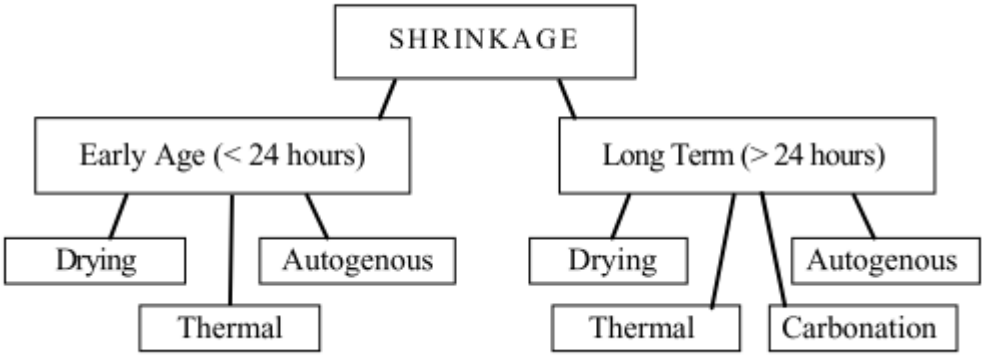

Figure 2.2 Shrinkage Elements and phases (Holt 2001).

It is not in the scope of this study to treat the long term effects but to give a thorough analysis on early-age effects and how to address them. These early-age effects are mainly drying shrinkage, autogenous shrinkage and thermal shrinkage/dilation.

2.3.1 Drying Shrinkage

Drying shrinkage refers to the variation in volume that occurs in a concrete member due to the loss of water to the environment and the accompanied decrease of its volume. This mechanism depends on the internal pore spaces and are therefore dependent on the moisture movement as well as time-dependent properties (Scherer 2015). If the evaporation rate surpasses the amount of bleed water rising to the concrete surface, the free surface from which the water evaporates moves into the concrete body and the evaporation continues then with the internal pore water. This difference in the amount of water in the concrete generates a variation in the hydration mechanism which in the end will produce a different behavior within the concrete leading to shrinkage.

Part of this shrinkage can be reversible and concrete will swell upon re-wetting (Holt 2001). One measure taken to control it involve the usage of surfactants (shrinkage reducing admixtures, SRA) that reduce the surface tension of the pore water and the shrinkage. Otherwise, the most common consequence of drying shrinkage is the appearance of surface cracks (Mindess & Young 1981).

2.3.2 Autogenous Shrinkage

Autogenous shrinkage is the macroscopic reduction in volume of cementitious materials when cement hydrates after initial setting, not including volume changes caused by temperature variation, external restraints or forces. Autogenous shrinkage occurs with no moisture transfer to the environment (Tazawa 1998).

The autogenous shrinkage is a chemical driven mechanism but while most of chemical shrinkage implies a microscopic variation of volume, autogenous shrinkage involves a macroscopic one. It is usually addressed in experimentation together with drying shrinkage since both mechanisms are difficult to dissociate. A deeper analysis on autogenous shrinkage can be found in (Holt 2001) and (Tazawa 1998).

Autogenous shrinkage depends on the water cement ratio (w/c), as presented in Figure 2.3, and the mineral composition of the binder. The higher the w/c ratio the smaller the autogenous shrinkage(Ji 2008). According to (Holt 2001) it can be disregarded for values over 0.45, as the amount of water will be enough for the concrete to reach full hydration.

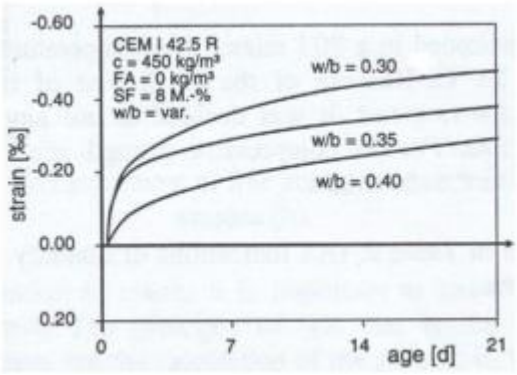

Figure 2.3 Influence of w/c ratio on autogenous shrinkage (Schießl et al. 2000).

2.3.3 Thermal Shrinkage/Dilation

Thermal shrinkage/dilation describes the change in volume caused in concrete due to the material being subjected to temperature fluctuations. Expanding with increasing temperatures and contracting with decreasing ones (Bjøntegaard 2011; Holt 2001). Part of the thermal dilation is elastic and will recover when temperatures go back to average values but there is a plastic part that develops into shrinkage.

The thermal dilation coefficient also known as coefficient of thermal expansion (CTE) is a property of concrete that describes the ratio at which its dimensions are altered due to the variation of temperature. It depends on the aggregate type (being a function of the coefficient of thermal expansion of the concrete mixture components), the w/c ratio, age and moisture condition among others (Holt 2001) and (Riding 2007).

Regarding influential elements, when analyzing w/c ratio research has shown that in the ranges between 0.32 to 0.44 there is no obvious change in concretes CTE (Zhou et al. 2014). On the contrary, while studying age, it has been found that the CTE shows a great variation during 15-30h after casting but develop to an almost constant value afterwards. This variation has minor influence on thermal stresses according to (Liu et al. 2014) and (Benboudjema & Torrenti 2008).

Thermal stresses coming from thermal strain can be reduced up to 50% with the usage of low CTE concretes, as this concrete design property have a major impact on cracking due to thermal strain (Riding 2007).

2.4 Degree of Hydration

The hydration process is a thermo-activated process, during which the concrete's properties develop. Therefore, there is a need to assess how these properties evolve in relation to how far the hydration process have gone. One way to solve this is to base the properties development on the parameter **degree of hydration (ξ)**, which is a measurement of the maturity of the concrete (Benboudjema & Torrenti 2008).This value varies from 0 to 1: being 0 for unhydrated and 1 for a fully hydrated concrete. This parameter can be used to describe the mechanical properties of the concrete such as the elastic modulus and strength, as well as the heat development and the main mechanisms involved in thermal cracking. This parameter allows to consider the effect of age and temperature simultanously in early age concrete (Liu et al. 2014).

Another element to take into account is that thermal dilation and autogenous shrinkage take place simultaneously. This generates a coupling of temperature dependent elements for modeling purposes. As thermal effects are impactful on concrete cracking, both the coefficient of thermal expansion and the hydration degree have been subjects of interest for long (Sellevold & Bjøntegaard 2006). The degree of hydration allows to handle these coupling issues and thermo-chemo-mechanical models are created based on this parameter.

2.5 Creep

In order to describe and understand the creep and relaxation behavior of concrete, one needs to understand the viscoelastic and plastic flows that can occur within the concrete. In general, when a material is loaded, it can go through three different types of deformations: elastic, plastic and visco-elastic.

In order to describe this type of deformations that are strongly dependent on time, it is common to use a strain-time relationship as shown in Figure 2.4. The plastic and viscous deformations are irreversible and would remain even if the material was unloaded. The elastic part on the other hand will be recovered upon unloading, and the part that is named delayed elastic deformation is the one that can be interpreted as a sort of creep (Emborg 1989).

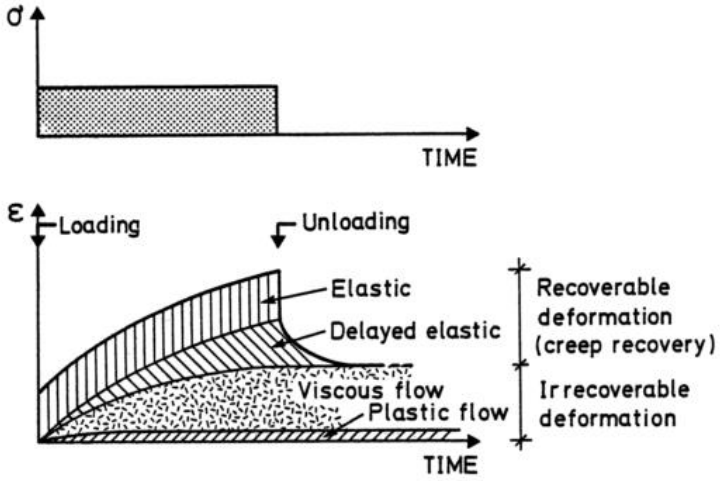

Figure 2.4 Strain-time diagram and the different kind of deformations that occur upon loading and unloading (Emborg 1989).

The viscous flow component will remain even if the concrete is unloaded, which makes it possible to be defined as a time dependent deformation that takes place for normal stress levels. It is possible to model the viscous flow, elastic and delayed elastic deformations by using a superposition method. Though it has been shown that there also are minor changes of the concrete's microstructure during these deformations, and therefore this method tends to overestimate the creep recovery at unloading and creep strain at loading (Emborg 1989).

The creep in a reinforced concrete structure is influenced by several factors. According to (Ji 2008) and (Emborg 1989) these can be either internal or external. The internal factors that have a large influence are connected to the material features that don't change after the concrete is poured into the mold. A few examples of this are the design strength, type of cement and E-modulus of the aggregate. External factors are ones that can change over time after the casting has been made, for example moisture and temperature conditions, load duration and type of loading.

An extensive amount of research has been done in the subject and when studying creep and relaxation of early age concrete, there are a few parameters that are often investigated. The age of the concrete upon loading, w/c-ratio, temperature history and development before, during and after loading (Bissonnette et al. 2007).
One of the difficulties is that the creep behaves different in compression and tension, according to (Atrushi 2003) for instance, instantaneous deformation in tension is found to be lower than under compression. The reason for this is a matter of discussion in research circles, but some suggestions are that the difference occurs due to micro cracking, debonding of the paste-aggregate interface and a difference in E-modulus in tension and compression (Hilaire et al. 2013).

According to (Ji 2008) there is also an inconsistency within the creep data that is obtained for both compression and tension. The conclusion that can be made from this is that the actual creep behavior is strongly affected by how the specimens are treated before and during the tests and what kind of test procedures that are used.

2.5.1 Creep in compression

The basic experimental and analytical considerations on creep are focused on creep in compression. According to (Briffaut et al. 2012) the creep strain rate is also affected by temperature variations and especially for massive structures where the concrete cure during high temperatures, up to 60° C. A high curing temperature can have a significantly effect on the basic creep strain rate with a factor of up to 2 or 3.

2.5.2 Creep in tension

According to experiments conducted by (Bissonnette et al. 2007) the tensile creep behavior has a large influence on the final stresses that are produced in the concrete due to restrained drying shrinkage. Another conclusion that has been made is that tensile creep is greatly affected by the age of the concrete upon loading. An early loading of the concrete, will results in a higher creep coefficient. Though it should be noted that the amount of available experimental data of tensile creep is limited, mainly due to difficulties that have related to get an accurate measurement of creep properties (Ji 2008).

2.5.3 Rheological models

One way to model the creep behavior is to use rheological models, which use a combination of elastic springs and viscous dashpot elements that are placed and connected, either in series or parallel. Two common models that are often used is the Kelvin-Voight model and Maxwell model.

The Kelvin-Voight model consists of a spring and a dashpot that are placed parallel to each other and Maxwell model is formed with a spring and dashpot placed in series, see Figure 2.5.

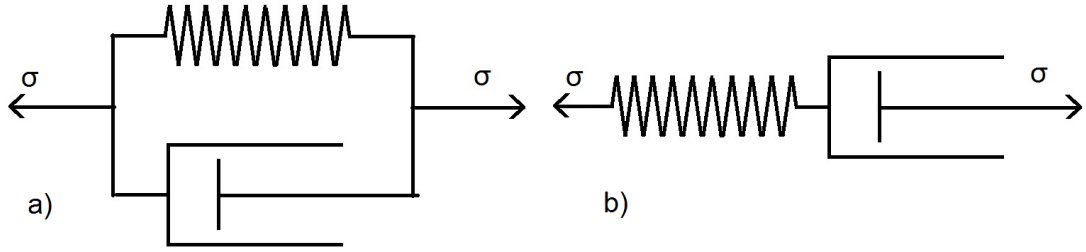

Figure 2.5 a) Kelvin-Voight model. b) Maxwell model.

The Kelvin-Voight model can be used to model the delayed elastic behavior (elastic part of the creep) and the Maxwell model can represent the viscous behavior. These two models can then be combined in order to be able to model creep behavior.

2.6 Restraint

The results when analyzing concrete structures are often deformations and stresses, these results can then be used to evaluate the risk of cracking in the structural members. In order to get a result and make the correct conclusion it's important to distinguish different types of strain. There are two different kinds of strain that can occur in a structure, stress-dependent strain and stress-independent strain. The stress-dependent

strain occur when a structural member is loaded by an external load, both instantaneous and during the whole loading time (creep).

The other type, stress-independent strain, are strains that are independent of the stress level and only create deformations. Though this stress free strain can only occur if the structural member is able to deform freely. If the movement of the member is prevented they will contribute to the stress-dependent strain. Two phenomenon that create stress-independent strains in concrete are shrinkage and thermal strains (Engström 2014).

If the structural member is subjected to stress-independent strains, due to for example shrinkage or thermal strains, it will require a certain degree of movement in the member itself. These movements can be handled by three basic cases, see also Figure 2.6:

- No restraints: the member is free to move and there are no boundaries which prevent it.
- Partially restrained: the member movement is partially prevented by certain boundary conditions which only prevents a certain degree of the movements.
- Fully restrained: The movements of the member are completely prevented by the boundary conditions.

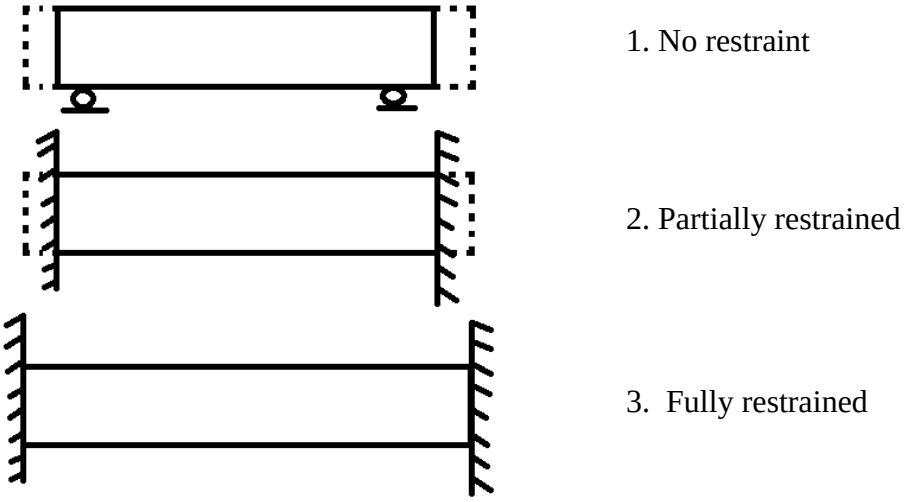

Figure 2.6 Principal sketch of restraints, adopted by (Engström 2014).

The restraint degree, which describes how much the concrete is restrained, is an important parameter to be able to predict early age cracking in concrete. The restraint factor, *R* is defined as ratio between the actual stress generated in the element, and the hypothetical stress at total restraint:

$$R = \frac{\sigma_{actual}}{\sigma_{Total\ restraint}} \quad (2.1)$$

The restraint factor will have a value of 1 in the case of full restraint and 0 when there is no restraint as shown in (Knoppik-Wróbel & Klemczak 2015) and (Engström 2014).

There are also two different kinds of restraints, often named internal and external restraint. The internal restraint is caused by the material itself and its components, where different parts of the cross-section prevent each other from moving. An example of this type of restraint is reinforced concrete, where the reinforcement can act as an internal restraint. External is created when the movement of the member is prevented by the boundary conditions. For concrete, this type of restraint could occur when an older structure is connected to a new, for example a wall that's going to be connected to an already cast ground slab (Emborg 1989; Engström 2014).

These types of restraints create restraining forces within the structural member, the size of these forces depend on the stiffness of the member itself and the stiffness of the boundaries.

2.7 Cracking

The appearance of cracks in concrete structures have been related to the concrete properties and the environment for a long time. Structures that are submitted to a high exposure class (placed in a severe or aggressive environment) and in particular submerged structures, such as tunnels, have a high requirement that no cracking should occur. Therefore, it is critical to be able to predict the cracking risk with a computer model. The prediction is of great importance since cracking deeply affects the concrete durability, since it has a negative effect on the permeability. An increased permeability can increase the risk of corrosion on the reinforcement and in the end have a negative effects on the service life (Riding 2007). Another factor to consider is that the cracking also influences the resistance of the concrete section in a negative way from a structural design perspective. This is the main reasons on why cracking needs to be considered and limited already in the design process.

According to (Emborg 1989) two types of cracks can occur:

- Surface cracks that is caused by internal restraints within the material, as the case with reinforcement or due to temperature gradients.
- Through cracks that occurs across the whole cross-section and is caused by the external restraints that arise due to connection of already existing adjoining structures.

For a restrained concrete specimen, as shown in Figure 2.1, it is possible to distinguish that the concrete experiences compressive stresses during the first part, which is when the hydration process starts and the temperature rises. The compressive stresses in the specimen continue to increase until the peak temperature is reached around ~36h. The cooling process then starts and rather soon the compressive stresses changes into tensile stresses which continue to grow as time progress.

The surface crack is a result of an uneven temperature distribution within the concrete structure. When the surface cools and wants to shrink, the shrinkage could be prevented by the warmer core of the structure or the reinforcement. This type of internal restrain creates tensile stresses in the surface layer and can cause it to develop cracks, but this type of surface crack usually closes, become compressed, when the entire structure has finally cooled down.

The other type of crack that can occur is the through crack which affects the whole cross-section of the structure. This type of cracking takes place due to external restraints which prevent the natural movement due to volume changes, see Figure 2.7.

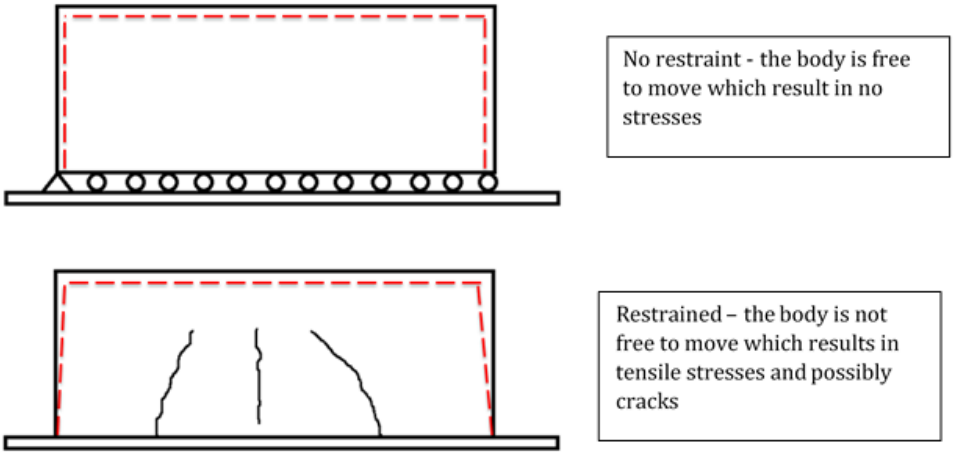

Figure 2.7 External restraint from the foundation which result in through crack.

Through cracks are cracks that tend to appear perpendicular to the restraint joint and at the ends these cracks often has an inclination which follow the principal stresses. The cracks often starts to develop near the joint, can be quite long and they also penetrate the whole thickness of the structure, see Figure 2.8.

Figure 2.8 Through cracking as an effect of external restraint (Bjøntegaard 2011).

A particular case of through cracks is usually noticed in cases similar to the one studied in the Marieholm Tunnel. In this type of structure, where there is a connection between the wall and slab, the decisive point for through cracks appear above the casting joint, see Figure 2.9.

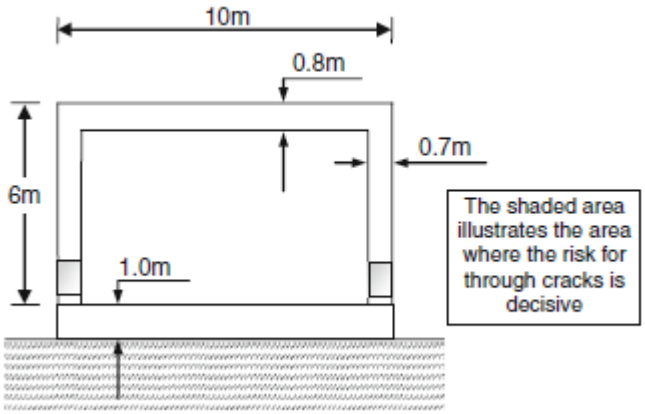

Figure 2.9 Critical Section of a tunnel for through cracks (Utsi & Jonasson 2012)

3 Early-Age Cracking Model

Several different approaches have been used during the last 30 years in order to solve the issue of early age cracking in concrete. Many of these studies encounter the same main problem which is connected to the complexity due to the amount of variables that are involved and the coupling between temperature and age. The different solutions presented for these problem varies from an initial idea of analytical flow options and simplified models, to more complex numerical models that are adapted to the usage of computational modeling software.

The risk of cracking is evaluated by comparing the tensile strength of the concrete and the self-induced tensile stresses during the hardening period. Therefore, one can identify several key aspects which have a large influence on the early age cracking.

According to (Bjøntegaard 2011) the main driving force that create early age cracking are the thermal dilation and autogenous shrinkage, while the other factors, seen in Figure 3.1, can be considered to be the response of the material itself and adjacent structures.

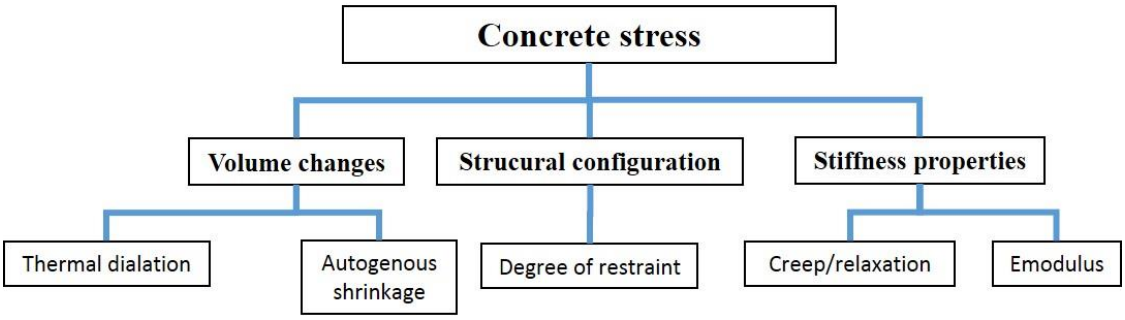

Figure 3.1 Schematic diagram of factors that influence the early age cracking of concrete, adopted from (Bjøntegaard, 2011).

This chapter will first introduce a simplified model in order to present the basic idea behind the stress calculation. Further on the basic idea of computer modelling is explained together with one method on how the different mechanisms can interrelate and be based on the degree of hydration.

3.1 Simplified model

There are several different models available to determine the risk of thermal cracking in concrete and one of them is a simplified method that is presented in (Bjøntegaard 2011).This method can be used for hand calculations and to give a good understanding of the principles that is being used for this type of problem. The method is based on simplified stress calculations which give an estimation on the risk of cracking for a concrete structure. This type of calculation method is often dependent on the fact that a realistic temperature distribution together with the degree of restraint are known for the analyzed structure. There are charts and tables available that can be used to estimate the degree of restraint or it can be based on previously made advanced computer simulations.

The method presented in (Bjøntegaard, 2011) is based on a parameter called age adjusted effective E-modulus (AEM) which only considers the phase when the tensile stresses start to appear during the cooling phase, see Figure 3.2. The strains can then be calculated according to:

$$\varepsilon_{tot}(t_2, t_3) = \varepsilon_{as}(t_2, t_3) + \varepsilon_T = \varepsilon_{as}(t_2, t_3) + (T_3 - T_2) \cdot \alpha \quad (3.1)$$

Where ε_{tot} is the total strain, t_2 is the time in days until zero stress, t_3 is the time in days when the crack risk should be determined, T_2 is the temperature at t_2, T_3 is the temperature at t_3, α is the thermal dilation coefficient, ε_{as} is the autogenous shrinkage.

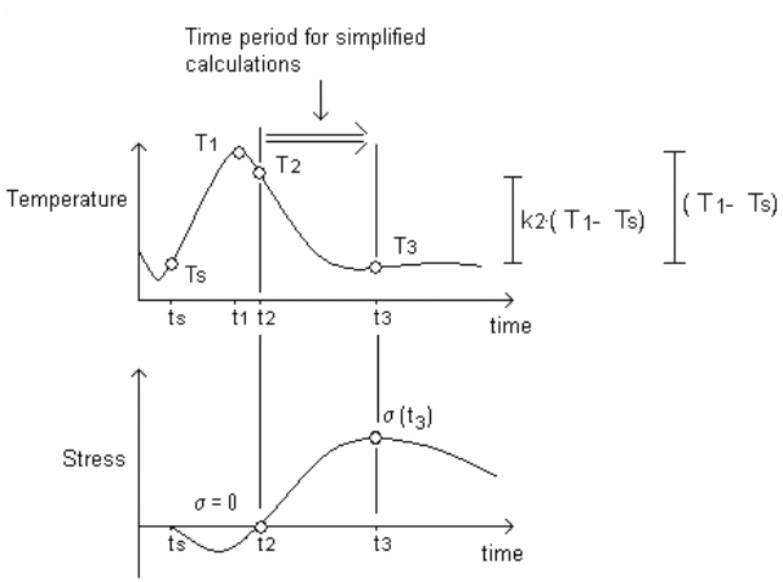

Figure 3.2 Considered time period and stresses for the simplified method (Bjøntegaard 2011).

In structural design, codes as Eurocode 2 (CEN 2004) use the effective E-modulus which is calculated by the usage of the creep factor, φ, according to: $E_{ef} = \frac{E_c}{1+\varphi}$,which is based on the assumption that the stresses are approximately constant in time. It is not possible to apply this directly on hardening concrete since it has a gradual stress development. Therefore the E-modulus is reduced by an aging coefficient, χ_{AEM}:

$$E_{AEM} = \frac{E_c(t_2)}{1+\chi_{AEM} \cdot \varphi(t_2, t_3)} \quad (3.2)$$

Where the ageing coefficient are calculated according to:

$$\chi_{AEM} = 0.69 + 0.005 \cdot t_2 \quad (3.3)$$

And the stress can then be calculated as:

$$\sigma(t_3) = \varepsilon_{tot}(t_2, t_3) \cdot E_{AEM} \cdot R \quad (3.4)$$

Where *R* is the restraint factor and combined with equation 3.2:

$$\sigma(t_3) = (\varepsilon_{as}(t_2, t_3) + (T_3 - T_2) \cdot \alpha_T) \cdot \frac{E_c(t_2)}{1+\chi_{AEM} \cdot \varphi(t_2,t_3)} \cdot R \qquad (3.5)$$

This is one way to estimate the risk of cracking in theory. The real behaviour is much more complex and several parameters change over time, which become to complicated to handle in handcalculations and therefore a computer based model is used instead.

3.2 Advanced computer based model

One common way to solve this complexity is to use the coupling mentioned in Section 2.4, with the usage of degree of hydration, ξ, as the core variable for both concrete properties and temperature evolution. This type of coupling have been used by several researchers and (Guenot & Torrenti 1994) developed different models for creep based on the degree of hydration. (Liu et al. 2014) later based their research on this work in order to do a more detailed analysis of the variation of Poisson's ratio, ν, and (Benboudjema & Torrenti 2008), developed the coupling including a more accurate interpretation of transient creep.

3.2.1 Degree of hydration

The coupling revolves around the usage of the degree of hydration which is defined with the Arrhenius law that describes kinetics of hydration (Brown et al. 1988):

$$\dot{\xi} = \tilde{A}(\xi) \exp(-\frac{E_A}{RT}) \qquad (3.6)$$

where E_a is the activation energy, R the natural gas constant, T the thermodynamic temperature (K) and $\tilde{A}(\xi)$ the normalized affinity, a function that characterizes the hydration process, as described in (Ulm & Coussy 1995).

3.2.2 Temperature evolution

The temperature evolution which drives the main mechanisms is described with an energy balance formula, considering the heat released from the hydration process:

$$C\dot{T} = \nabla(k\nabla T) + L\dot{\xi} \qquad (3.7)$$

Where L is the latent heat of hydration, k the thermal conductivity and C the volumetric heat capacity (Lacarrière 2007).

3.2.3 Stress

The usual choice for cracking prediction is based on a strain model such us the Elastic Damage Model (Benboudjema & Torrenti 2008):

$$\tilde{\sigma} = E(\xi) \cdot \dot{\varepsilon}_{el} \qquad (3.8)$$

Where $\tilde{\sigma}$ are the effective stresses, E the elastic stiffness tensor and $\dot{\varepsilon}_{el}$ the elastic strains.

3.2.4 Material properties

The stress is according to Equation 3.8 depending on the elastic modulus and elastic strains. The following Section presents how these factors depend on the degree of hydration.

Elastic Modulus

The Young Modulus increases with hydration according to:

$$E(\xi) = E_{\infty} \cdot \left(\frac{\xi - \xi_0}{\xi_{\infty} - \xi_0}\right)^{\beta} \qquad (3.9)$$

Where ξ_0 is the degree of hydration for the time t_0, when the concrete starts to gain resistances, ξ_{∞} the final hydration degree , E_{∞} the young modulus for $\xi = \xi_{\infty}$ and β a value dependant on the type of concrete.

Poisson´s ratio

The Poisson ratio is dependent on the degree of hydration along the hydration process according to the next relationship:

$$\upsilon(\xi) = 0.18 \cdot \sin\frac{\pi\xi}{2} + \frac{1}{2}\exp(-10\xi) \qquad (3.10)$$

Which is based on the fictitious degree of hydration for basic creep of early age concrete purposed by (Schutter & Taerwe 2000).

3.2.5 Strain components

This can be decomposed as:

$$\dot{\varepsilon}_{el} = (\dot{\varepsilon} - \dot{\varepsilon}_{bc} - \dot{\varepsilon}_{au} - \dot{\varepsilon}_{th}) \qquad (3.11)$$

Where $\dot{\varepsilon}_{bc}$ are the basic creep strains, $\dot{\varepsilon}_{au}$ the autogenous shrinkage strains, $\dot{\varepsilon}_{th}$ the thermal variation strains and $\dot{\varepsilon}$ the total strain. The transient thermal creep has not being considered as a simplification.

3.2.6 Autogenous Shrinkage

Based on the Eurocode 2 EN 1992-1-1(CEN 2004) the autogenous shrinkage is obtained in the following way:

$$\varepsilon_{ca}(t) = \beta_{as}(t) \cdot \varepsilon_{ca}(\infty) \quad (3.12)$$

Where the final shrinkage is:

$$\varepsilon_{ca}(\infty) = \frac{5}{2}(f_{ck} - 10) \cdot 10^{-6} \quad (3.13)$$

And

$$\beta_{as}(t) = 1 - \exp(-0.2t^{1/2}) \quad (3.14)$$

Where f_{ck} is the characteristic cylinder strength of concrete at 28 days.

3.2.7 Thermal dilation

The thermal dilation is given by:

$$\dot{\varepsilon}_{th} = -\alpha \cdot \dot{T} \quad (3.15)$$

Where α is the coefficient of thermal dilation. Which is taken as constant with a value of 10 $\mu\varepsilon / °C$ according to (CEN 2004).

3.2.8 Creep

The basis for the definition of the creep modelling is the usage of Kelvin-Voigt degree of hydration-based chains, based on physical observations, such as the one shown in Figure 3.3. The number of cells in the Kelvin-Voigt chains varies among the different models.

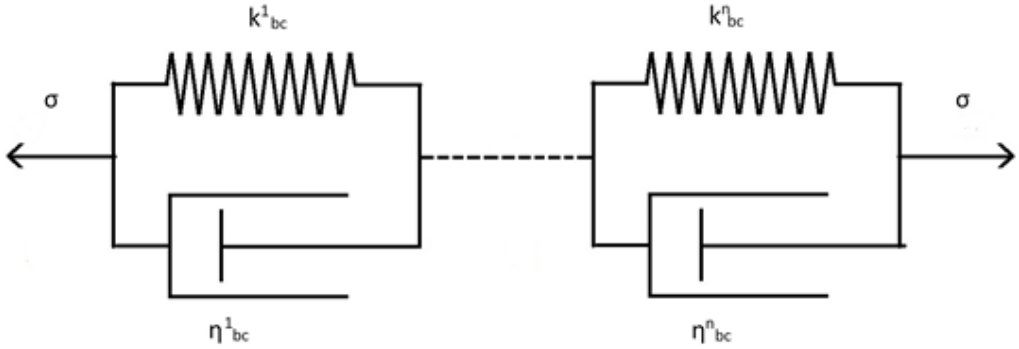

Figure 3.3 Two cell Kelvin-Voigt degree of hydration-based chain.

In (Benboudjema & Torrenti 2008), the equilibrium equation of a cell is presented as:

$$\dot{\tilde{\sigma}} = \dot{\tilde{\sigma}}^{i}_{sp} + \dot{\tilde{\sigma}}^{i}_{ds} \quad (3.16)$$

Where $\tilde{\sigma}^{i}_{sp}$ are the effective stresses acting on the spring and $\tilde{\sigma}^{i}_{ds}$ the effective stresses in the damper, for a Kelvin-Voigt unit *i*.

The stresses in the spring are obtained with:

$$\tilde{\sigma}_{sp}^{i} = k_{bc}^{i}(\xi) \cdot \dot{\varepsilon}_{bc}^{i} \qquad (3.17)$$

Where $k_{bc}^{i}(\xi)$ is the stiffness of the spring and ε_{bc}^{i} is the basic creep strain both for the Kelvin-Voigt unit *i*.

At the same time, the stresses in the damper are described by:

$$\tilde{\sigma}_{ds}^{i} = \eta_{bc}^{i}(\xi) \cdot \dot{\varepsilon}_{bc}^{i} \qquad (3.18)$$

In which $\eta_{bc}^{i}(\xi)$ is the damper's viscosity in the Kelvin-Voigt unit *i*.

The inclusion of the degree of hydration dependency is presented in (Hauggaard et al. 1999) and considered along with the relationships introduced by (Schutter 1999):

$$k_{bc}^{i}(\xi) = k_{bc,\infty}^{i} \cdot \frac{0.473}{2.081 - 1.608\xi} \cdot \xi^{0.62} \qquad (3.19)$$

Where $k_{bc,\infty}^{i}$ is the final stiffness when the hydration is complete and ξ the degree of hydration.

Describing the relationship between the stiffness of springs and dampers viscosity as:

$$\tau_{bc}^{i} = \frac{\eta_{bc}^{i}(\xi)}{k_{bc}^{i}(\xi)} \qquad (3.20)$$

Combining these equations together a differential equation for each Kelvin-Voigt unit *i* according to (Benboudjema & Torrenti 2008):

$$\tau_{bc}^{i} \cdot \dddot{\varepsilon}_{bc}^{i} + (\tau_{bc}^{i} \frac{\dot{k}_{bc}^{i}(\xi)}{k_{bc}^{i}(\xi)} + 1)\ddot{\varepsilon}_{bc}^{i} = \frac{\ddot{\sigma}}{k_{bc}^{i}(\xi)} \qquad (3.21)$$

Finally the temperature effect must be taken into account, as it modifies the strength of the concrete, this is considered by modifying the spring stiffness and the damper viscosity:

$$\begin{cases} k_{bc}^{i}(\xi, T) = k_{bc}^{i}(\xi, T_0) e^{\frac{E_{ac}}{g}(\frac{1}{T_c} - \frac{1}{T_0})} \\ \eta_{bc}^{i}(\xi, T) = \eta_{bc}^{i}(\xi, T_0) e^{\frac{E_{ac}}{g}(\frac{1}{T_c} - \frac{1}{T_0})} \end{cases} \qquad (3.22)$$

Where E_{ac} is the creep activation energy and $T_0 = 273$ K

3.2.9 Cracking

The basic crack check provided in (CEN 2004) is to ensure that the attained stress is lower the concrete's tensile strength. A safety factor of 0.7 is often considered, although in this particular case cracking should not occur or should be of little impact as it is a submerged structure with strict design limitations regarding cracking (Olofsson & Uhlan n.d.).

3.3 DIANA Model

Diana divides the analysis into two different phases, according to the type of analysis, which includes: the non-linear heat flow and the non-linear structural analysis. Together defined as heat flow-stress staggered analysis.

3.3.1 Non-linear Transient Heat Flow

Diana uses as input the initial temperature field, the thermal boundaries and the concrete hydration.

Initial Temperature Field
An initial temperature field can be applied as a first estimate of the solution to come, or as the initial temperature value for the elements.

Thermal Boundaries
The thermal boundaries (conductive, radiative or convective) must be defined in the model. The materials that act as boundaries should be provided with values for conductivity and capacity (as it is a transient heat analysis). For the transient heat analysis the time dependency of the boundary conditions should be also specified.

Concrete Hydration
For the early-age concrete heat problem, the hydrating concrete acts as an internal heat source. To simulate the hydration process of the concrete the variable heat of hydration ($\dot{\xi}$) is described as the momentary cumulative heat production divided by the total heat production:

$$\xi = \frac{\int_0^t q(\xi,T)dT}{\int_0^\infty q(\xi,T)dT} \tag{3.23}$$

The amount of heat produced is a function of temperature history, as such the momentary heat production can be defined as:

$$q(\xi,T) = H_u \cdot q_\xi(\xi) \cdot q_T(T) \tag{3.24}$$

With H_u the maximum value of heat production rate, q_ξ degree of reaction dependent heat production and q_T temperature dependent heat production. For this second one Diana uses:

$$q_T(T) = e^{-\frac{c_A(\xi,T)}{T}} \quad (3.25)$$

Where c_A is the constant of Arrhenius that describes the Arrhenius equation dependent on the degree of reaction.
The main output from the heat flow analysis is nodal temperatures and either degree of reaction or equivalent age.

A more detailed description of the ways this variables can be implemented can be found in (Diana 2014).

3.3.2 Non-linear Structural

The structural problem is solved the same way as the linear one, but the non-linearity comes from the dependence of parameters on variable factors such as temperature or maturity. As such, the problem solved is:

$$K \cdot u = f \quad (3.26)$$

Where *K* is the system stiffness matrix, *u* a vector of unknown nodal variables (namely displacements and rotations) and *f* the vector of the nodal forces.

From the displacements obtained and through the usage of the finite element method stresses and strains are obtained. DIANA adds the incremental strains and stresses based on modified elastic parameters to the previous stress state:

$$\sigma_i = \sigma_{i-1} + E_i \cdot \Delta\varepsilon_i = E_{i-1} \cdot \varepsilon_{i-1} + E_i \cdot \Delta\varepsilon_i \quad (3.27)$$

Material Properties
As the material properties such us the young modulus or coefficient of thermal expansion are maturity dependent, this requires the usage of a nonlinear analysis.
The material properties dependence on maturity or temperature is defined through the material model.

Thermal Strains
From the temperature results obtained on the heat flow analysis and in combination with the coefficient of thermal expansion the thermal strain is calculated as in (3.15).

Shrinkage Strains
The way the shrinkage strains are calculated depends on the material model used. For Eurocode material model for instance, this is based in the notional size and the age at the end of curing. User supplied functions can be used, these can be maturity dependent.

Creep Strains
Similarly to shrinkage this heavily relies on the material model, in this case for Eurocode it depends on notional size and age of loading/age at the birth of the element. There is a specific function for creep at high temperatures in which creep strain is obtained as:

$$\dot{\varepsilon}^{tr} = \frac{\alpha\phi}{f_c}\dot{T}\sigma \qquad (3.28)$$

With ϕ the creep factor, α the coefficient of thermal expansion and f_c the uniaxial compressive strength.

Phased Analysis

A way of considering the pouring of concrete is by including a phased analysis where elements become progressively active in the structure. This is considered in the calculations as shown in Figure 3.4.

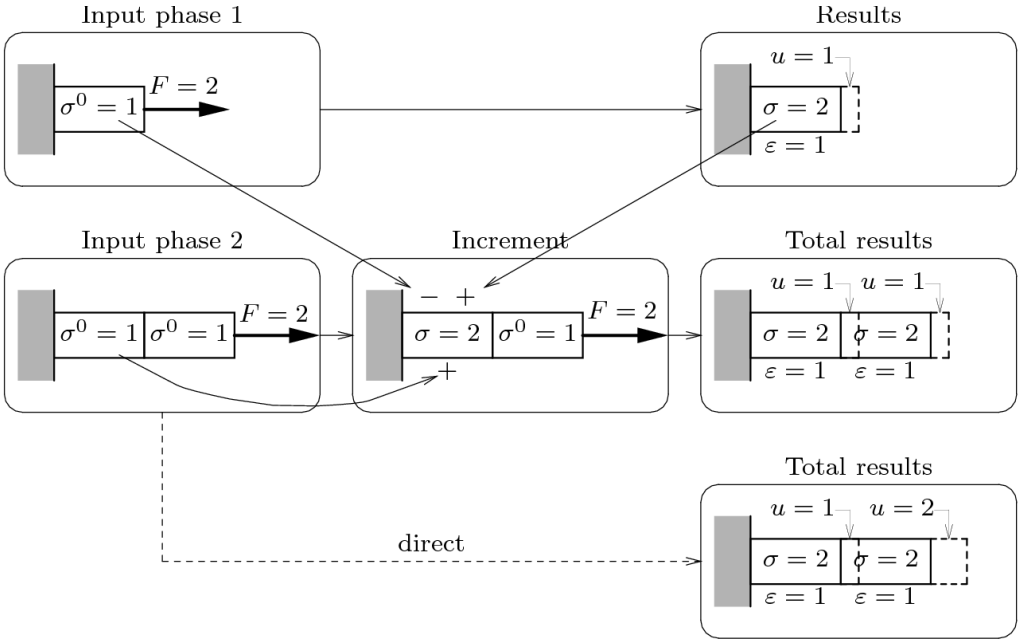

Figure 3.4 Phased analysis influence on calculation of strain/stress (Diana 2014).

4 Modelling Software

For the modelling of the mock up different software options were investigated. In this chapter, information on their benefits and limits is provided. It is important to state that there are plenty of software alternatives, from general software like Abaqus, Ansys, Lusas or Midas, to Contest, Femmasse Heat or b4cast, which are softwares with a focus on the calculation of hydration based problems in hardening concrete. A special focus has been made on the DIANA 10, OOFEM, Code Aster, Athena and HACON.

4.1 DIANA 10

DIANA is a software developed by TNO DIANA for the modelling of concrete structures, and the version DIANA 10 was just recently released. As so, it provides a wide variety of alternatives both design-wise and when it comes to analysis options. There is extensive literature on the usage of Diana, such us (Eierle 1999) and (Ji 2008).

It includes the option of non-linear analysis for creep, time dependant temperature and maturity, as well as a potentially very interesting features such as coupled flow stress analysis. There is also a Multi-directional fixed crack model included in the program for temperature and maturity dependant cracking, which is based on a strain decomposition in elastic, crack and plastic strain.

The variables can be modified with functions dependent on temperature, maturity or concentration. For shrinkage and creep, as well as other material definitions, different material codes are already implemented in the software. It also allows the creation of subroutines for built in materials.

The post-processing phase offers options for cracking and stress results. In addition all the modelling can be developed in the same software that integrates pre and post processing with analysis, within the Diana Interactive Environment.

More information about Diana can be found in its website http://tnodiana.com/.

4.2 OOFEM

Oofem is a free finite element code with object oriented architecture for solving mechanical, transport and fluid mechanics problems. It has been developed since 1997 by the Department of Structural Mechanics of the Faculty of Civil Engineering in the Czech Technical University in Prague, the structure and the idea behind it is showed in (Patzák & Bittnar 2004).

This free software provides plenty of different tools for structural analysis, the more interesting ones regarding early age concrete analysis are the staggered analysis which is a temperature analysis followed by a structural one based on it; as well as its transport module that allows for coupled heat and mass transfer problems. There is not specific information to early age concrete analysis in its manuals, but the correct usage of the previously mentioned tools could be implemented into modelling of an early age concrete problem, with the advantage of involving a free software tool that can be modified and improved for the particular problem in question.

Regarding material modelling, it provides various creep models dependant on age as well as a damage model based on the microprestress-solidification theory which is well described in (Di Luzio & Cusatis 2013) and includes a wide variety of parameters.

Further documentation and information on the different versions can be found in http://www.oofem.org/en/oofem.html.

4.3 Code Aster

Code Aster is an open source software that allows the study of structural mechanics behaviour of structures mainly applied to the usage of deformable solid mechanics, developed in particular to study the components of materials or machines used in the field of electricity production and transmission. The formulation used in hydration processes is shown in (Bottoni 2012). It allows the study of temperature development in a solid as well as modelling the hydration and the drying of concrete, as well as creep cracking coupling.

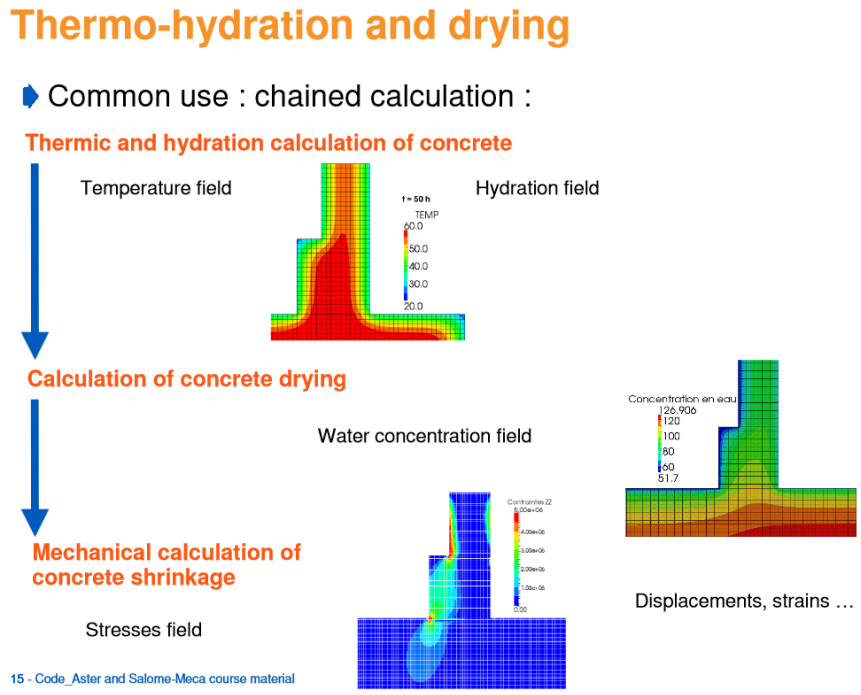

Figure 4.1 Extract from Code Aster thermal analysis manual.

It also includes mechanisms to study thermo-hydro-couplings which would allow for an extensive study of early cracking in concrete if the relative humidity is also taken into account, as can be seen in Figure 4.1. There is the possibility of modelling reinforced and pre-stressed concrete both in 3D and 2D models.

A wide variety of information is provided on their website http://www.code-aster.org/spip.php?rubrique2, where an active forum can offer help and learning materials can be found.

4.4 ATENA

ATENA is a commercial software developed by Cervenka Consulting for the simulation of concrete and reinforced concrete structures, including cracking, crushing and reinforcement yielding. Its theoretical basis and usage has been shown in (Cervenka et al. n.d.)

Regarding analysis options, a heat and moisture transport analysis including hydration is provided as one of the examples of usage for this tool, with the modelling of cooling pipes included. Even while not having the creep commands in the native version, there is a graphical interface for it ATENA-Gid.

It provides a user friendly approach with the disadvantages of a less customizable tool that is also not free. On http://www.cervenka.cz/products/atena/ detailed information on this software can be found as well as documentation and an online forum.

4.5 HACON

HACON is a computer program developed as a joint project between the Division of Structural Mechanics in Lund University and Vattenfall Utveckling AB. This software allows for 2D and axisymmetric analysis of hardening concrete problems, allowing for heat development calculations based on the degree of hydration and temperature. It allows also for phased analysis, as well as stress analysis along the whole process, and takes into consideration creep, stress induced thermal strain, autogenous shrinkage and crack development, for further information consult (Dahlblom & Lindemann 2000).

4.6 Choice of software

Provided all the choices, DIANA 10 allows for a balanced approach to the modelling intended in this master thesis. While being adaptable in some aspects, such as defining variables, it also comes as a structured software, with a clear work flow, that allows for a simplified approach to the task in hand. And extensive documentations with examples for an easier approach to the program.

Future considerations can be made on the complexity attained in the model being able to apply even a phased analysis that might be interesting for the purpose of this study.

5 Marieholm tunnel

The background for this thesis is the construction of the Marieholm tunnel under the river Göta älv in Gothenburg. This tunnel will be around 500 meters long and will have three driving lanes in each direction.

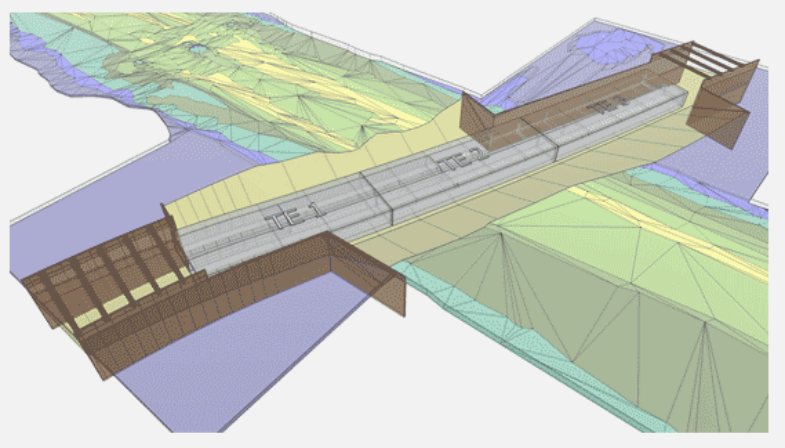

Figure 5.1 Principal sketch over the Marieholm tunnel and the three immersed sections.

The middle part of the tunnel is divided into three large sections, where each section is about 100 meters long, 30 meter wide and 10 meters high. These sections are constructed in a dry dock before they are immersed and connected on the river bottom, as seen in Figure 5.1 (Trafikverket 2015).

In order to verify the results that are obtained in the developed 3D FEM-model in DIANA, see Chapter 8, a large scale trial casting of a tunnel segment has been done, where data such as temperature distribution within the segment, external temperature etc have been measured.

5.1 Geometry

The tunnel segment that was analyzed is a 7 meter long wall segment of the tunnel, see Figure 5.2. There is a casting joint placed 2050 mm from the top. The bottom part was casted first and 57 days later the top part was casted.

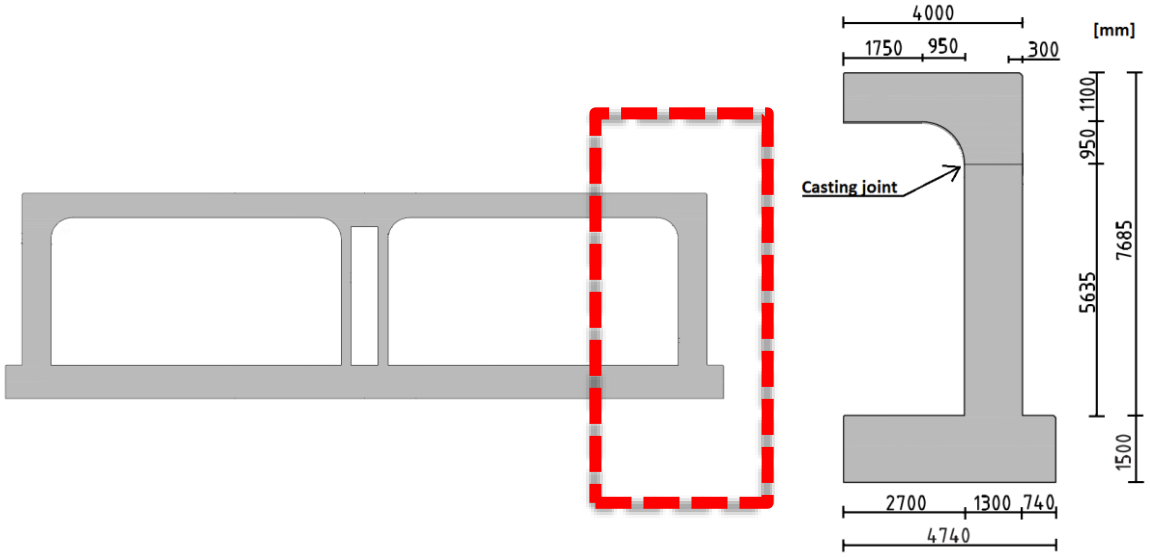

Figure 5.2 Cross-section of the tunnel and the analyzed tunnel segment.

5.2 Given data

The large scale trial casting provides information on the temperature profile along the time within the element but also an external temperature curve which can be used when applying boundary conditions.

This trial casting occurred in two phases as can be seen in Table 5-1, with the second casting including the roof slab.

Table 5-1 Casting Times

Start/end times for measurements	
Start time cast 1	**End time cast 1**
2015-12-15 15:53	2016-01-11 11:23
Start time cast 2	**End time cast 2**
2016-03-09 07:52	2016-03-21 08:22
Time between starting times:	
Hours:	2031,991667
Seconds:	7315170

First Cast

The mock-up itself was monitored through 16 different probes that where placed inside the segment. The position of the probes in the bottom part be can be seen in Figure 5.3.

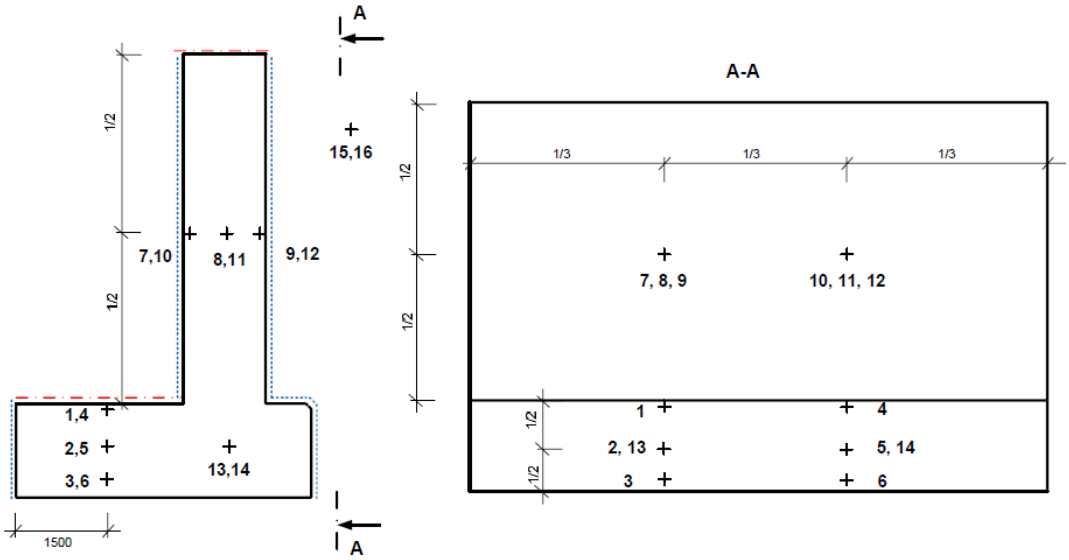

Figure 5.3 Thermal gauges positioning first cast.

For the first cast period, Probe 15 and 16 measured the external temperature and the obtained distribution can be seen in Figure 5.4, where time=0 is equal to the moment when the first casting starts.

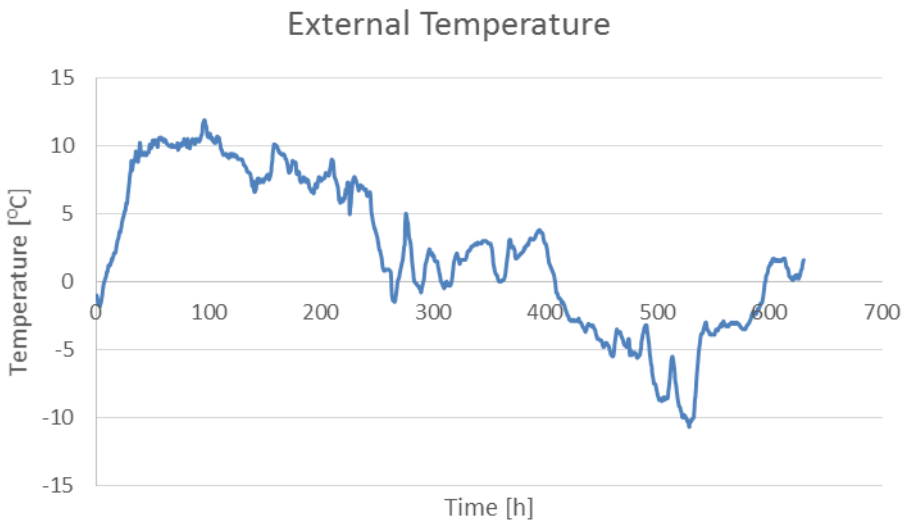

Figure 5.4 First cast, external temperatures measurement.

Second Cast

In the top part 14 probes where used which were placed according to Figure 5.5.

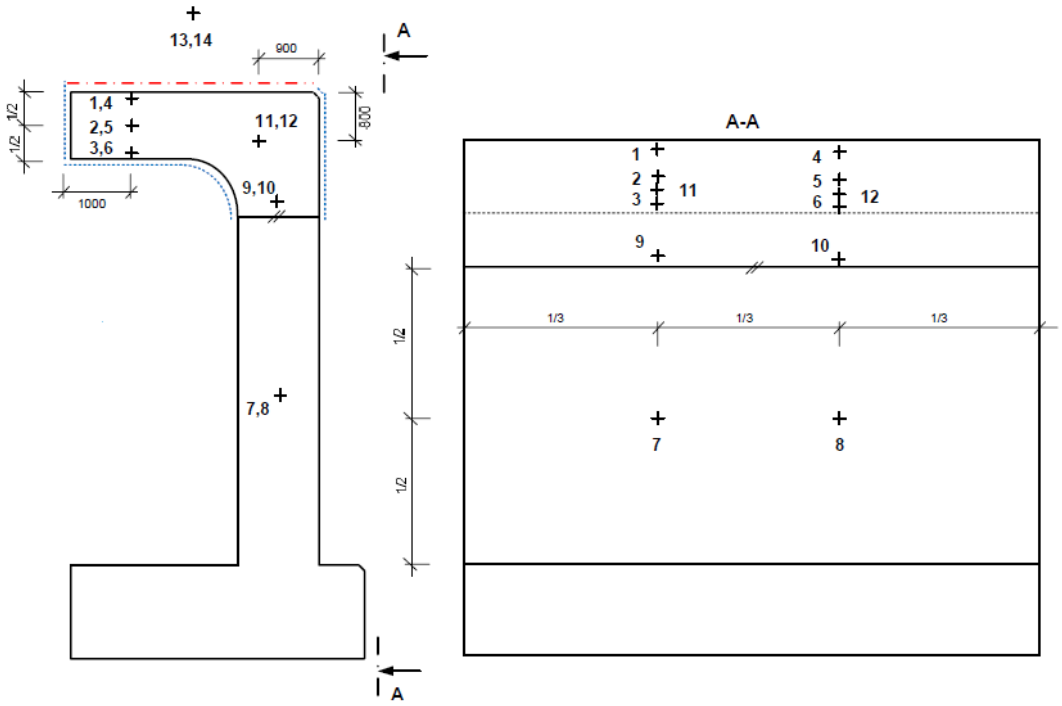

Figure 5.5 Thermal gauges positioning second cast

For the second cast period, Probe 13 and 14 measured the external temperature and the obtained distribution can be seen in Figure 5.6, where time=0 is equal to the moment when the second casting starts.

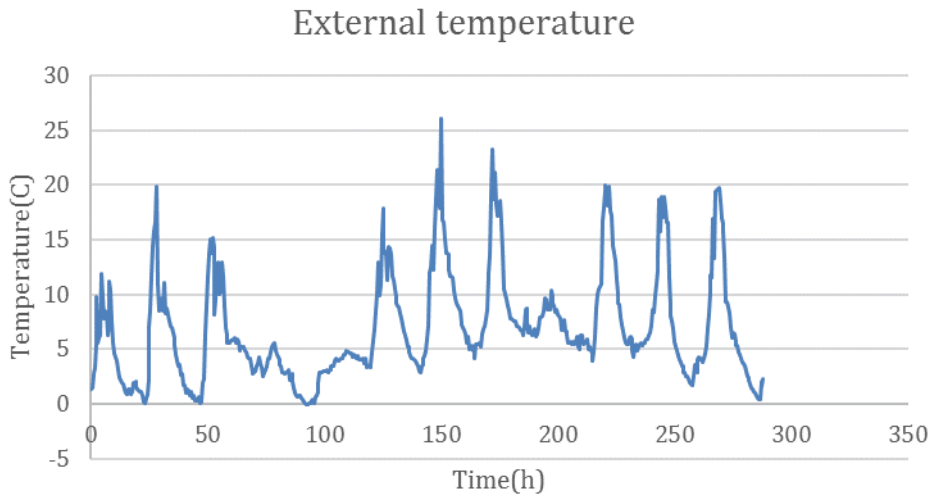

Figure 5.6 Second cast external temperatures measurements.

The cement used in the concrete is CEM I 42.5 N SR3 MH/LA, Anläggningscement which is a type 1 Portland cement. The chemical composition of this cement, which can be seen in Table 5-2, is used together with HYMOSTRUC in order to estimate the adiabatic temperate development, Arrhenius constant, conductivity and specific heat capacity. See appendix 1 for a complete table on material properties

Table 5-2 Concrete mix design and Chemical composition of the cement.

Properties			
		Value	Unit
Specific Surface (Blaine for Cement)		338	m^2/kg
Particle density of the concrete		3182	kg/m^3
Compressive strength (Cement)	1 Day	12.1	MPa
	2 Days	23.1	MPa
	28 Days	54.5	MPa
Strength Class		C35/45	-
W/C		0.395	-
Air Content		4.2	%
Proportions:	Cement	415	kg/m^3
	Water	164	kg/m^3
0-2mm	Sand	700	kg
4-8mm	Crushed	189	kg
8-16mm	Crushed	227	kg
16-25mm	Crushed	718	kg
Total Density		2411	kg/m^3

Cement Composition	
Component	**Amount [%]**
CaO	64
SiO_2	21.6
Al_2O_3	3.7
MgO	0.95
Na_2O	0.1
K_2O	0.63
Cl	0.01
SO_3	2.6
Fe_2O_3	4.5
C_2S	18.5
C_3S	57.8
C_3A	2.2
C_4AF	13.7

While HYMOSTRUC simulates the concrete hydration of a cube and provides a wide variety of results with respect to this, the adiabatic curve obtained from it differs heavily form the expected result. This implies a lack of accuracy in the final temperature profile

output, for this reason it was finally disregarded and a simple model was generated in Contest to obtain a precise adiabatic heat development curve.

Both curves can be seen in Figure 5.7.

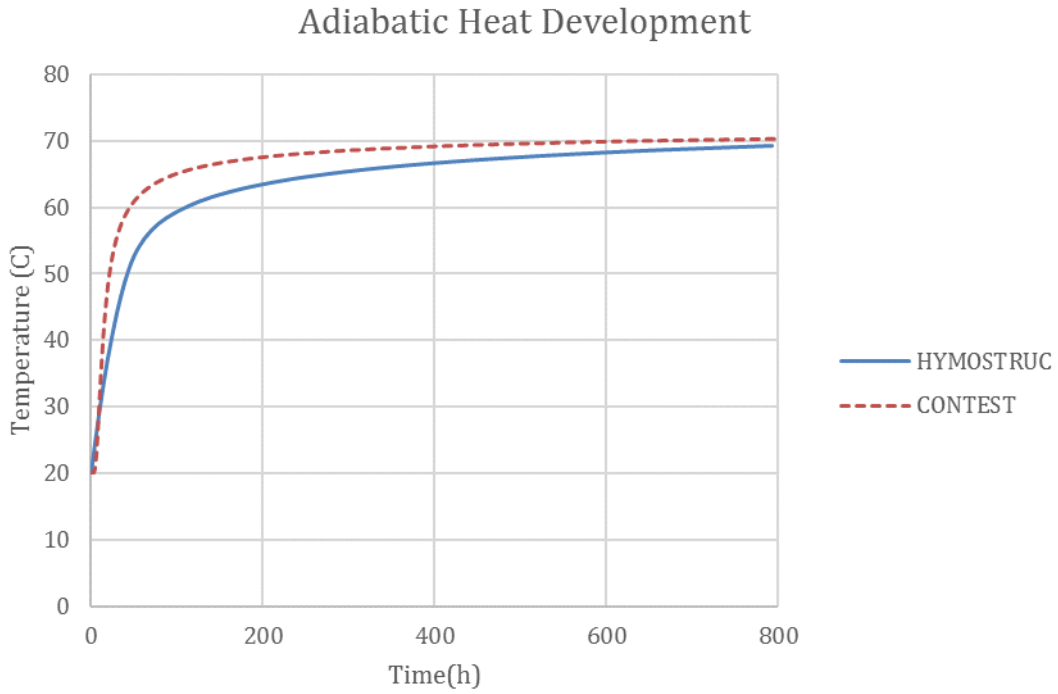

Figure 5.7 Adiabatic heat development curve comparison.

6 Finite element-analysis of tunnel wall segment

As a way of approaching the problem, a simple cube was used to test the different variables and its interactions before implementing them in the model. This allowed for a simplified view on each of the mechanisms involved in early-age cracking, that later were implemented in the complete model.

6.1 Geometry

For the purpose of the project the mock-up geometry was adapted to the modelling needs imposed by Diana. Initially an approach including the modelling of the formwork and surrounding tarpaulin was used, but aiming for simplicity they were removed applying their effects as boundary conditions, diminishing drastically the amount of elements in the model and with little to no deviation in the results.

This same reason motivated the study of half the mock-up, as symmetry conditions can be applied in the middle section, therefore diminishing the amount of elements and making it more efficient from a computational time perspective.

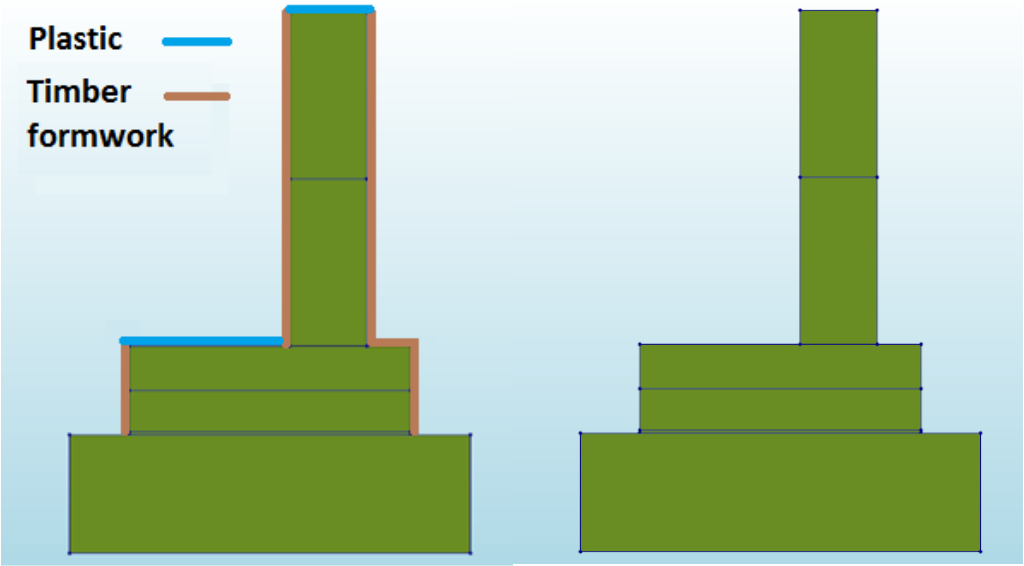

Figure 6.1 To the left is the model with formwork and to the right the model without formwork used in the analysis for the first cast.

A 2 meters volume of soil was included in the model to offer a restraint condition closer to reality, the width and length are adopted to create 1 m wide stripes surrounding the mock-up, based on the CONTEST model created for the same purpose.

Afterwards, the mock-up was divided into 5 solids, as shown in Figure 6.1, to simulate in Diana the pouring of the concrete, with the usage of phased analysis. This was considered relevant since there was 12 hours difference between the casting of the bottom slab and the first measurement of concrete in the mid-point of the wall, that if not considered would lead to significant deviations in the influence of the hydration.

Finally, the roof slab corresponding to the second cast was added to the geometry for the complete representation of the real mock up as shown in Figure 6.2.

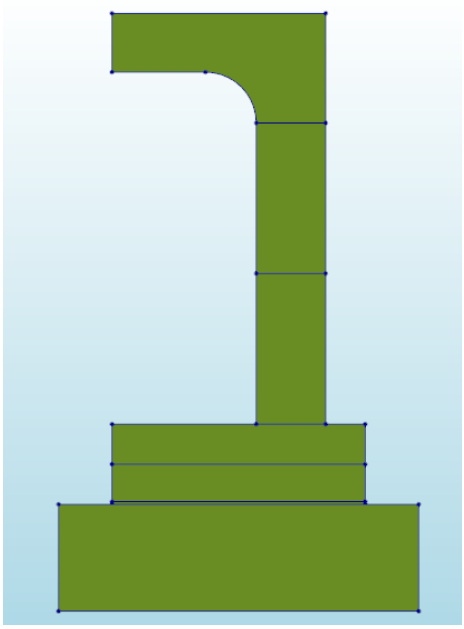

Figure 6.2 Complete Geometry

6.2 Element type

When it comes to the kind of elements used, the main considerations to take into account are: element complexity, distribution of strain and stress over the element and computational load. From all the options presented in DIANA, it is important to clarify that not all structural elements are available for staggered structural-flow analysis, as not all of them can be transformed from structural elements to flow elements.

Two main differences can be found between the elements, the shape and the number of nodes. Regarding the general shape the available alternatives are: tetrahedron, pyramid, wedge and brick. To get a more detailed analysis but at the cost of computational time, this shapes can be used with nodes not only in the apex but also in the midpoint of the edges.

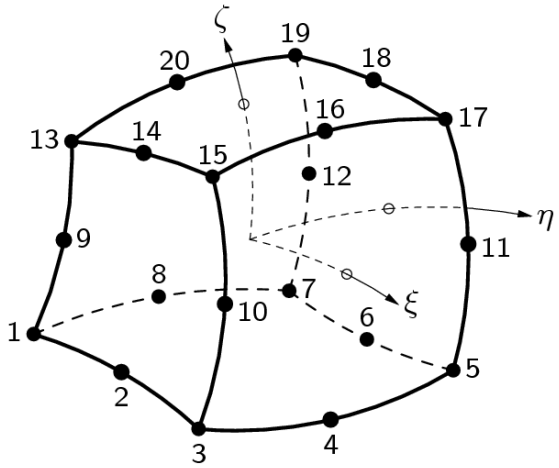

Figure 6.3 Example of element CHX60

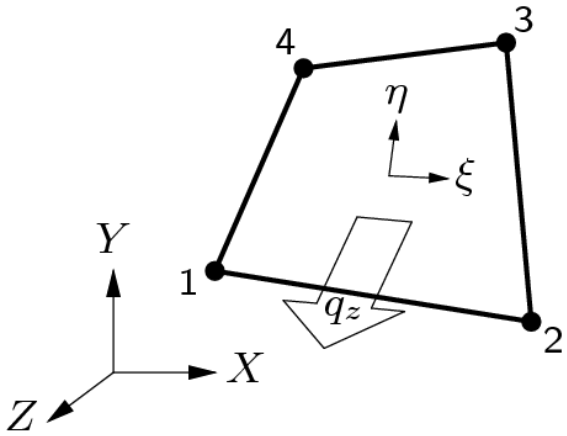

Figure 6.4 Example of Element BQH4T

Tetrahedron elements only provide constant stress and strain distribution over the element, while wedge elements offer a linear approximation of it. The rest of the element types give a constant value of strain and stress in the direction studied, but linear in the perpendicular directions.

Brick elements CHX60, shown in Figure 6.3, were the majority in a mock-up model with a prismatic shaped as they adapt greatly to it, while for the thermal problem, the usage of boundary elements was required and elements BQH4T were used for this purpose, this can be seen in Figure 6.4.

The BQH4T boundary elements don't have mid-side nodes, but DIANA internal conversion makes them compatible with the brick CHX60 elements.

6.3 Boundary conditions

When it comes to boundary conditions two aspects where considered, in parallel with the analysis used. This is structural restraint and thermal boundaries.

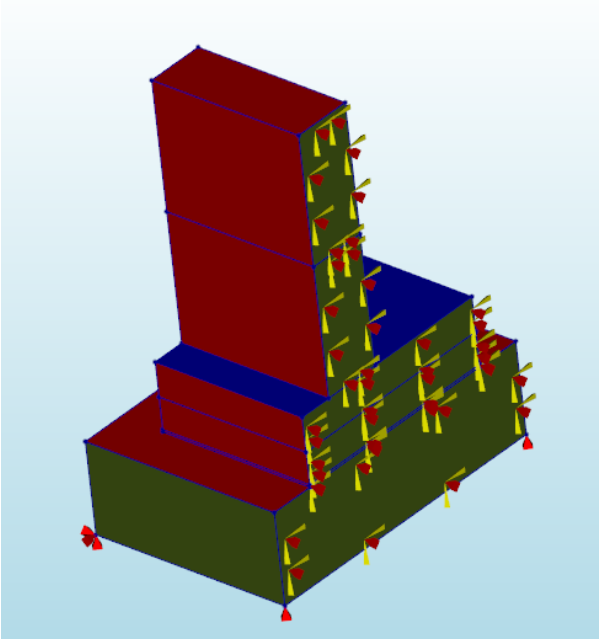
Figure 6.5 Support positioning, symmetry conditions and thermal boundaries.

The structural restraint was imposed in the bottom part of the cube, and symmetry conditions were imposed in the central section as shown in Figure 6.5.
For the thermal problem, every exterior face was defined as a thermal boundary, applying a profile of temperatures obtained from the measurements of the mock-up as external thermal loads.

In addition, the phased analysis lead to the study of the addition of temporary boundary faces for each phase in the process, and its comparison to a model without intermediate boundaries as can be seen in Section 9.1.4.

6.3.1 Formwork and plastic

In order to keep the model simple, the formwork and the polyethylene tarpaulin that are surrounding the concrete were removed and a modified boundary conditions was applied straight onto the concrete surfaces.

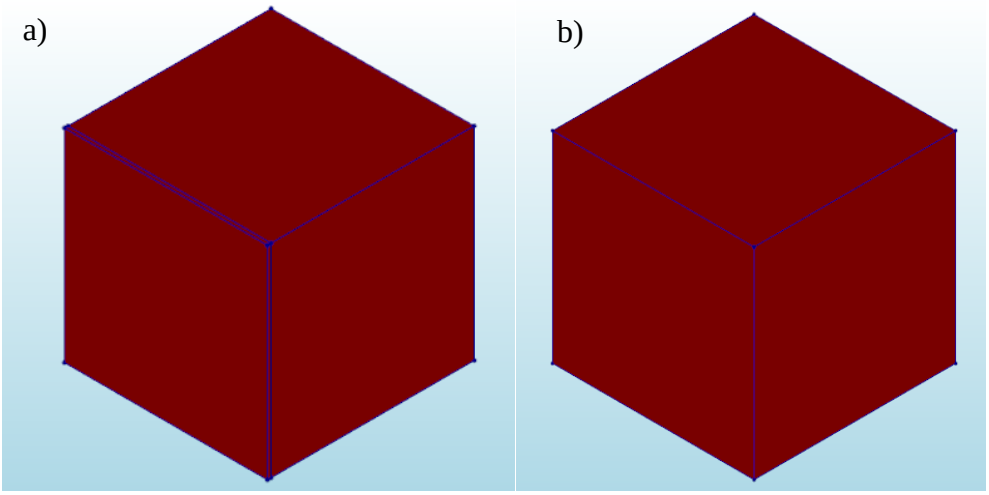

Figure 6.6 a) Model with formwork/plastic elements. b) Model with the boundary conditions applied on concrete surface.

To find out what values to use for the convective power, the base cube was used and first modelled with one side covered by the formwork and polyethylene. This model was then copied and another model was created where the formwork/polyethylene was removed, and the boundary condition that was previously applied on the outer surface of the formwork/plastic was moved onto the concrete surface, see Figure 6.6.

Both models where then analysed and the conduction coefficient in the model without the formwork/plastic geometry was modified until the same temperature development could be seen in both cases. This was measured by first analysing the temperature development at the final time step (after 24h) for one single node, until the difference was approaching 0, see Figure 6.7.

With formwork				Without formwork			
node nr	Conduction coefficient [W/mK]	temp [°C]		node nr	temp [°C]	Conduction coefficient [W/mK]	Diff
298	7,777	34,839374		298	33,89052	7,777	0,948856
				298	33,8494	8	0,989976
				298	34,49217	5	0,347204
				298	35,39351	2	-0,55413
				298	34,90307	3,5	-0,0637
				298	34,78637	3,9	0,053
				298	34,84415	3,7	-0,00478
				298	34,82957	3,75	0,009805

With plastic				Without plastic			
node nr	Conduction coefficient [W/mK]	temp [°C]		node nr	temp [°C]	Conduction coefficient [W/mK]	Diff
298	18	19,929015		298	19,83562	18	0,09339
				298	19,90541	17	0,023603
				298	19,90701	16,5	0,022004
				298	19,91185	10	0,017168
				298	19,92839	10	0,000624
				298	19,92178	9,5	0,00277
				298	19,92907	9,8	-5,2E-05
				298	19,92873	9,9	0,000286

Figure 6.7 Table showing the iterative process of finding the right conduction coefficient.

When the difference was small enough, the temperature development with the new conduction coefficient was plotted for a single node; which made it possible to verify that not only a single value correlated well, but also the temperature development during all time steps, see Figure 6.8.

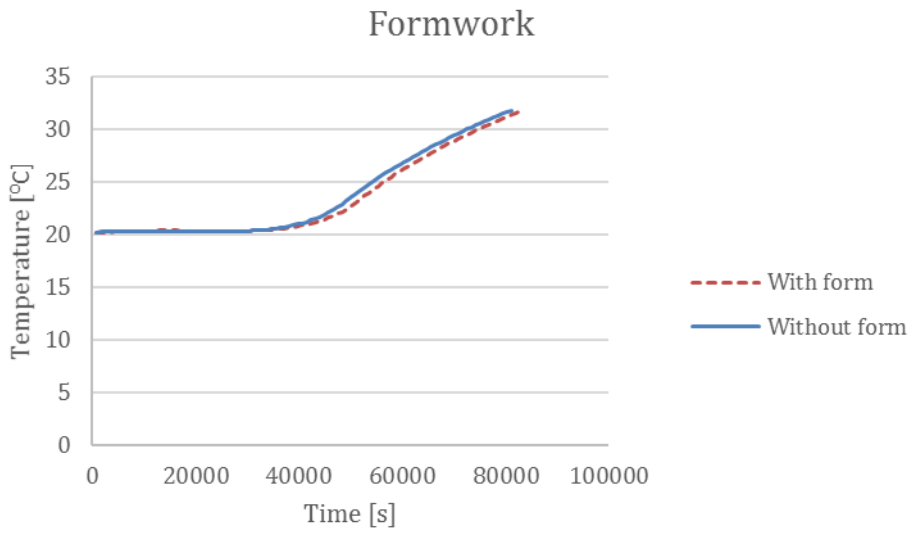

Figure 6.8 Plot used to verify that the temperature development is the same for both cases.

This resulted in that the formwork and polyethylene elements in DIANA could be replaced with a new boundary condition applied onto the concrete surface. This simplified the model and increased the calculation efficiency due to reduction in total number of elements.

6.4 External temperatures

The model simulates the whole stress and temperature development of the element. Unfortunately there was no measurements for the temperatures of the time in between both castings. To solve this an average temperature of 1 °C was assumed, which offers a restrictive boundary condition and allows for the cooling of the first cast. The final exterior temperatures used can be seen in Figure 6.9 .

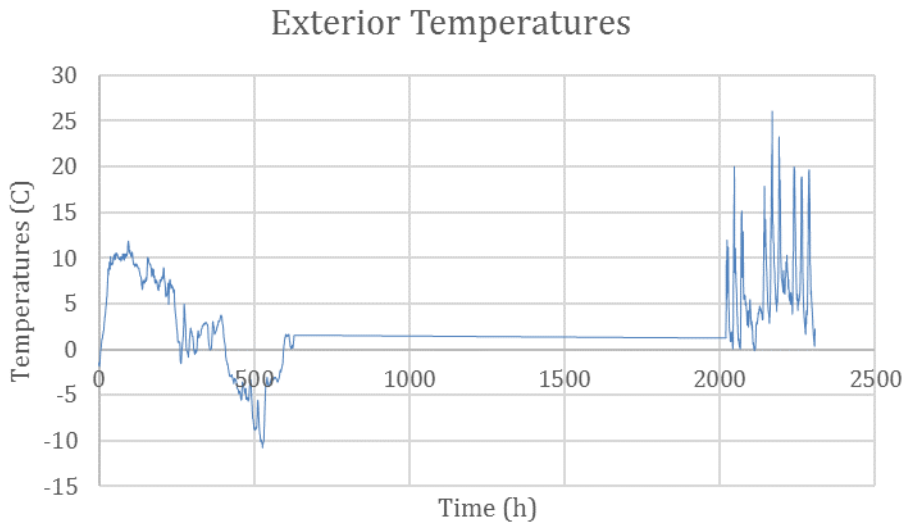

Figure 6.9 Complete exterior temperatures profile.

6.5 Material model

From the different alternatives provided by Diana, the Eurocode model was used as a basis, where the needed parameters were modified for a more accurate resemblance to the real material.

To better control the different variables, a material model was created with formulation for maturity dependent parameters. This was done for the elastic modulus, Poisson ratio and shrinkage, including also its own creep function and strength gain based on maturity for a potential crack analysis.

6.5.1 Elastic Modulus, viscoelasticity

The formulation for the elastic modulus comes from (Singh et al. 2013) where two different methods for maturity dependent elastic modulus are discussed, the CEB-FIP method and the ACI 209 method.

CEB-FIP

The basic formula established in the CEB-FIP method is:

$$E_{ci}(t) = \beta_E(t) \cdot E_{ci} \qquad (6.1)$$

Where E_{ci} is the concrete elastic modulus at an age of 28 days, and $\beta_E(t)$ a coefficient depending on the maturity of concrete:

$$\beta_E(t) = \left[\beta_{cc}(t)\right]^{0.5} \qquad (6.2)$$

Where $\beta_{cc}(t)$ is described as:

$$\beta_{cc}(t) = \exp\left[s\left\{1-(\frac{28}{t/t_1})^{0.5}\right\}\right] \quad (6.3)$$

Where t is the maturity of the concrete (days), t_1 is 1 day, and s a coefficient which depends on the type of concrete as seen in Table 6-1.

Table 6-1 s-values for different concrete types.

	High strength	Rapid Hardening	Slow Hardening
s=	0.2	0.25	0.38

More details on young modulus and maturity dependent methods in Appendix 2.

Poisson Ratio

The formulation used in (Hattel & Thorborg 2003) for maturity dependent Poisson modulus was used.

$$\nu(t_E) = \nu_0 + (\nu_\infty - \nu_0)\exp\left[-\left(\frac{\tau_\nu}{t_E}\right)^{\alpha_\nu}\right] \quad (6.4)$$

Where $\nu(t_E)$ is maturity dependent Poisson ratio, ν_0 initial Poisson ratio, ν_∞ final Poisson ratio and both τ_ν and α_ν fitting parameters. For further information on this consult Appendix 2.

Adiabatic heat development

A special study was done regarding adiabatic heat development as can be seen in chapter 5.2. Different adiabatic curves and its influence is discussed in chapter 9.1.2.

Activation Energy

The activation Energy was studied as well, as a defining factor in the heat development, for this the Bogue formulation (Folliard et al. 2008) was used, based on the composition of the concrete as can be seen in Appendix 1.

$$\begin{aligned} E_a &= 41320 + 8330\cdot\left[(C_3A + C_4AF)\cdot\rho_{cement}\cdot Gypsum\cdot\rho_{cement}\right] \\ &-3470\cdot Na_2O_{eq} - 19.8\cdot Blaine \\ &+2.96\cdot\rho_{Flyash}\cdot\rho_{CaO-Flyash} + 162\cdot\rho_{GGBFS} - 516\cdot\rho_{SF} \\ &-30900\cdot WRRET - 1450\cdot ACCL \end{aligned} \quad (6.5)$$

Where C_3A, C_4AF and gypsum are the mass percentage of the clinker minerals and gypsum in the cement, ρ_x is the percentage of binder component x in the mixture (cement, fly ash or GGBS), *Blaine* is the Blaine finesse of the cement, *WRRET* is the ASTM Type A&D water reducer/retarder and *ACCL* is the ASTM Type C calcium-nitrate based accelerator both in % of solids per gram of cementitious material.

Obtaining an activation energy of:

$E_a = 28724$ J/mol

6.6 Load cases

The only load case considered involves the self-weight of the mock-up which is the only relevant load. The temperature output from the thermal flow acts also as a thermal load in the structural analysis, but is converted as such automatically by Diana after every heat flow analysis introduced as thermal strains.

6.7 Shrinkage

The Eurocode function for shrinkage is based on two parameters the notional size and the element age, therefore it does not consider maturity values from previous heat flow analysis (Diana 2014).

For the autogenous shrinkage a maturity dependant function was implemented. This was based on the tests done in (Chu et al. 2012) for a concrete C35 at 40˚C curing temperature. These can be seen in Figure 6.10.

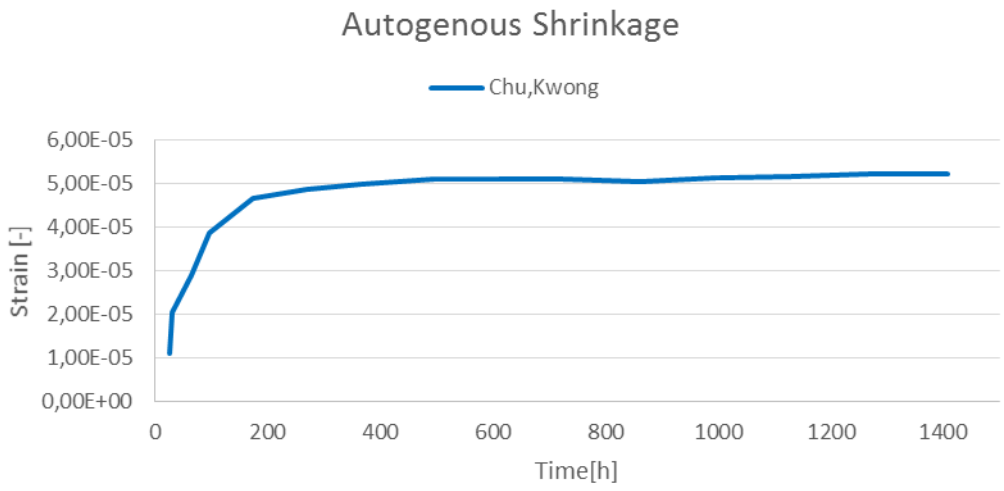

Figure 6.10 Shrinkage user-supplied function.

An alternative function obtained from Hymostruc, was studied in order to analyze shrinkage influence, this can be seen in Section 9.2.1.

6.8 Creep

6.8.1 Eurocode Model

Creep is applied according to (CEN 2004). DIANA establishes a number of kelvin chains in order to simulate creep behaviour. The maximum number of units that is generated is 10, as can be seen in Figure 6.11, but the program automatically reduces this number if it's needed to achieve a unique fit. In order to calculate the creep, Eurocode uses the parameter notional size and element age. These parameters are included in the calculations and therefore DIANA does not use any calculated or given maturity from a potential flow analysis.

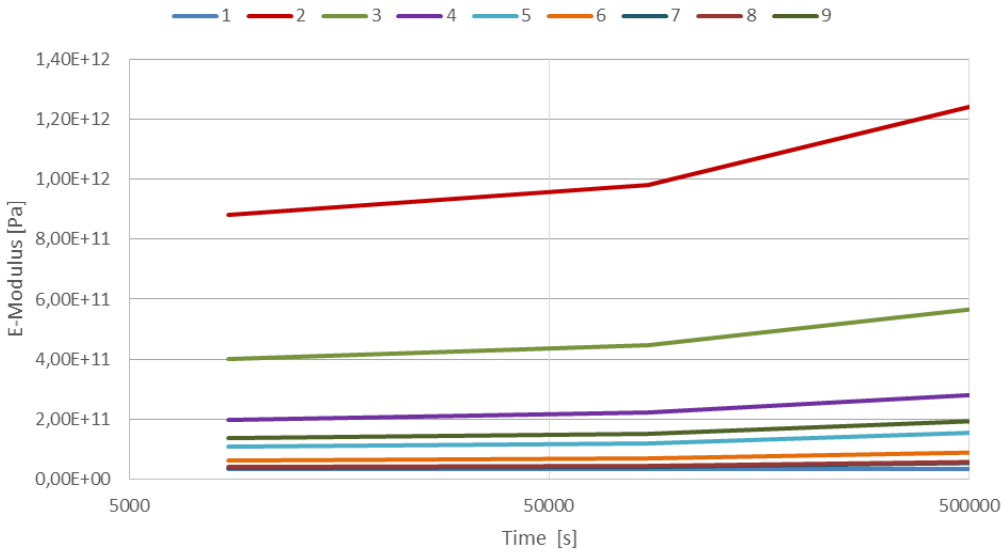

Figure 6.11 Kelvin chains as calculated by DIANA.

The function CREEPN is used by DIANA to calculate the creep strains in the structure, this function depends on the notional size and the age of the concrete when the element first appears, disregarding any previous maturity calculations (TNO DIANA 2008).

6.8.2 User supplied model

Creep was defined in two different ways, as established by Diana, transient creep was defined through uniaxial creep following equation 3.28.

On the other hand, long term creep was defined through viscoelasticity with the usage of a power law.

$$J(t,\tau) = \frac{1}{E(\tau)}\left(1+\varphi\cdot\tau^{-d}\cdot(t-\tau)^{p}\right) \qquad (6.6)$$

Where p is the power of the creep function that depends on the loading time τ , φ is the creep coefficient and *d* is the power of the part of the creep function that depends on the loading time.

6.9 Analysis

In order to make an analysis based on the degree of hydration, a staggered heat flow – stress analysis was made. First the structural elements are internally transformed into flow elements, then the heat flow problem is solved for each phase, the temperature output is applied as input for the structural analysis, acting as thermal strains.

Finally, the structural non-linear analysis is solved giving as main result the stresses and strains in the structure. The nonlinear analysis is needed as the material properties from the flow model depend on the temperature.

The output requested contains thermal strains, shrinkage strains, creep strains, total stress, maturity and temperature.

In addition to this, it was integrated into a phased analysis that allows for a simulation of the concrete pouring, and therefore a more accurate study of the hydration of the structure.

The phases were established according to the data from the temperature gauges placed in the mock-up and were based on the time when a sudden increase of temperature occur. This sudden increase mark the time when the concrete height reached the level of the gauge. Figure 6.13 shows an example, where the time when there is a jump in the temperature is marked in green. The height and position of the gauges is known therefore it's possible to estimate how the concrete is poured. The results can be seen in Figure 6.12.

29	2015-12-16 05:38	-1,4	-1,2	-0,7	----
30	2015-12-16 06:08	-1,5	-1,3	-0,6	----
31	2015-12-16 06:38	-1,5	-1,2	10,8	----
32	2015-12-16 07:08	-1,4	-0,8	9,8	----
33	2015-12-16 07:38	-0,4	0,7	9,1	----
34	2015-12-16 08:08	-0,4	1	9	----
35	2015-12-16 08:38	-0,3	1,4	8,9	----
36	2015-12-16 09:08	-0,3	1,3	9	----
37	2015-12-16 09:38	0	6,1	9,2	----
38	2015-12-16 10:08	0	11,5	9,3	----
39	2015-12-16 10:38	0,5	13	9,4	----
40	2015-12-16 11:08	1,1	13,4	9,5	----
41	2015-12-16 11:38	1,3	13,8	9,6	----
42	2015-12-16 12:08	1,2	14	9,7	----
43	2015-12-16 12:38	1,1	14,2	9,7	----
44	2015-12-16 13:08	1,3	14,5	9,8	----
45	2015-12-16 13:38	1,3	14,7	9,9	----
46	2015-12-16 14:08	1,5	14,9	10,2	----
47	2015-12-16 14:38	11,4	15,2	10,3	----
48	2015-12-16 15:08	9,6	15,5	10,6	----
49	2015-12-16 15:38	9,1	15,9	10,8	----

Figure 6.13 The sudden temperature increase is marked with green and allows for an estimation of the pouring process

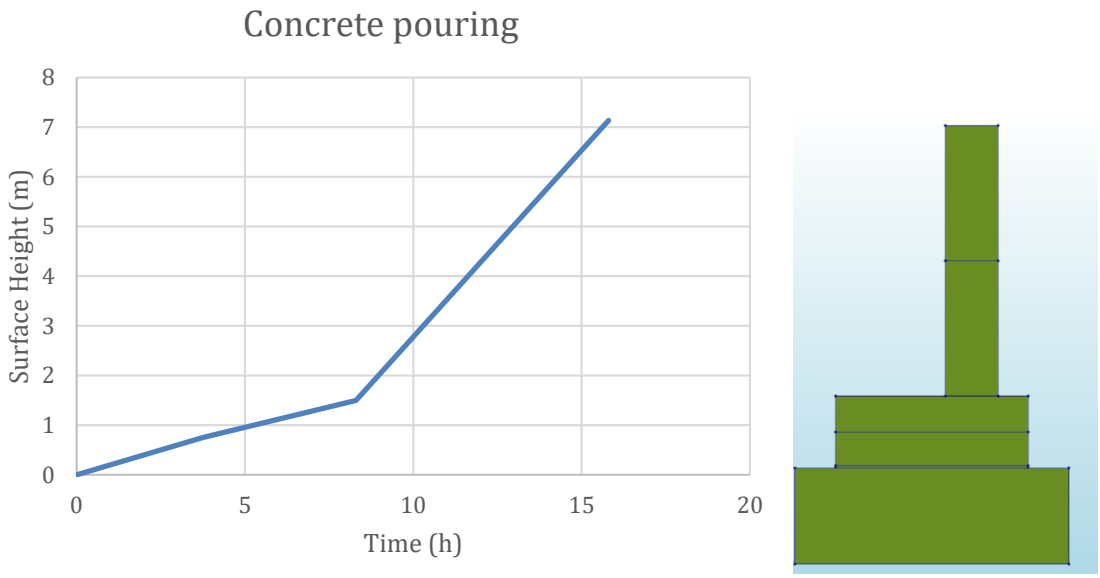

Figure 6.12 Picture showing the pouring process.

The final data used for the model is shown in Table 6-2. Starting time, t_0, and end time, t_1, is only used to estimate the length of each phase. How long each phase actually runs is then decided by the step size and number of steps. Therefore the total run time is 2299 hours, while the end time is 2319. 20 hours disappears due that the step size has to be an integer.

Table 6-2 Phased analysis as implemented in DIANA model.

Times and steps for phases								
Phase	**Starting time T_0 [h]**	**End time T_1 [h]**	**[h]**	**[s]**	**Step size [h]**	**Step size [s]**	**Number of Steps**	**Surface height [m]**
1	0	3,5	3,5	12600	0,1	360	35	0,05
2	3,5	8	4,5	16200	0,1	360	45	0,75
3	8	11,8	3,8	13680	0,1	360	38	1,5
4	11,8	15,55	3,75	13500	0,15	540	25	4,3175
5	15,55	120	104,45	376020	1	3600	104	7,135
6	120	404,55	284,55	1024380	24	86400	11	7,135
7	404,55	2032	1627,45	5858820	1627,45	5858820	1	7,135
8	2032	2080	48	172800	0,5	1800	96	9,185
9	2080	2319	239	860400	2	7200	120	9,185
				Total time	2299			

7 Model Verification and Limitations

Developing a model that accurately resembles reality involves a wide range of challenges. This is due to the simplifications that are needed in different steps of the process that can be taken for lack of relevance in the final result or for software limitations. The most important will be mentioned in this chapter as a basis for future development of the model or discussion of the results.

7.1 Relative Humidity

The main simplification that is made is the consideration of the relative humidity, this is a parameter that directly influences several of the main parameters involved in the process such as the coefficient of thermal expansion (Yeon et al. 2009), shrinkage and creep (Atrushi 2003) among others. Software like code-aster allows for a coupled thermal-relative humidity analysis, but this should be done also with the addition of the stress analysis itself, which makes for a complex system. An alternative to this would be the usage of input coming for values obtained in experimentation, with controlled relative humidity conditions.

7.2 Heat Development

When it comes to the heat development some simplifications where made, the main mechanism considered is convection which is modelled through the formwork and the thermal properties of the concrete.

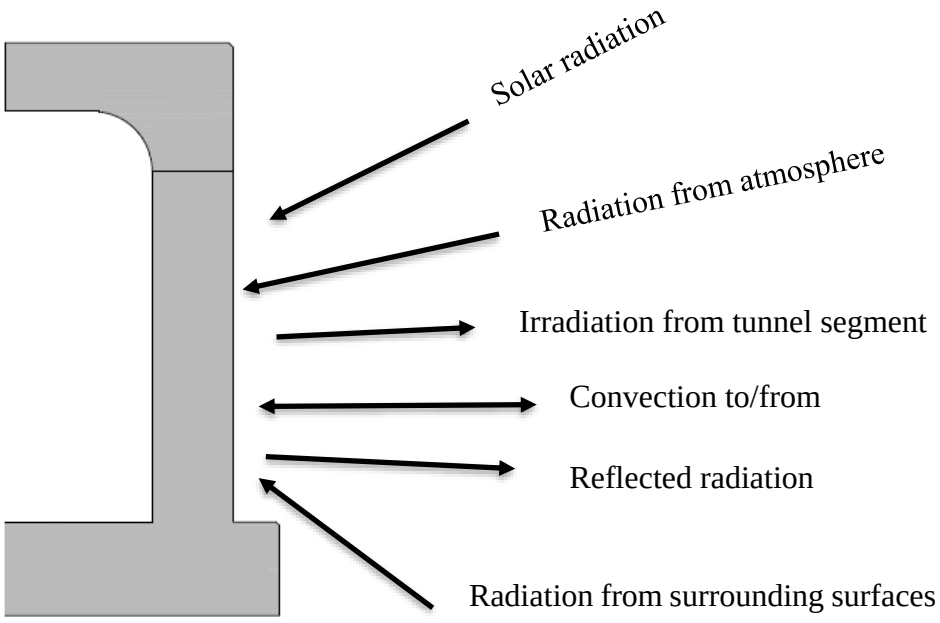

Figure 7.1 Heat Mechanisms adopted from (Riding 2007).

For a more accurate analysis models like the one presented in (Riding 2007) which considers radiation (solar, atmospheric and surface emitted) and shading as well, would consider more in depth elements involved in the temperature development of the concrete element.

7.2.1 Formwork

The modelling of the formwork was already mentioned briefly in Section 6.3.1. In initial stages the formwork was modelled as well, this has the advantage of modelling with higher accuracy the boundary surfaces with the cost of an increase on the amount of elements and the usage of elements more prone to be ill shaped. Since the relevant element for this study is the concrete mock-up the formwork was in the end modelled by modifying the conductivity properties of the exterior boundaries, but for a more accurate analysis its modelling should be considered.

7.2.2 Soil initial conditions

For every thermal analysis an initial temperature needs to be stated for all the elements. This has a major relevance for the concrete and its hydration as stated discussed in (Ji 2008). The Diana software requires an initial temperature field and only allows one, which forces the initial temperatures of both the soil and first phase concrete to be the same. This implies a higher temperature (20° C) on the soil than what it is assumed and stablished in the boundary conditions (5° C), making it longer to converge into the actual temperature of the soil and simultaneously diminishing the amount of heat lost by the soil/mock-up interface.

7.3 Soil-Mock-up interaction

From the structural point of view, the connection between the soil and the mock-up is defined in the model as perfectly connected. No friction is considered which might have an influence on the real restraint to which the structure is subjected to.

For instance while modelling in Contest it can be noticed an increase of stresses if there is a restraint factor of 0.2, so this might have a direct influence in the final stresses measured and should be taken into account.

7.4 Phased analysis

As a way of modelling the concrete pouring the model was divided in 5 phases. This was considered relevant as there is more than 12 hour's difference between the beginning of the concrete pouring and the time when concrete reaches the mid-point of the wall. This comes with a clear limitation which is the accuracy of this way of modelling.

7.4.1 Concrete pouring

The optimal way of including this would be a finer mesh which progressively includes new elements, resembling therefore the pouring process.

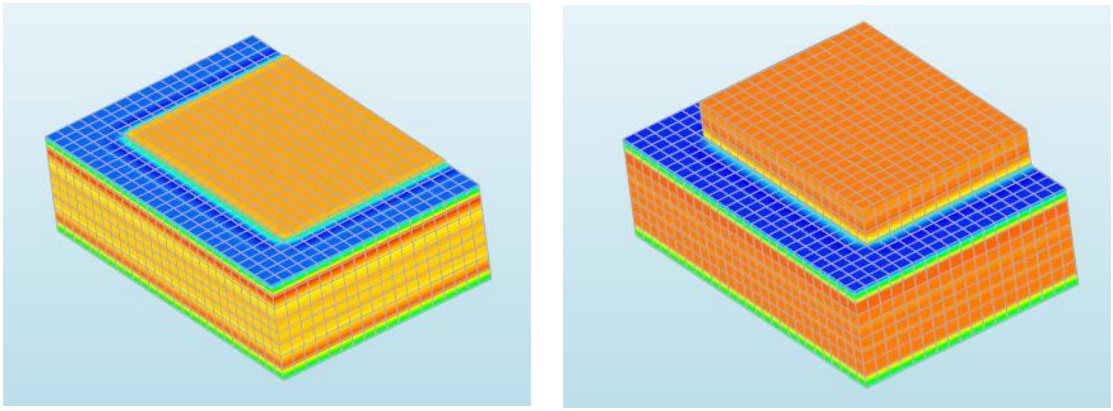

Figure 7.2 Step one in phases 1 and 2

A limitation coming from the phasing of the structure is related to the boundaries and how finite elements work. Along a phase a number of elements are active, and they represent the existing structure. However, the phasing is done in a finite number of steps, which means that the intermediate states of the structure are not represented accurately. This becomes more relevant when thinking on the boundary conditions applied to the structure. The upper surface is in reality where the concrete is being poured, therefore its thermal state goes from being subjected to exterior temperature (when no concrete is on top) to increasingly having a thicker layer of concrete above. On the contrary, in the model geometrical variable boundaries cannot be defined, which means that the active elements remain subjected to exterior temperatures for the full length of the phase, this can be seen in Figure 7.2.

This limitation comes directly from the finite element method but its effects can be decreased with a higher number of phases or a variation in the external temperatures applied. Its effects are discussed in 9.1.4.

7.4.2 Boundary faces

An indirect effect caused by the phased analysis comes from the way the thermal problem is solved.

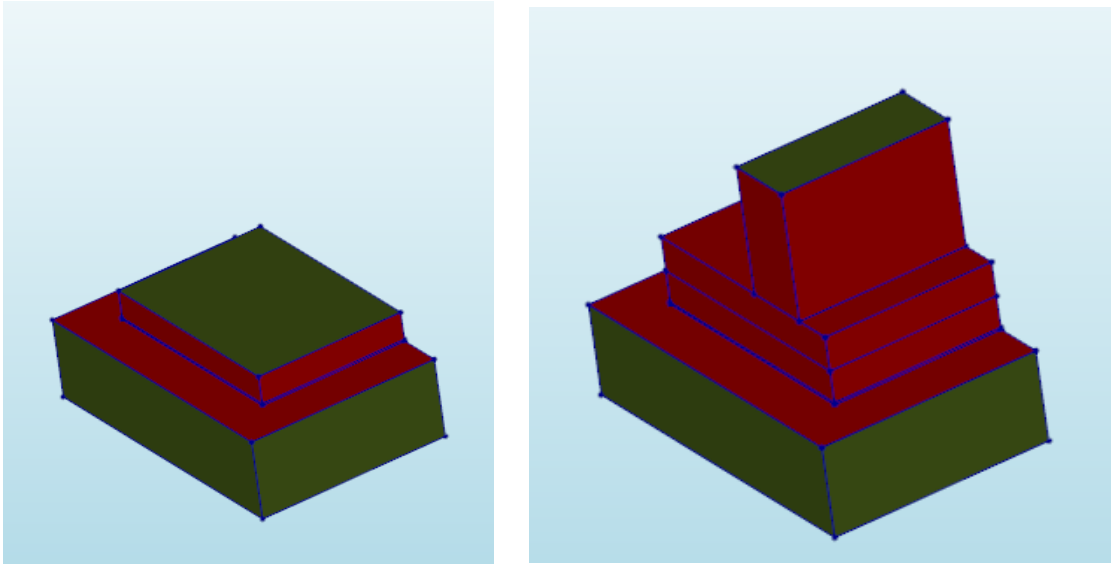

Figure 7.3Boundaries in Phase 2 and Phase 4

In each phase, the upper face of the solids active during the phase would act as a boundary as well. As it can be seen in Figure 7.3, where red faces represent the boundary interfaces, this has a minor effect when most of the structure is already active since the surface itself is rather small in comparison, but it might be quite relevant in initial stages when it represents up to 45% of the boundary of the structure.

The main problem with the modelling of this "Intermediate boundaries" comes when applying the exterior conditions to which they are submitted. Applying directly the exterior temperatures would have direct incongruences as concrete is poured on top of the intermediate boundaries. This led to the conclusion that a modified exterior temperature should be applied in order to offer more accurate results, this has being discussed and could probably be included in future and more developed analysis.

7.5 Mesh

In order to verify the mesh and ensure that the results were independent of the element sizes, a sensitivity analysis was done. The chosen node for this study was placed in the first phase to ensure that there was values available for all time steps, see Figure 7.4. It was also chosen since its position is fixed from a geometrical perspective and exist at the same coordinates for all tested meshes.

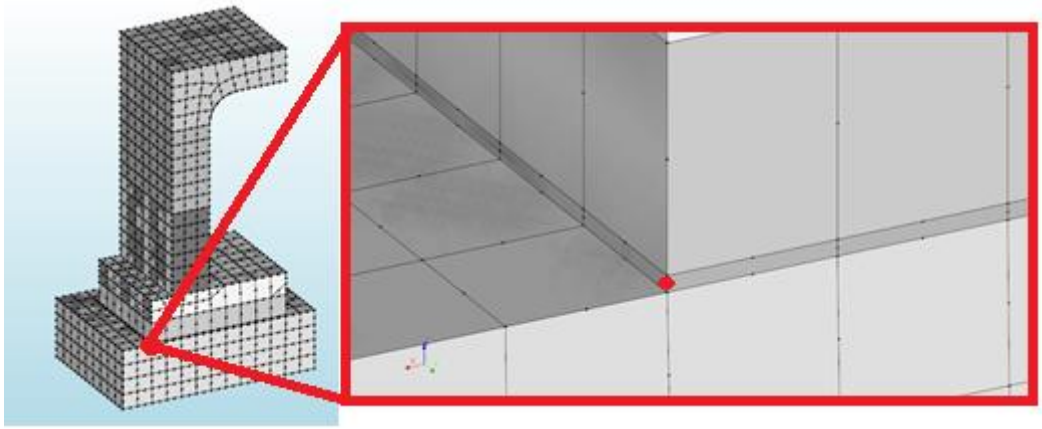

Figure 7.4 The node that was used in order to verify the mesh.

Three different meshes was compared both regarding heat development and resulting stresses. The computational time and number of elements was also analyzed and the results can be found in Table 7-1.

Table 7-1 Number of elements and calculations times for each mesh.

Mesh size [m]	0.5	0.4	0.3	0.2
Number of elements [-]	1890	3619	7157	22710
Calculation time [min]	31	62	177	3600

The element size appears to have a small influence on the final results for both the temperature development and stresses, see

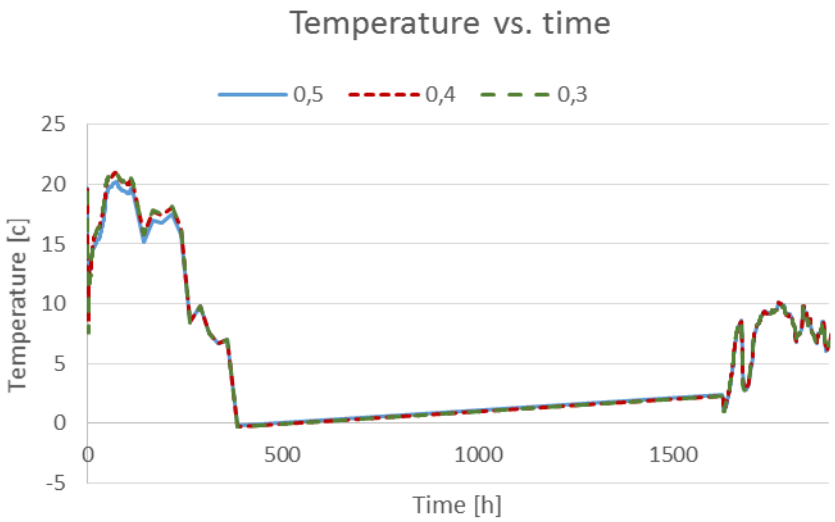

Figure 7.5. Although this difference was considered to be small enough to be disregarded and a mesh size of 0.3 m was used in the final model. This can also be motivated by studying the computation times, since one of the objectives of the thesis was to develop a working model and to include critical parameters, a short calculation time was desired to be able to do several analyses and identify potential issues.

7.6 Verification of model

In order to verify the validity of the model two main lines of actuation were took, namely the creation of an equivalent Model in a 2D tool, that also allows for a comparison between them, and a comparison with results from (Ji 2008).

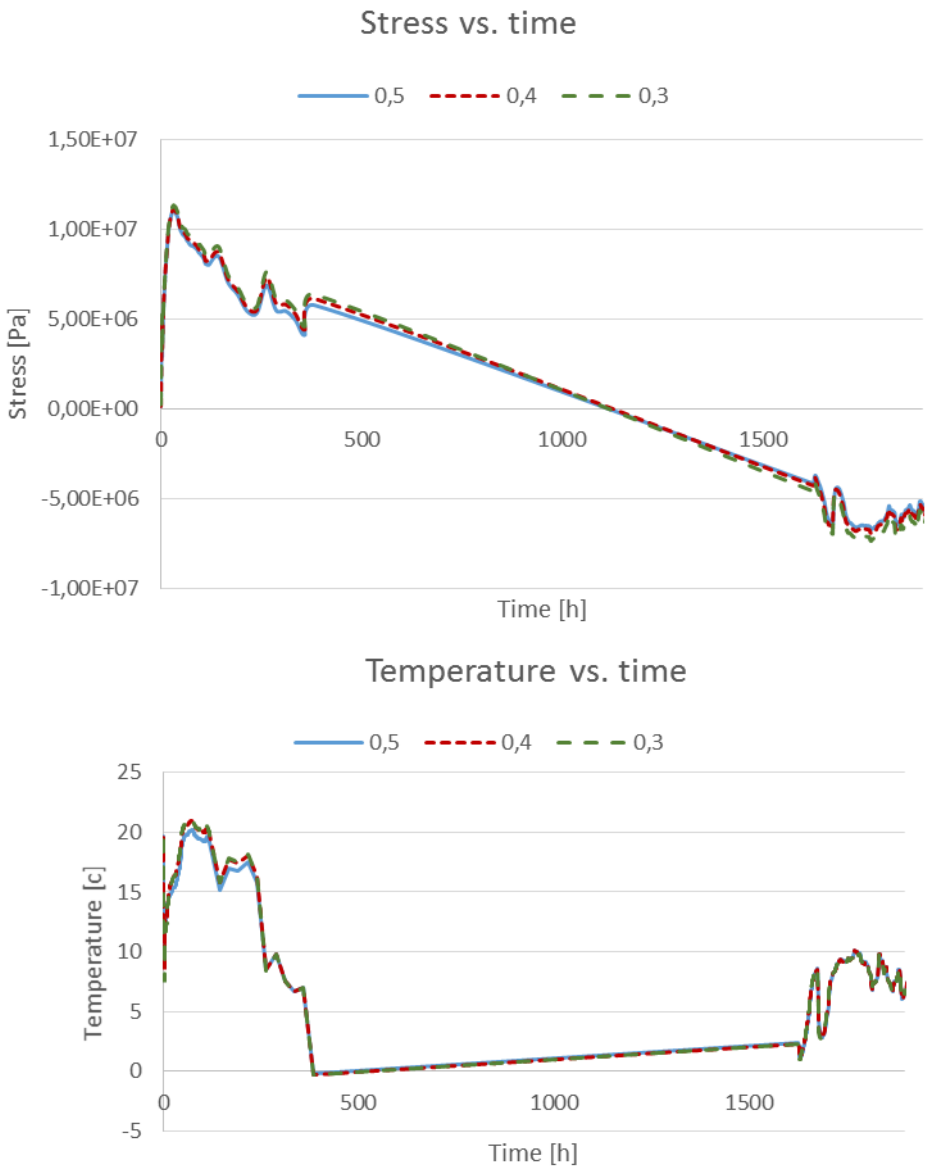

Figure 7.5 Top diagram shows the stress development and the bottom diagram shows the temperature development for the chosen node.

7.6.1 Contest Model

A Model was created with the tool CONTEST, with the addition of parameters taken from the real measurements made on the mock-up, a comparison between both models can be seen in Chapter 9.
The results from CONTEST are presented in Chapter 8 and in more detail in Appendix 5.

8 Results

The results are presented in three sections where first the thermal analysis from DIANA is presented followed by the structural analysis. The last section contains the most important results from the analysis that was done in CONTEST.

8.1 Non-linear Heat flow

From the nonlinear heat flow analysis two main results were obtained, the temperature profile and the degree of hydration in every point for all time steps. An example for the mid-point of the wall is presented in Figure 8.1, which shows the temperature from casting up to 2000h. The degree of hydration can be seen in Figure 8.2.

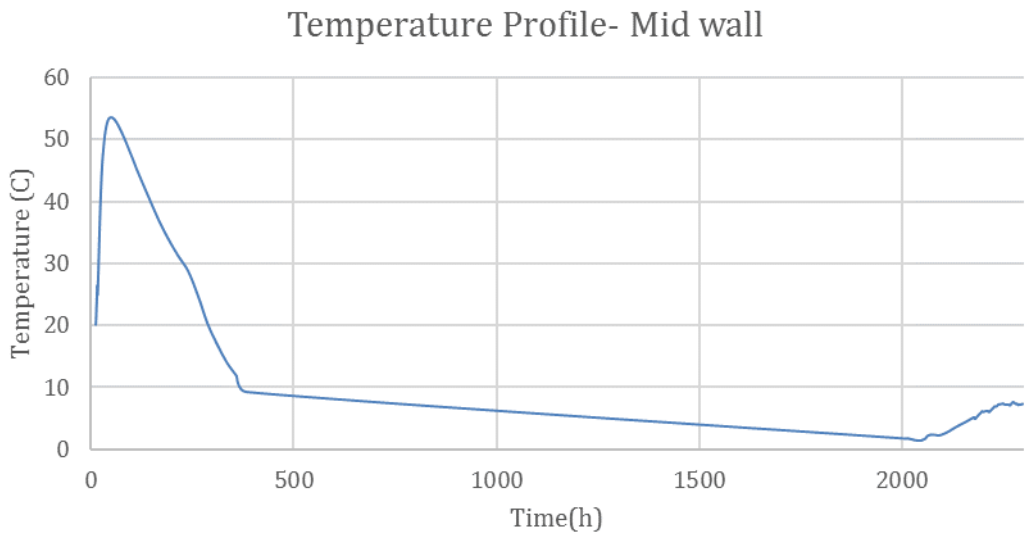

Figure 8.1 Temperature profile in the mid-point of the wall.

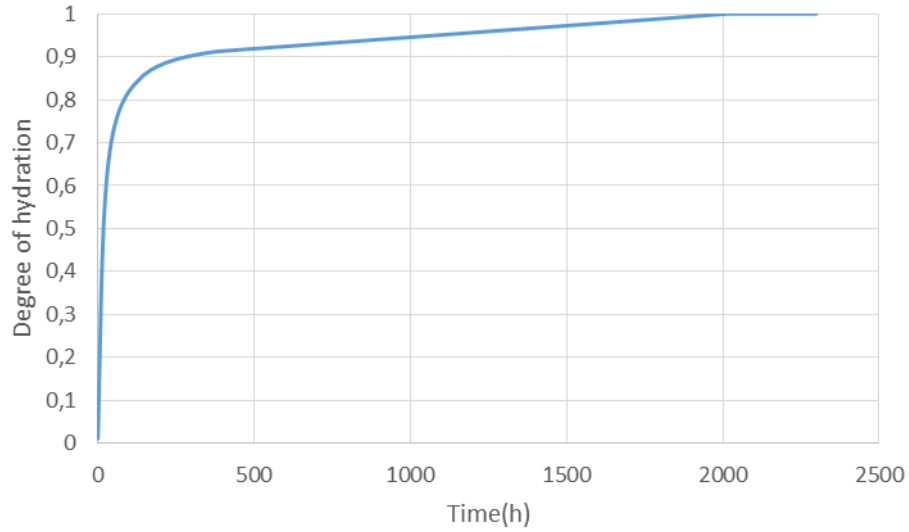

Figure 8.2 Degree of Hydration in the mid-point of the wall

The results from the thermal analysis in the second cast were also obtained, and are show for the centre point of the roof slab in Figure 8.3.

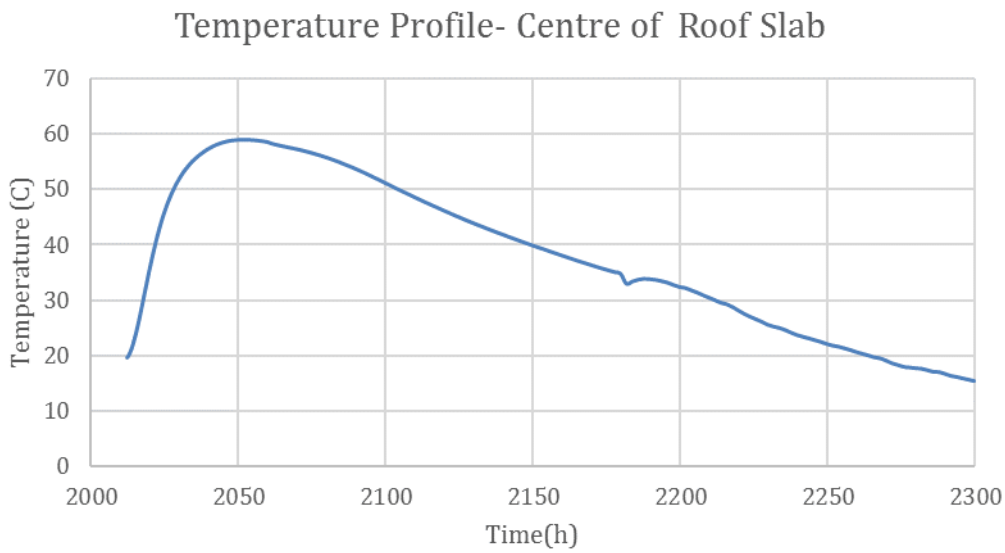

Figure 8.3 Temperature profile in the center of the roof slab

A comparison was also made between different types of concrete, where the composition was altered which changed the adiabatic curve. Apart from the curve obtained with Contest, two other cement compositions where analysed; one which contained 60 % fly ash and one that had 40% blast furnace slag based on data from (Ji 2008). The results can be seen in Figure 8.4.

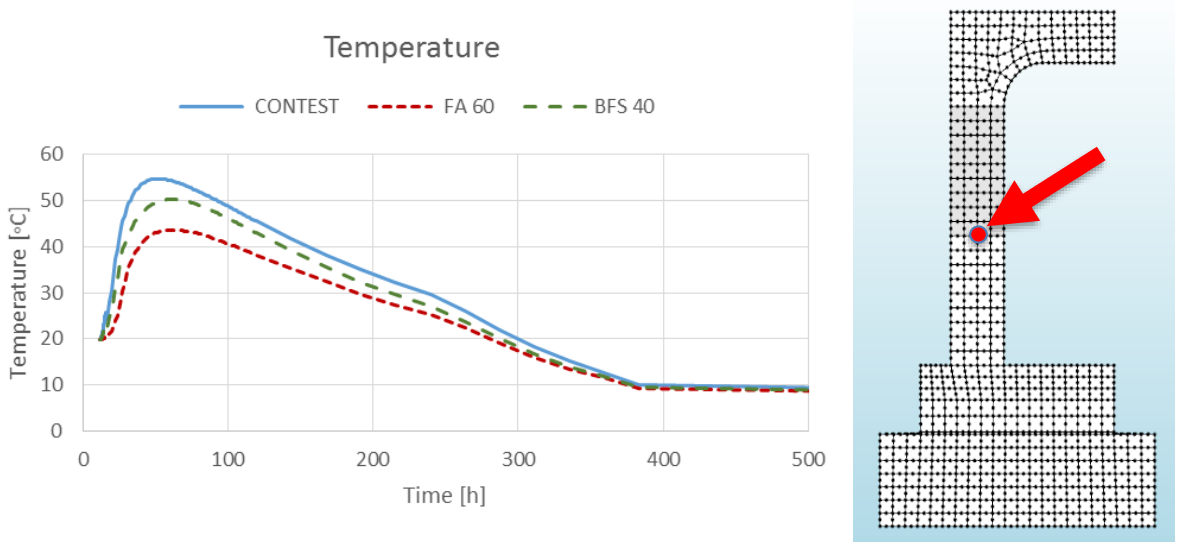

Figure 8.4 Temperature development of the segment for different adiabatic curve, the studied node is marked by the arrow.

8.2 Non-linear Structural Analysis

From the non-linear structural analysis two main parameters where obtained, stresses and strains. Two different geometrical points were chosen to show the stress and strain in critical points, one in the bottom of the first cast, and one close to the joint in the second cast, see Figure 8.5.

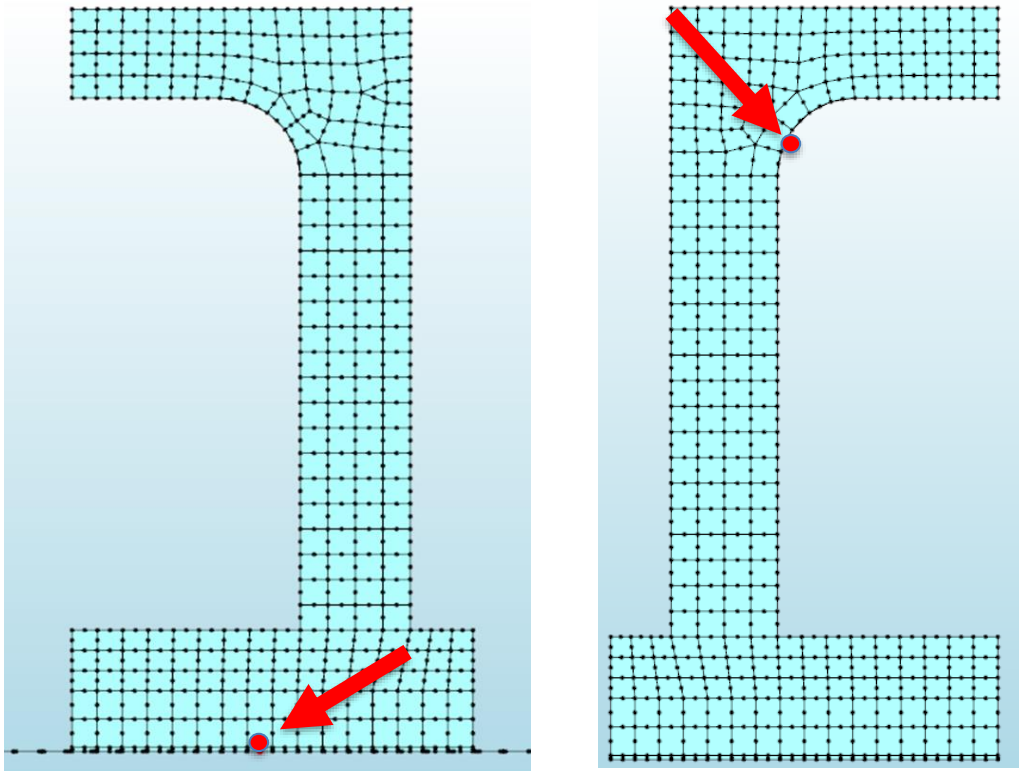

Figure 8.5 Selected nodes to show stress/strain results.

The locations of the nodes where chosen with regard to where restraint stresses occur. The one in the left is present along all the phases, and it's a critical point due to the soil restraint. The upper node shown to the right is a node situated close to the connection between the wall and the roof slab. Here the restraint is created from casting and connecting the roof slab to the old wall.

It is important to highlight that the behaviour is not a simple one and in order to fully understand the behaviour the complete structure should be studied, since singular nodes might differ from the global result. One advantage from the 3D design, is that the whole structure can be studied for all time steps. To give an idea of the structural behaviour an analysis of nodes in different phases of the structure was done and its results can be seen in Section 9.2.4.

8.2.1 First Cast

Stresses

The three principle stresses for the bottom node can be seen in Figure 8.6Figure 8.5. This node reaches a maximum tensile stress of 2.6 MPa after 263 h. Figure 8.7 is a contour plot of the stress profile at 120 h, to allow for a comparison with the maximum stress time according to CONTEST.

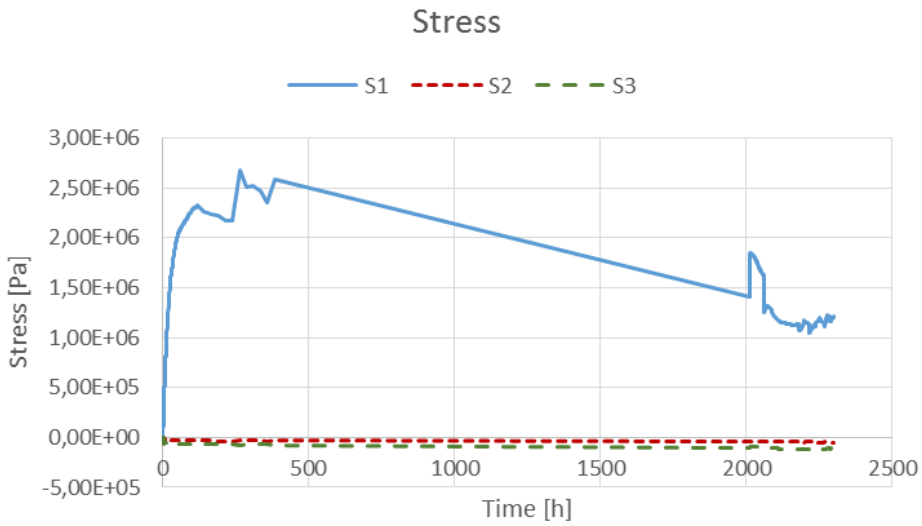

Figure 8.6 Stress development in exterior slab-node.

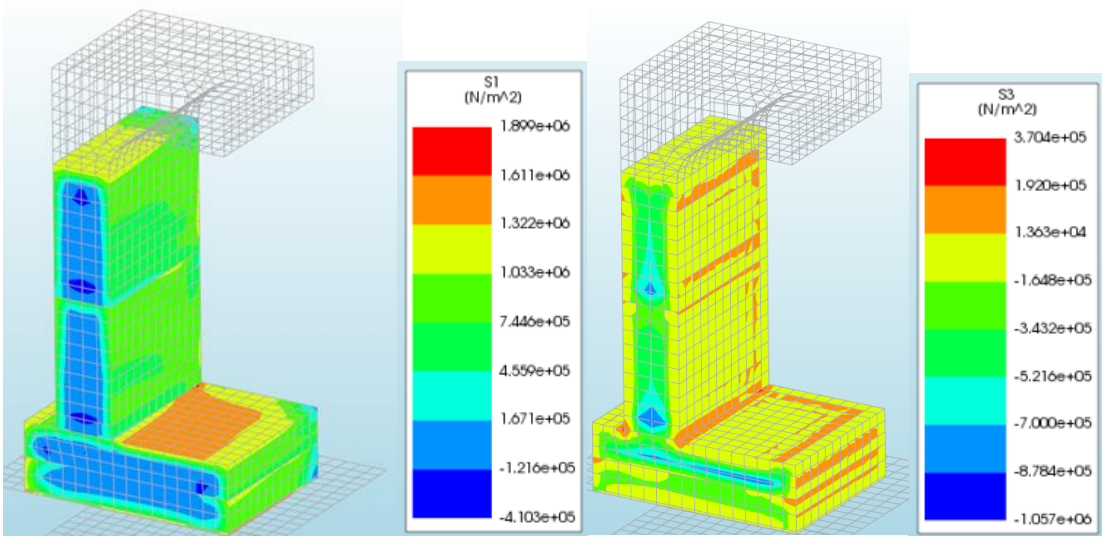

Figure 8.7 Contour stress plot at 120 hours.

Strains

Regarding strains a strain profile is shown in Figure 8.8 with the total strain and its different components. For a more detailed view on creep strains they can be seen in Figure 8.9 . Contour plots for every kind of strain are shown in Figure 8.10.

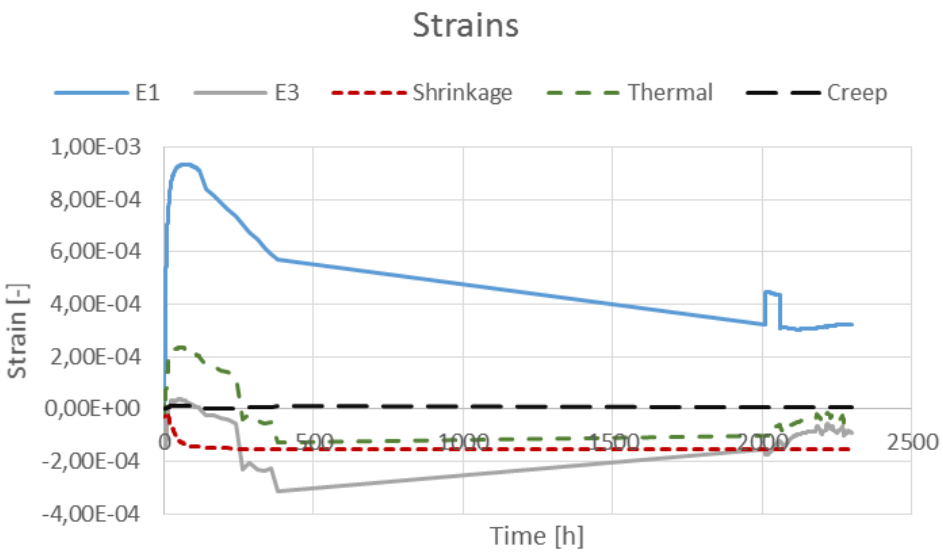

Figure 8.8 Total strain and main components

Figure 8.9 Creep strain for the bottom node.

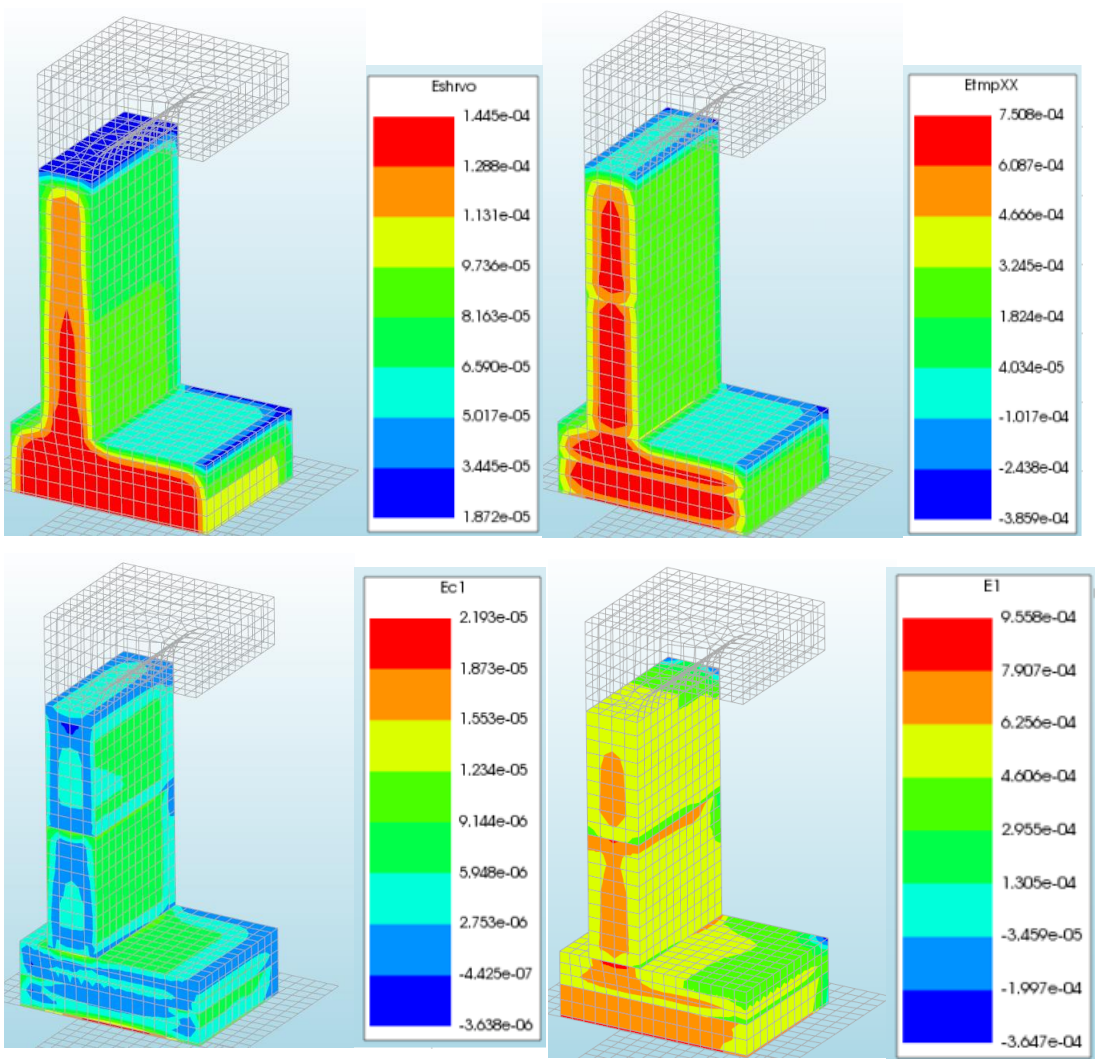

Figure 8.10 Contour plot for different strains at 120h, top left is shrinkage, top right thermal, bottom left creep and bottom right is total principle strain.

8.2.2 Second Cast

Stresses

The three principle stresses for the node in the upper part, close to the joint can be seen in Figure 8.12. For the upper part the time is calculated from the moment that the upper part appears in the model (not the total time elapsed). Maximum tensile stresses occur after 120h and their value is 1.01 MPa. A contour plot for the stresses for this time can be seen in Figure 8.11.

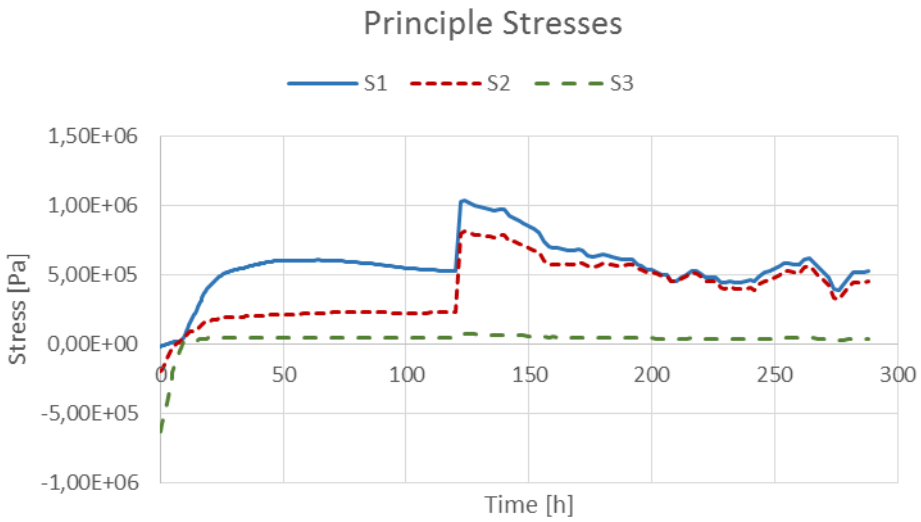

Figure 8.12 Principle stress development for the node in the upper part.

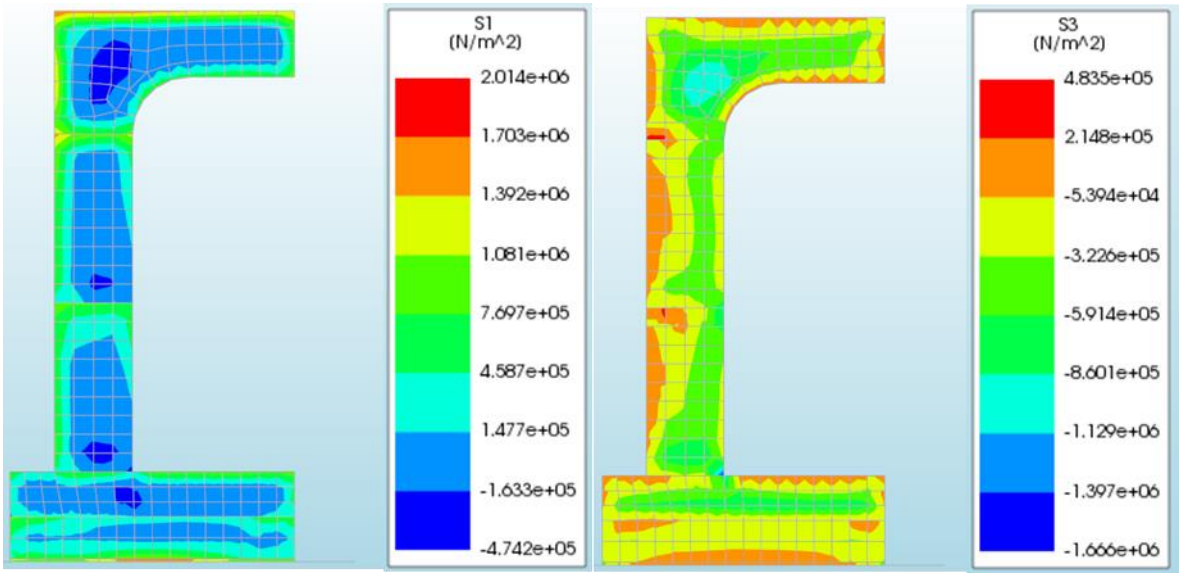

Figure 8.11 Contour plot for the principle stresses S1 and S3 at 120h after the second cast is made.

Strains

The strain profile for both the different components (E1) and total strains are shown in Figure 8.13. The creep strain is very small compared to the other components and therefore a detailed graph for this can be seen in Figure 8.14. A contour plot at 120 hours for all types of strains can be seen in Figure 8.15.

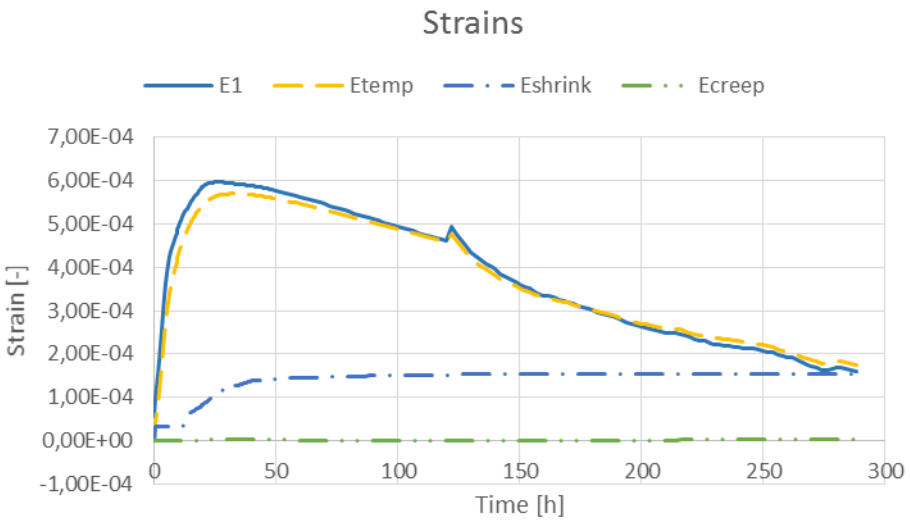

Figure 8.13 Strains both in terms of the principle strains and the contribution from each parameter.

Figure 8.14 Creep strains for the node close to the roof slab joint.

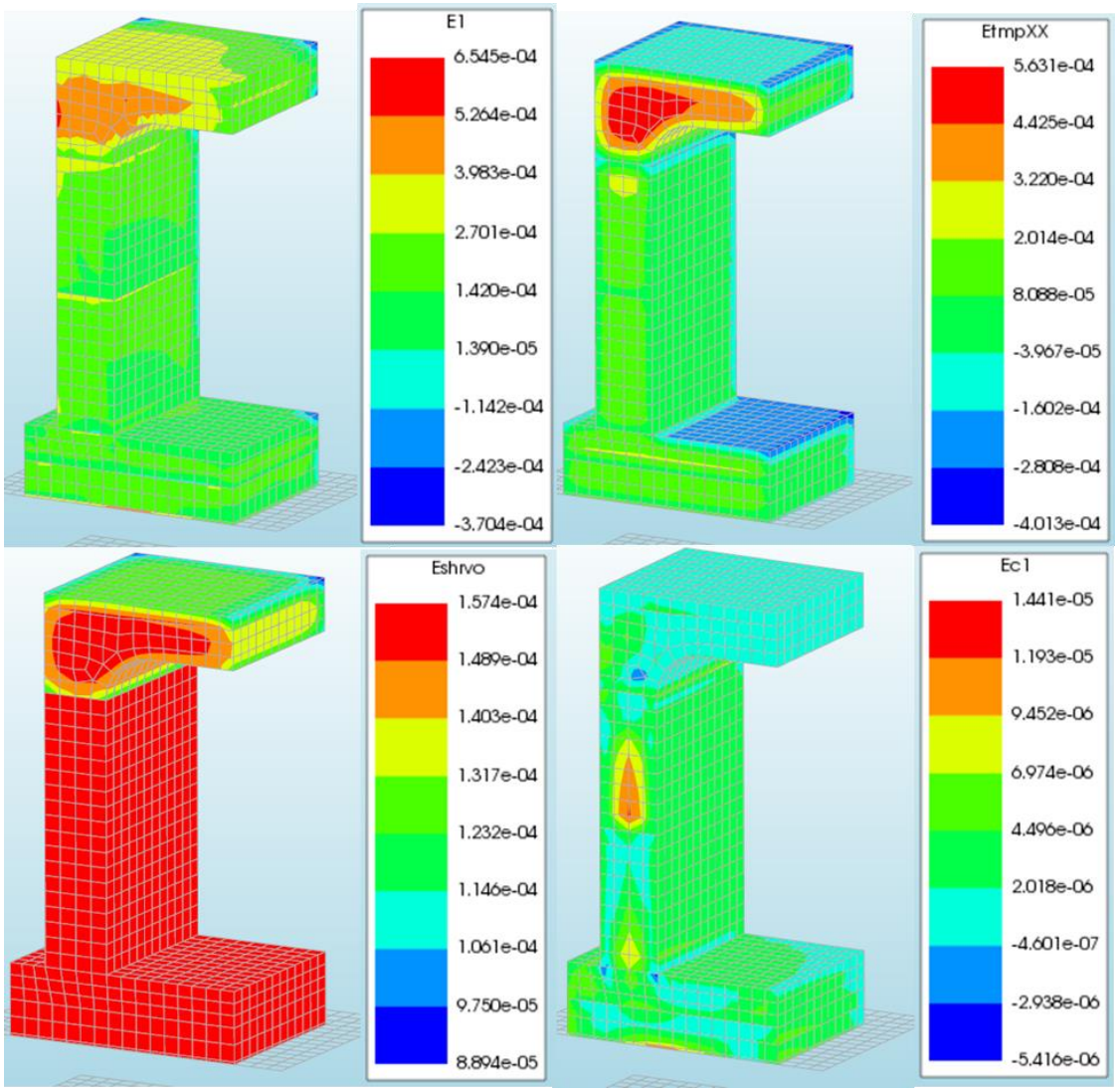

Figure 8.15 Contour plot for different strains at 120h, top left is shrinkage, top right thermal, bottom left creep and bottom right is total principle strain.

8.3 Contest

According to the 2D model made in the software Contest Pro the maximum temperature of the tunnel segment will occur after 62 hours and reach a maximum temperature of 57.5 ^{o}C, see Figure 8.16.

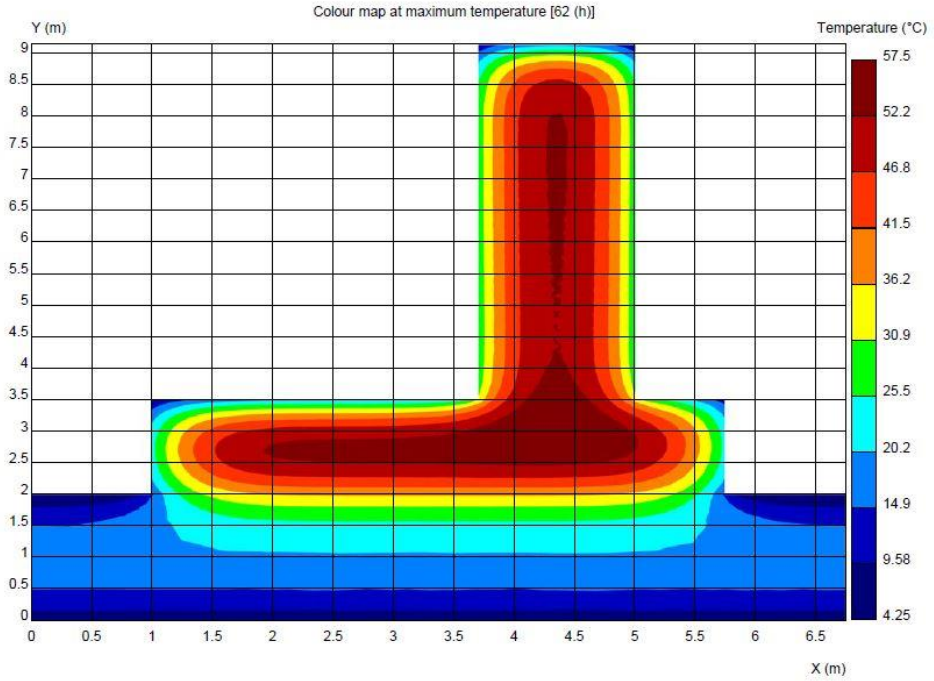

Figure 8.16 Maximum temperature according to Contest Pro.

The maximum tensile stresses appears after around 120 hours and have a value of 2.2 MPa, see Figure 8.17. It is important to realize that Figure 8.17 shows the maximum values of tensile and compressive stress in the block that represents the mock-up, not only for a specific geometrical point.

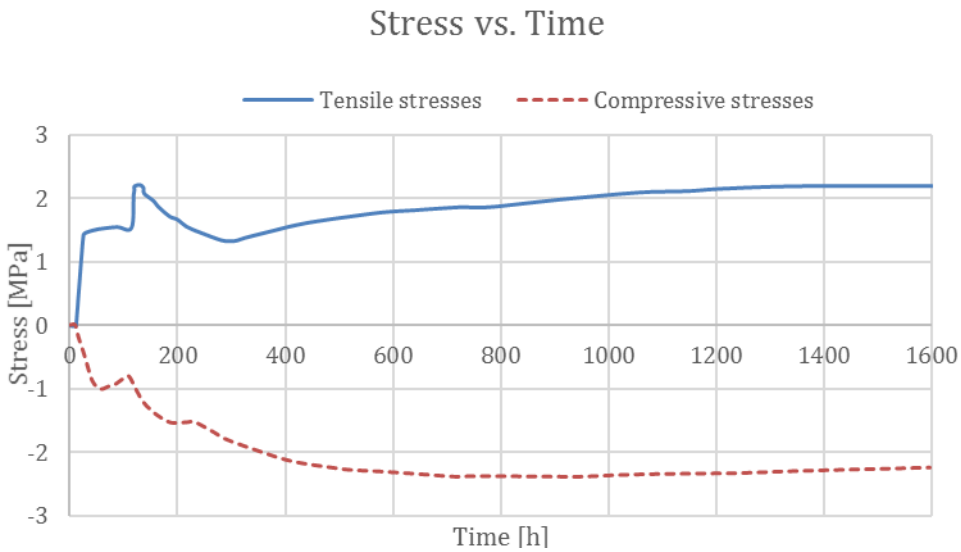

Figure 8.17 Stress development over time.

The complete report together with all input used in Contest can be found in Appendix 5.

9 Discussion

In this part a discussion and comparison will be made on the obtained thermal profiles with focus on the difference between a 3D and a 2D model, the influence of the adiabatic curve, the usage of phased analysis and the intermediate surfaces. This is followed by discussion of the stress/strain results and how the different parameters; shrinkage, creep and coefficient of thermal expansion, affect the results.

9.1 Thermal Profile

As a result of the thermal flow analysis the main result obtained is the thermal profile together with the level of maturity. This allows for different comparisons both from the modelling point of view as well as the accuracy of the different models that were used.

9.1.1 Comparison 3D Model and 2D Model

One of the goals of this master thesis was to compare the obtained results in a 3D analysis with the results from a commonly used software that only consider 2D. It is important to say that this comparison is not perfect, as 2D software has limitations but allows to see how it can resemble the results obtained in the mock up measurements, as shown in Figure 9.1.

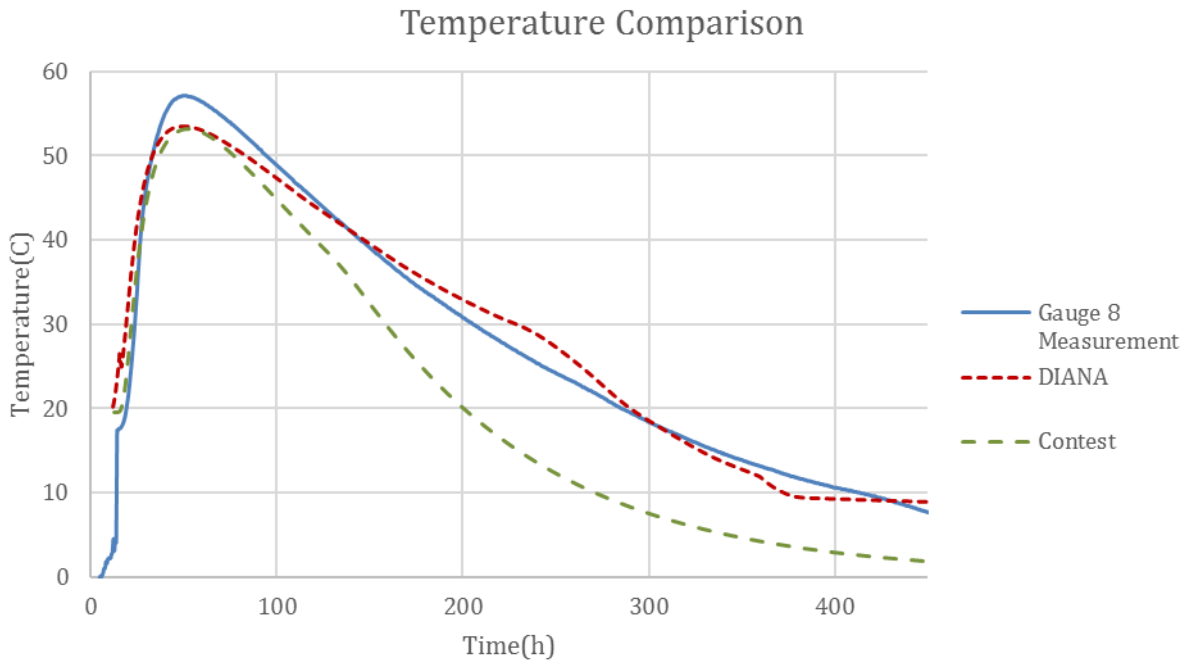

Figure 9.1 3D and 2D comparison to real measurements

It is noticeable how the peak temperature is similar in both models and around 3 degrees less than the gauge measurements. This is due to the usage of the same adiabatic heat development curve, which is not the same as the real one. Yet the implementation of the additional heat boundaries together with realistic input (such as ambient temperatures measured) makes the DIANA results more close to reality than the ones obtained from CONTEST.

On the other hand, CONTEST offers the option of a movable boundary. This is applied to the upper surface and resembles better the pouring of the concrete, which would make for a really interesting option in DIANA.

9.1.2 Adiabatic Curve Influence

A comparison was also made between different types of cement, each one with a unique adiabatic curve. As expected an adiabatic curve which had a smaller temperature development resulted in lower maximum temperatures for the whole segment. Though an interesting effect was found between the CONTEST and BFS40 curves, their adiabatic curves have the same maximum temperature, but the maximum segment temperature is about 5 ˚C lower, see Figure 9.2. This effect probably due to a slower rate of hydration, which implies a slower heat development. In semi-adiabatic conditions and due to the dimensions of the section a rate of heat development will result in lower maximum temperature. Under adiabatic conditions the maximum final temperature will be the same, as can be seen in Figure 9.2.

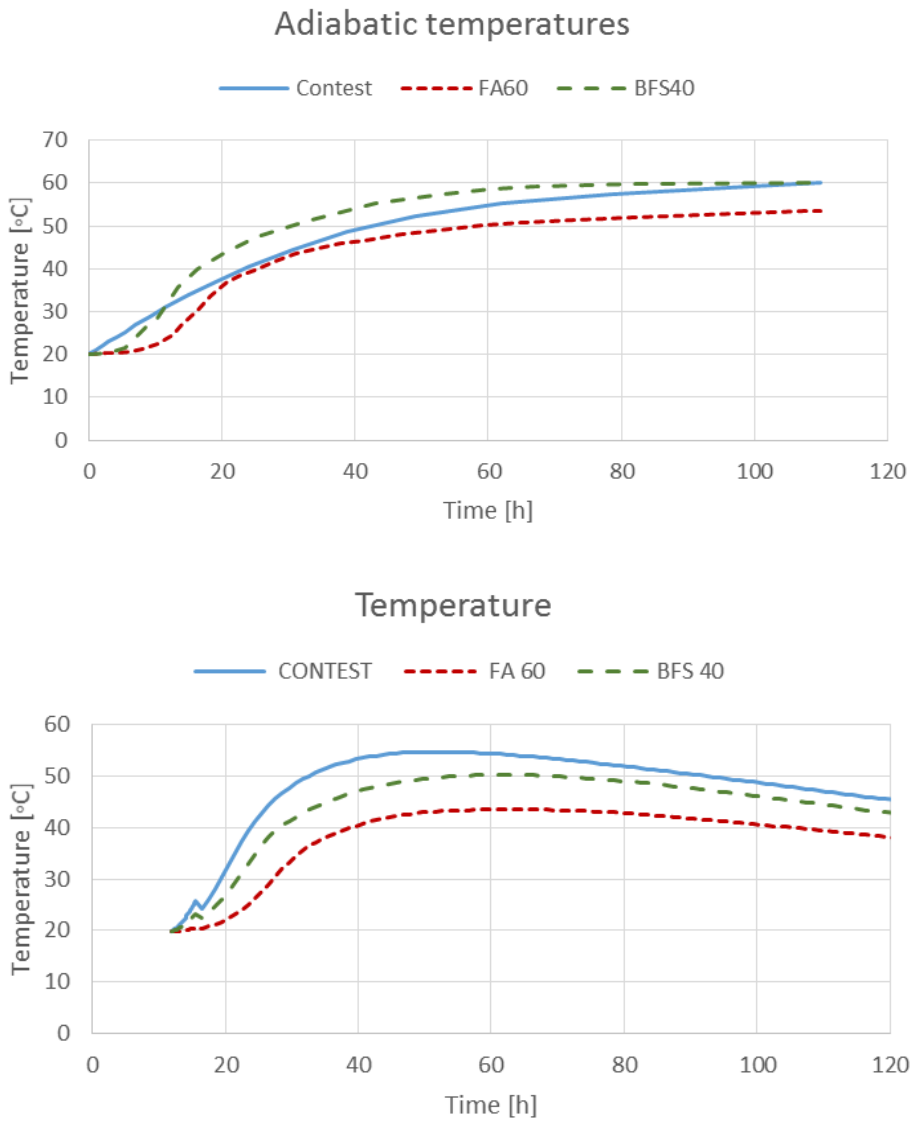

Figure 9.2 Adiabatic Heat Development and resultant temperatures

The temperature development starts at 11.8 h the moment of appearance of the elements in the phased analysis. The discontinuity in the beginning of the curves in the bottom

graph in Figure 9.2**Fel! Hittar inte referenskälla.** is due to the appearance of the elements from the next phase, which have an initial thermal field of 20 °C. The discontinuity is there for all three curves, just with different magnitudes due to a higher temperature difference between the previous phase and new phase.

9.1.3 Impact of phased analysis usage

While CONTEST allows for the definition of a variable interface that simulates the concrete pouring, this was not an option in DIANA. The impact of the usage of phased analysis versus a non-phased one was studied through the creation of a model without phases.

The results from the non-linear thermal analysis can be seen in Figure 9.3, through the temperature profile attained in the structure at a given time.

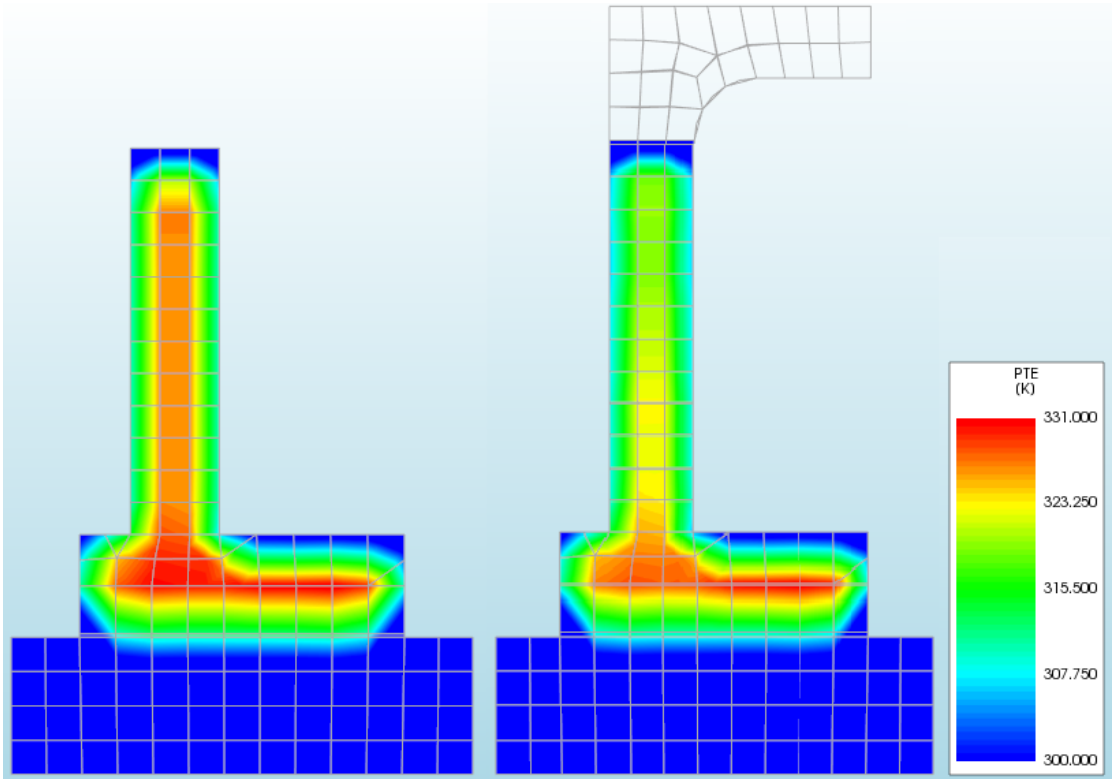

Figure 9.3 Temperature profile at 32h, left Non-Phased analysis, right Phased Analysis.

The temperature profile along the first 120 h can be seen in Figure 9.4 for a point in the center of the wall. While in the phased analysis elements appear progressively, in the non-phased one all appear at the same time t=0.

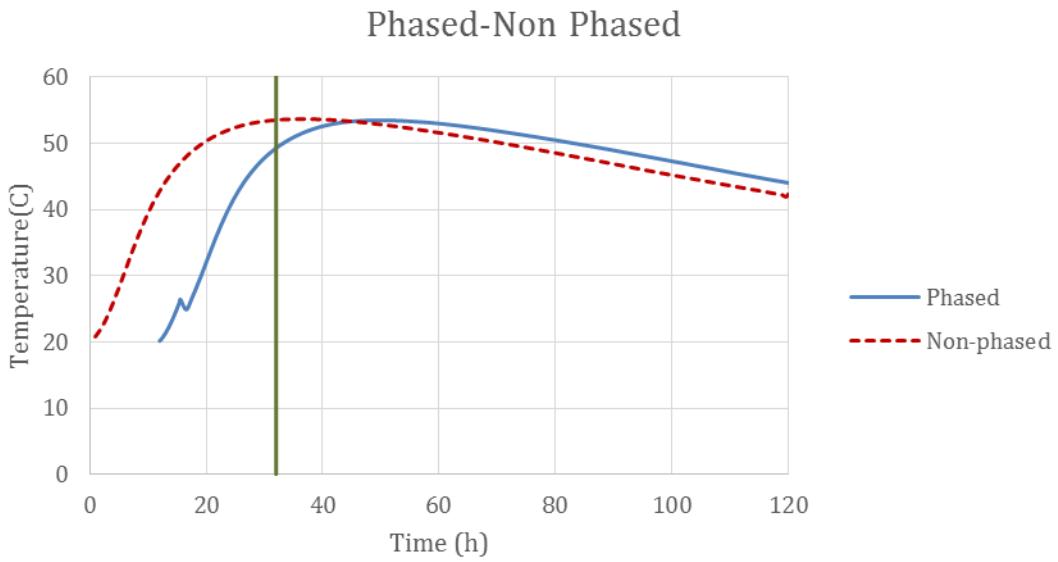

Figure 9.4 Temperature profile in a node for Non-phased and Phased analysis.

The temperature development is more realistic when considering the phased analysis, where temperatures develop progressively as in reality. In the non-phased analysis the maximum temperature occurs at 32 h, while in the phased one and in the measurements form the mock up this happens around 50h, as can be seen in Figure 9.4.

Something noticeable is that this difference is bigger higher up in the structure as the elements were added later in the phased analysis, with a final difference of almost 12h. As such, the very bottom elements behave in the same way since they are in a similar point of hydration while, a real difference is seen higher up in the structure.

9.1.4 Impact of intermediate Interfaces

A direct consequence of the implementation of a phased analysis is the need of modelling the boundaries in the intermediate states of the structure along the pouring process.

To address this issue and taking into account the limitations of the software, two different models were created. The first one with no intermediate interfaces, representing an adiabatic heat development in the surfaces of concrete in contact with the air. The second one, applying external conditions along each phase. While none of them is totally accurate, they represent the upper and lower limits of heat loss/gain that the structure will experience, as can be seen in Figure 9.5.

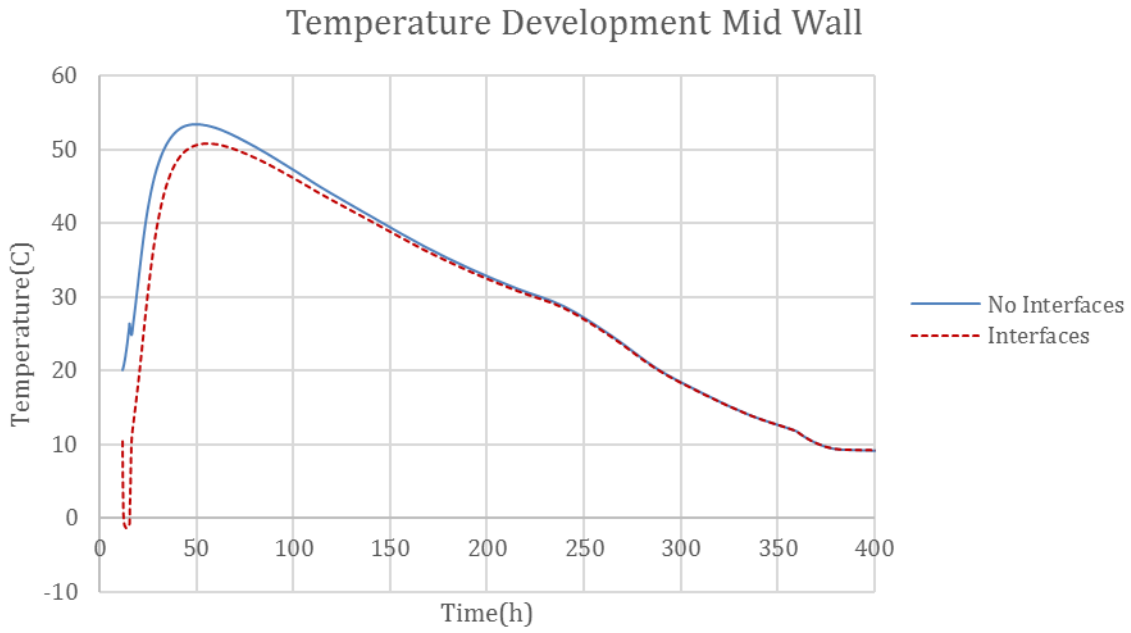

Figure 9.5 Interface Influence

The deviation that can be noticed in the beginning of the interfaces result is due to modelling issues. The studied node is a boundary element along the phase 4, which generates a different behaviour. As expected the model with no interfaces reaches a higher temperature and acts as a top boundary for the real results (in this case there would be no heat loss through horizontal intermediate interfaces). In the same way the model with interfaces shows the opposite situation where the heat loss is higher than the real one as it doesn't consider the concrete poured in the duration of the phase.

9.2 Stress/Strain

In the following section a discussion is made on the results obtained in the structural analysis and how the different mechanisms; shrinkage, creep and thermal dilation coefficient influence the final results.

9.2.1 Shrinkage Influence

As a way of studying the influence of shrinkage the material model was modified with different maturity dependant shrinkage properties, the ones tested are shown in Figure 9.6 and the stress results for the bottom node in Figure 9.7.

A first conclusion is that the function from HYMOSTRUC is probably not only autogenous shrinkage but also considers drying shrinkage hence the higher values. On the other hand, the values from (Chu et al. 2012) are more accurate and therefore more reliable. As expected shrinkage together with thermal strains are the main mechanisms influencing the stress in the element, especially in early ages. The concrete dilation increases as temperature increases due to the hydration process, while autogenous

shrinkage partially counteracts this effect when the elements are subjected to tensile stresses, in elements with little to no restrain.

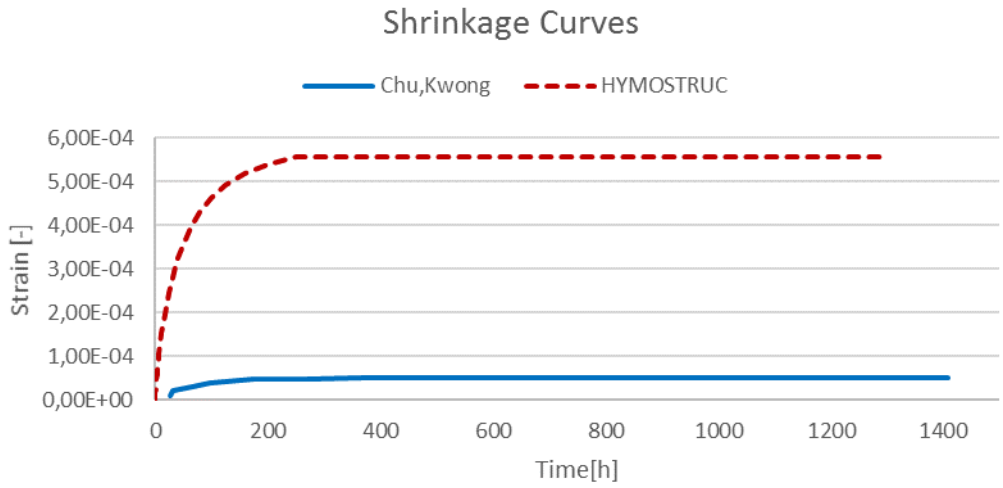

Figure 9.6 Shrinkage Curves from Hymostruc and (Chu et al. 2012).

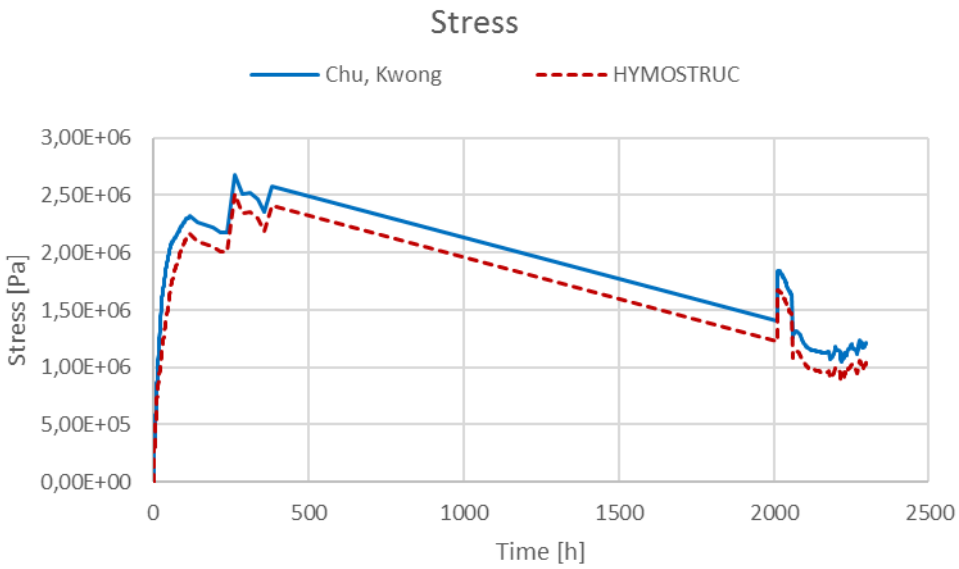

Figure 9.7 Stress development in a node for different shrinkage curves.

9.2.2 Creep Influence

To analyse the influence of creep the model was run with the upper and lower boundary values of the creep coefficient, this is 2.35 and 1.6 respectively. The strain values obtained can be seen in Figure 9.6 (for the creep strains) and Figure 9.7 (for the total strains). The influence of creep has proven small in comparison to thermal and shrinkage strains to the extent were it appears that could be disregarded. The simplified functions used in the material model are not able to show its relevance in early ages, as well as its different behaviour in tension and compression.

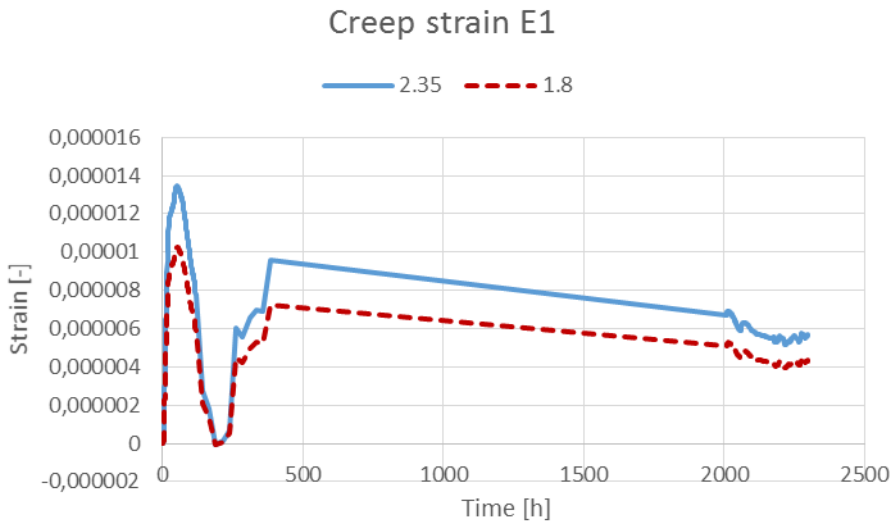

Figure 9.6 Creep Strain

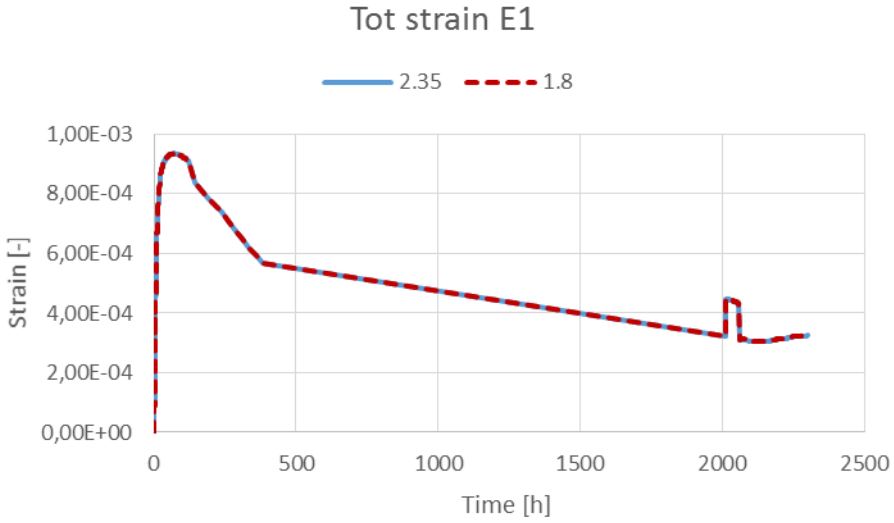

Figure 9.7Total Strain

9.2.3 CTE Influence

In order to study the influence that a variation of the CTE values would have on results, an analysis based on the Eurocode material model were made. It was not done for the user supplied material since for this one CTE is maturity dependent. The results from this analysis can be seen in Figure 9.8. As expected thermal dilation is one of the driving mechanisms in stress development for this type of structure. Therefore, is relevant to study how a variation on the coefficient of thermal expansion influences the stresses. The results for 1.2×10^{-5}, 1.1×10^{-5} and 1.0×10^{-5} (1/K) show that an increase of 0.2×10^{-5} in the CTE can generate up to 1 MPa in additional tensile stresses. This effect has to be taken into consideration, given that it is around 25% of the capacity for a C35/45 concrete.

The stress results belong to the model using Eurocode material model, which had low values for shrinkage generating the high stresses that can be seen in Figure 9.8. In this case the CTE is not maturity dependent and this is the reason why the analysis was done

with the Eurocode material model provided by DIANA and not with the user supplied material model.

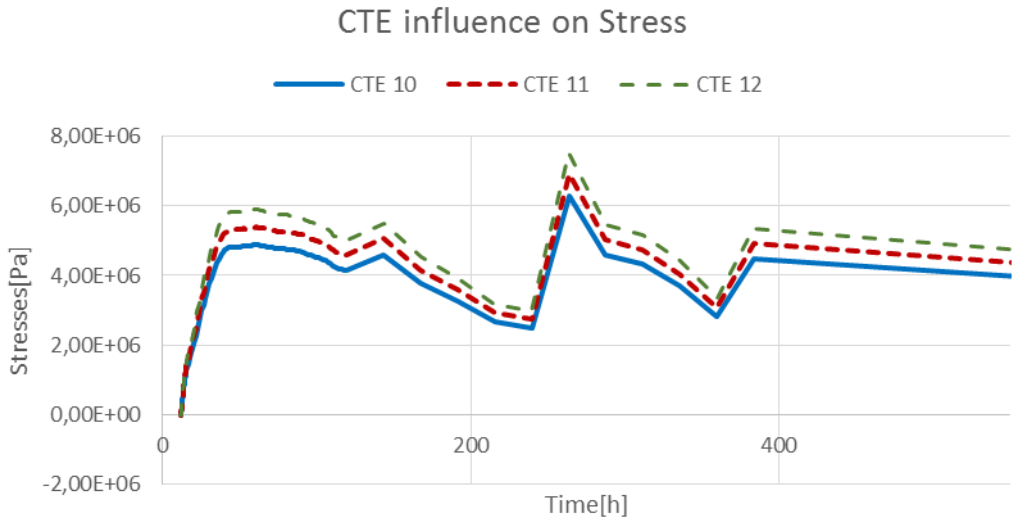

Figure 9.8 Influence of CTE variation in stresses.

9.2.4 Structural Behaviour

As a simplified way of showing the structures behaviour three positions in the structure were studied, looking in detail at the behaviour of a node and two surrounding it. This was done for 3 different phases.

Subjected to exterior temperature influence, the exterior nodes show in general a tensile behaviour, mostly because of the high temperature gradients. On the other hand, interior nodes which have higher levels of restrain show compressive stresses along the whole process. Intermediate positioned nodes show a behaviour similar to the one noticed by (Ji 2008) and (Bjøntegaard 2011), with a compressive behaviour in the first 24 hours and a tensile stress development coincident with the cooling. A comparison between these three behaviours can be seen in Figure 9.9.

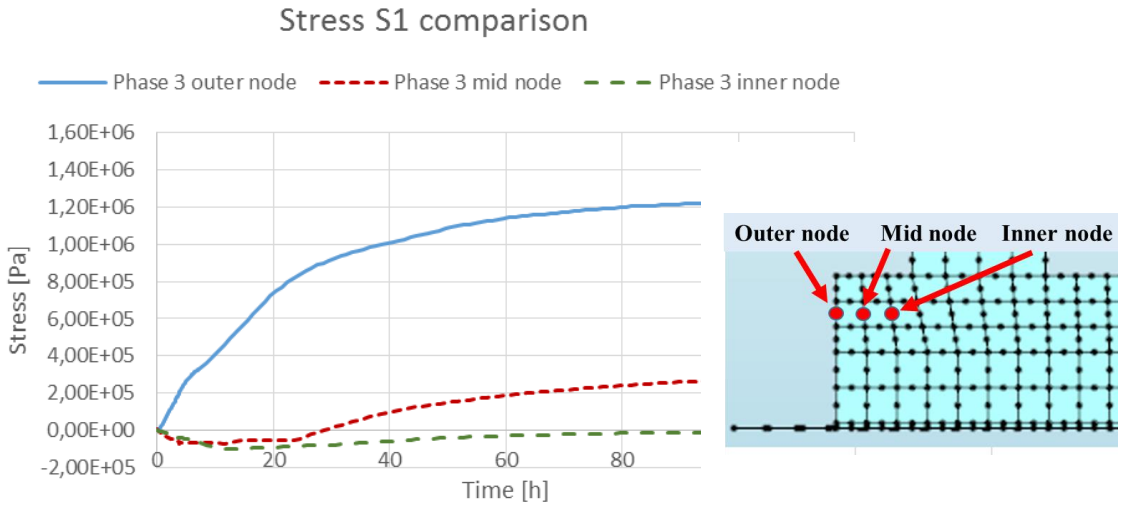

Figure 9.9 Stress S1 comparison

9.2.5 Crack analysis

Although the addition of crack models was not in the scope of this study a simple approach to it was done by comparing the stress and the strength gain for a critical node in the bottom of the slab and for a node in the roof slab, see Figure 9.10.

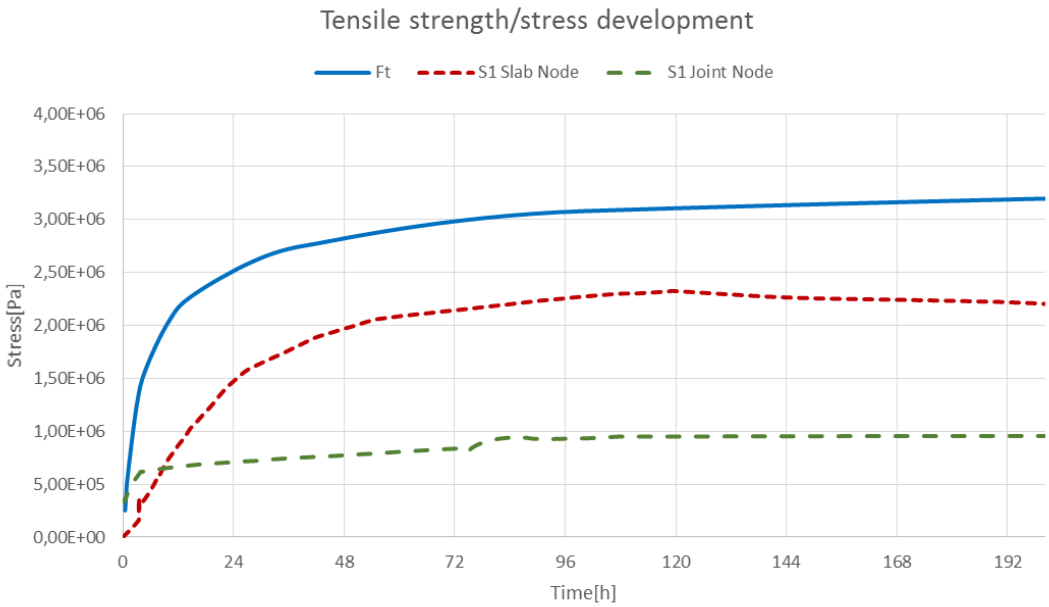

Figure 9.10 Stress/strength comparison.

These results show the need for a more thorough analysis into restraint and its influence in stresses. Finally the compressive strength gain is shown in Figure 9.11 as used in the material model definition.

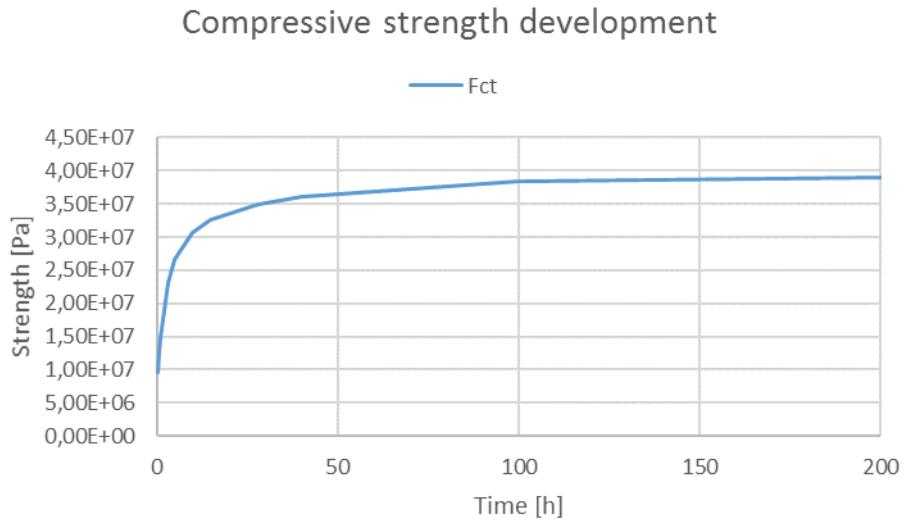

Figure 9.11 Characteristic Compressive growth due to maturity gain.

10 Conclusions

A Diana model was successfully created that allowed for a simplified prediction of cracking in concrete. This model included thermal effects, shrinkage and creep through the definition of the material model, as well as the modelling of restraint through the definition of the phased analysis and the supports. However, working with the recently released version DIANA 10 did cause some additional work and de-bugging which was time-consuming.

The model proved to be able to accurately give a simulation of the temperature development, as shown by the comparison to the temperatures measurements on the gauges and its comparison to the results from the model. Although this is true, the analysis could be made more accurate if the basis input from the materials used was more complete.

Regarding stresses, the results from DIANA show values in the range of the analysis from CONTEST. For a good representation of stresses, a more thorough study on restraint as well as creep and shrinkage in early ages and its effect should be done. Unfortunately, the results from modeling could not be compared to any measured strains in the mock-up as initially expected.

When it comes to cracking, the developed model can provide an initial understanding of the structural behavior and stress state, but for an accurate prediction of crack development a model which considers cracking, and includes reinforcement should be implemented.

The values from CONTEST are a good starting point for verification, as they allowed for an initial approach to assess the accuracy of the model. Since the developed model aims to improve the accuracy of CONTEST itself, it might not be the best way of assessing its validity. For this reason, the consulted research from (Ji 2008) proved useful to provide an understanding of the mechanisms influencing cracking.

It is relevant to mention that along the modelling phase different simplifications were made partially due to the limitations (as shown in Chapter 7) and for the sake of simplicity, for instance the usage of a modified value for conductivity in the boundaries to simulate them and avoid including the formwork as elements had minor to no influence in the results.

The usage of user supplied material models allows for a better control and understanding of the model since every mechanism that needs to be modelled can be defined as wished. On the contrary, built-in material models include variables and functions that are not customizable, difficult to understand and which therefore can complicate the analysis and even make it fail.

In conclusion, the 3D modelling allows for a better study of the structure and more factors can be considered that are otherwise disregarded in 2D modelling. Even if it comes with more computational cost it allows for a more realistic way of simulating the behavior of the structure. On the other hand, 2D analysis offer a wide variety of output in a faster and easy way, while 3D is not as straight forward when it comes to results interpretation. Hence, a combination of 2D and 3D analyses could be a way

forward. For example, 3D for more accurate temperature and moisture simulations and to assess the restraint, while 2D could be used to check the stresses etc.

10.1 Further development

The problem treated here is a complex one, this means that lots of different mechanism are involved and all of them would deserve a thorough analysis regarding its dependence on temperature, maturity and relative humidity. Some clear actuation lines can be considered:

- A more realistic model would be obtained by modelling the reinforcement of the element and the cooling pipes, as their influence in the strains and temperature development respectively are relevant for the final solution.
- A study of DIANA material models that analyses their capabilities and limits, in order to find one that is completely maturity dependant and therefore more accurate.
- Regarding the main mechanisms involved in early age cracking, namely autogenous shrinkage, thermal shrinkage and creep, the measurement of their individual influence could be found interesting through the comparison of different functions that describe their behaviour.
- The implementation of a crack/damage model could allow for a visualization of the crack generation and its prediction that would be helpful for the reinforcement design for structures were cracking is allowable.
- The establishment of an accurate input based on experimentally determined material properties for the material to be used, to decrease lack of accuracy from the approximations done.

11 Appendix

Appendix 1 - Indata for DIANA

Main Materials

Main Material= CEM I 42.5					
CEB-FIP 1990	**Value**	**Units**	**Program Value**	**Program Units**	**Source:**
Concrete class			C35	-	
Cement type			Normal rapid Hardening	-	
Ambient temperature			293,15	K	
Notional size oh member h			0,15	m	
Realtive ambient humidity RH in %			80	%	Standard
Aggregate type			Quartzite	-	
Direct input					
Young's modulus			34000000000	N/m^2	Contest
Young's modulus at 28 days			34000000000	N/m^2	Contest
Poisson's ratio			0,2	-	Contest
Thermal expansion coefficient			1*10^-5	1/K	Contest
Mass density			2411	kg/m^3	Calculated
Characteristic strength at 28 days			35000000	N/m^2	Data from ingemar, see email
Mean compressive strength at 28 days			35000000	N/m^2	Data from ingemar, see email
Creep					
Creep based on model code			Yes	-	
Concrete age			Concrete age at loading	-	
Concrete age at birth of element			28800	s	
Shrinkage					
Shrinkage based on model code			Yes	-	
Concrete age at end of curing period			0	s	
Heat flow					
Conductivity			2,1	W/mK	
Capacity	1000	J/kgK	2411000	J/m^3K	Contest
Conductivity/capacity function			Element age dependent	-	
			Element age [s]	0 43200 86400 7.2e6	
			Conductivity [W/mK]	2.1 2.1 1.7 1.7	
Heat of hydration method			Preprocessing	-	
Adiabatic heat development			*See next page*	-	Own contest model
Equivalent age calculation			Arrhenius	-	
Reference temperature			293,15	K	
Arrhenius constant	3454,7	K	6000	K	Calculated according to A*1000/R

Main Material= Soil Coarse Grained					
Soil	**Value**	**Units**	**Program Value**	**Program Units**	**Source**
Linear material properties					
Young's modulus			120000000	N/m^2	
Poissions Ratios			0,4	-	
Mass density specification			Dry density and porosity		
Density			2200	kg/m^3	Contest report
Porosity			-	-	
Heat flow					
Conductivty			2,1	W/mK	Contest report
Capacity	1400	J/(kgK)	3080000	K/m^3K	Contest report

Constants:			
Gas constant	R	8,31447	J/mol K
Activation energy	A	30,15	KJ/mol

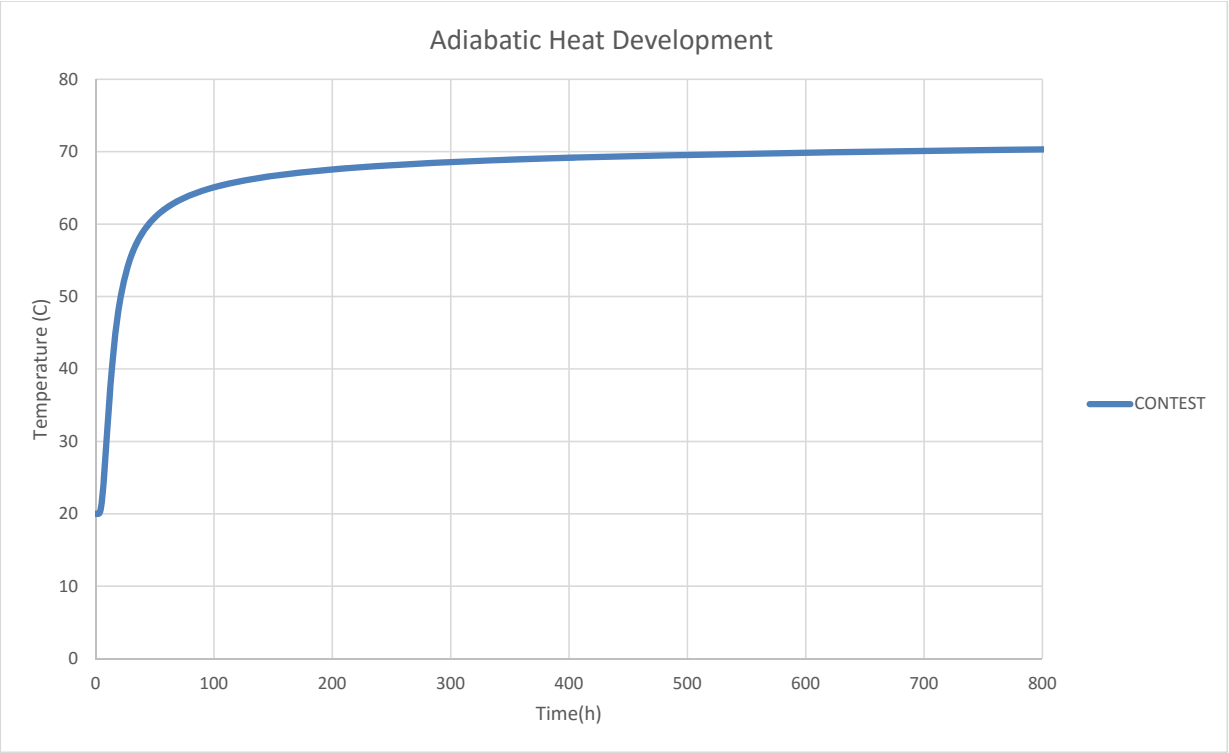
Adiabatic Heat Development
Temperature (C)
80
70
60
50
40
30
20
10
0
0
100
200
300
400
500
600
700
800
Time(h)
CONTEST

Boundary materials

CEM 1 Boundary

Boundary element	Value	Units	Program Value	Program Units				
Boundary properties heat flow								
Discharge type			Convection only	-				
Conduction coefficient			500	W/m^2K	Contest			
Convective power			1	-				
Convective function			No dependency	-				

Soil Coarse Grained Boundary

Boundary element	Value	Units	Program Value	Program Units				
Boundary properties heat flow								
Discharge type			Convection only	-				
Conduction Coefficient			80	W/m^2K	Contest			
Convective power			1	-				
Convection function			No dependency	-				

Timber Formwork Boundary

Boundary element	Value	Units	Program Value	Program Units				
Boundary properties heat flow								
Discharge type			Convection only	-				
Conduction Coeffici	7,78	W/m^2K		3,7	W/m^2K			
Convective power				1	-			
Convection function			Time dependent	-				
Time-conduction coefficient			Time [s]	0	432000	432001	864000	Contest
			Conduction Coefficient [W/m^2K]	3,75	3,75	500	500	Contest

Tarpaulin(plastic cover) Boundary

Boundary element	Value	Units	Program Value	Program Units				
Boundary properties heat flow								
Discharge type			Convection only	-				
Conduction Coeffici	18	W/m^2K		9,8	W/m^2K	Calculated		
Convective power				1	-			
Convection function			Time dependent	-				
Time-conduction coefficient			Time [s]	0	432000	432001	864000	Contest
			Conduction Coefficient [W/m^2K]	9,8	9,8	500	500	Contest

Interface Boundary

Interface Boundary	Value	Units	Program Value	Program Units	
Linear matieral properties					
Type			3D surface interface		
Normal stiffness modulus -z*			10000000000	N/m^3	See main material CEM I
Shear stiffness modulus -x*			0	N/m^3	See main material CEM I
Shear stiffness modulus -y			0	N/m^3	
Heat Flow					
Conduction Coefficient			500	W/m^2K	Contest

Concrete compositions

Properties			
		Value	**Unit**
Specific Surface (Blaine for Cement)		338	m^2/kg
Particle density of the concrete		3182	kg/m^3
Compressive strength (Cement)	1 Day	12.1	MPa
	2 Days	23.1	MPa
	28 Days	54.5	MPa
Strength Class		C35/45	-
W/C		0.395	-
Air Content		4.2	%
Proportions:	Cement	415	kg/m^3
	Water	164	kg/m^3
0-2mm	Sand	700	kg
4-8mm	Crushed	189	kg
8-16mm	Crushed	227	kg
16-25mm	Crushed	718	kg
Total Density		2411	kg/m^3

Admixtures			
Name	**% of CEM**	**Type**	**ASTM Type**
Master Glenium 51/18	0.6	Water reducing	A
Master Air 100	0.008	SuperPlast	F
Master Set 401 Lent	0.2	Retardant	B

Density and weight fractions			
	Content	**Density**	**Fraction [%]**
	kg/m3	kg/m3	
Cement	415	3182	0.1304
Water	163.93	1000	0.1639
Aggregate	1134	2835	0.4
Sand	698.68	2650	0.2636
Total	2411.61		

Activation Energy

Component	
Method 2.4.1	
% Cement	0,172084209
Gypsum	3,7
Na20 eq	0,51454
% FlyAsh	0
% Cao in Fly ash	0
% GGBFS	0
% Silica Fume	0
WRRET	0,6
ACCL	0
Method 2.4.2	
CaSO4	0
xH2O	0
K2SO4	0
Calculated activation energy	**A [J/mol]**
Method in 2.4.1	28724
Method in 2.4.2	17016

Cement Composition

Component	Amount [%]
CaO	64
SiO_2	21,6
Al_2O_3	3,7
MgO	0,95
Na_2O	0,1
K2O	0,63
Cl	0,01
SO_3	2,6
Fe_2O_3	4,5
C2S	18,5
C3S	57,8
C3A	2,2
C4AF	13,7

Appendix 2 - Material parameters used in user-supplied model

Elastic modulus					
t [days]	**t [s]**	**bcc(t)**	**be(t)**	**Ec(t) [Mpa]**	**Ec(t) [Pa]**
0,2	17280	0,066667	0,2582	8778,8075	877880750
0,5	43200	0,197735	0,444674	15118,9085	1511890848
0,8	69120	0,292579	0,540906	18390,8002	1839080022
1	86400	0,342024	0,584828	19884,1453	1988414533
2	172800	0,503881	0,709846	24134,7655	2413476546
5	432000	0,710627	0,842987	28661,5509	2866155092
15	1296000	0,912502	0,95525	32478,4896	3247848960
28	2419200	1	1	34000	3400000000
40	3456000	1,04168	1,020627	34701,3302	3470133023
45	3888000	1,054216	1,02675	34909,5069	3490950686
50	4320000	1,064939	1,031959	35086,5929	3508659294
55	4752000	1,074251	1,036461	35239,664	3523966399
60	5184000	1,08244	1,040404	35373,7234	3537372342
65	5616000	1,089716	1,043895	35492,4238	3549242379
70	6048000	1,09624	1,047015	35598,5029	3559850288
100	8640000	1,124921	1,060623	36061,1728	3606117284
200	17280000	1,169362	1,081371	36766,5994	3676659937
500	43200000	1,210265	1,10012	37404,0926	3740409258
1000	86400000	1,231419	1,109693	37729,5657	3772956573
5000	432000000	1,260227	1,122598	38168,3402	3816834019
10000	864000000	1,267151	1,125678	38273,0559	3827305586
15000	1296000000	1,270231	1,127045	38319,5384	3831953841

Value	
Eci [Mpa]	34000
s	0,25
t_1 [days]	1

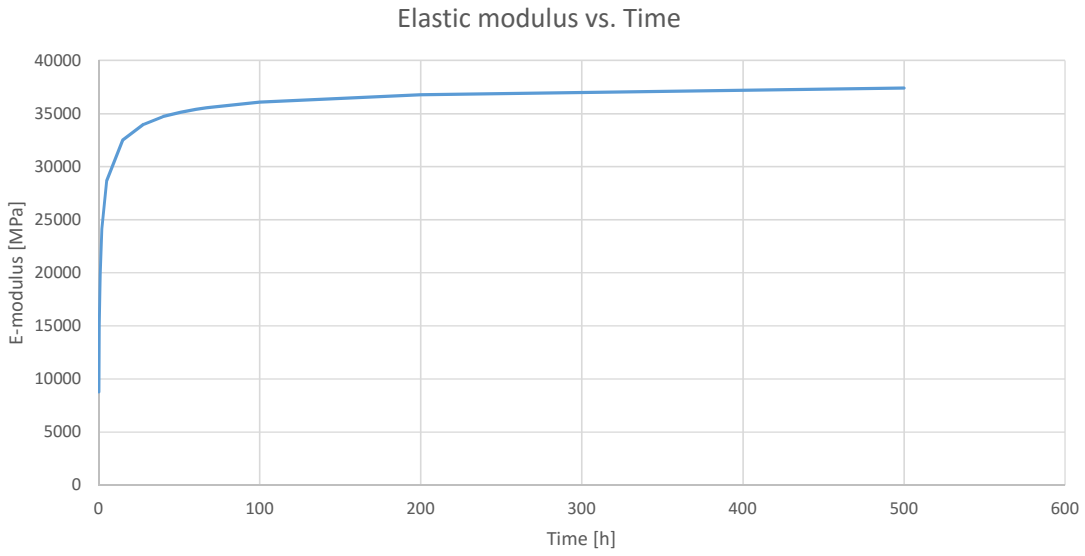

Coeffiecient of thermal exansion	
Time [s]	**CTE [1/K]**
0,00000E+00	3,67480E-05
1,56522E+04	3,67480E-05
1,95652E+04	2,86179E-05
2,73913E+04	2,14634E-05
3,52174E+04	1,56098E-05
4,69565E+04	1,23577E-05
8,21739E+04	1,49594E-05
1,25217E+05	1,65854E-05
1,87826E+05	1,62602E-05
2,50435E+05	1,46341E-05
3,13043E+05	1,30081E-05
3,71739E+05	1,10569E-05
4,61739E+05	1,04065E-05
5,67391E+05	1,04065E-05
6,22174E+05	1,04065E-05

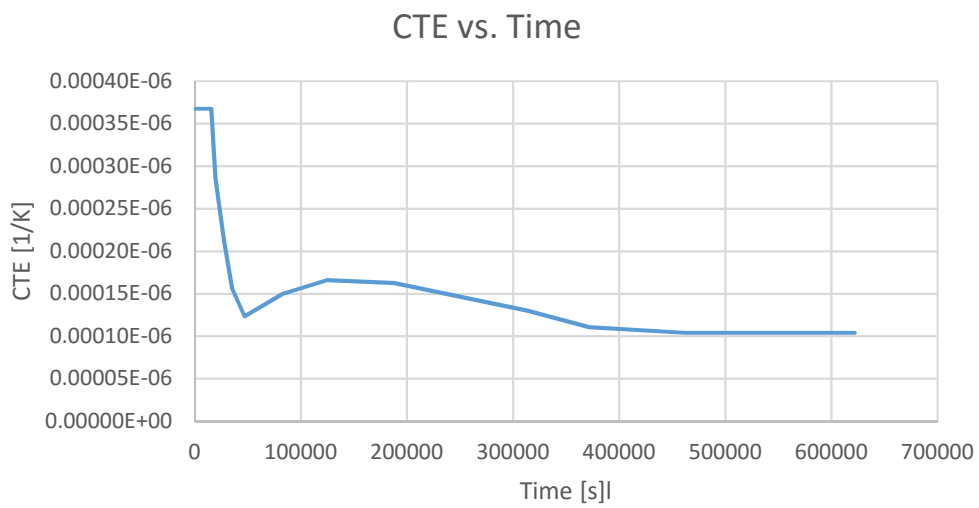

Fitting parameters				
v_0	v_{inf}	t_{auf}	α_v	h [s]
0,34	0,17	14,9	0,78	53640

Poisson's Ratio			
Days	hours	SEC	v(te)
0,2	4,8	17280	0,324875
0,5	12	43200	0,287967
0,8	19,2	69120	0,265169
1	24	86400	0,254688
2	48	172800	0,22622
5	120	432000	0,200325
15	360	1296000	0,183603
28	672	2419200	0,178494
40	960	3456000	0,176471
45	1080	3888000	0,175913
50	1200	4320000	0,175454
55	1320	4752000	0,175069
60	1440	5184000	0,174741
65	1560	5616000	0,174458
70	1680	6048000	0,174211
100	2400	8640000	0,173198
200	4800	17280000	0,17187
500	12000	43200000	0,170917
1000	24000	86400000	0,170535
5000	120000	432000000	0,170153
10000	240000	864000000	0,170089
15000	360000	1296000000	0,170065

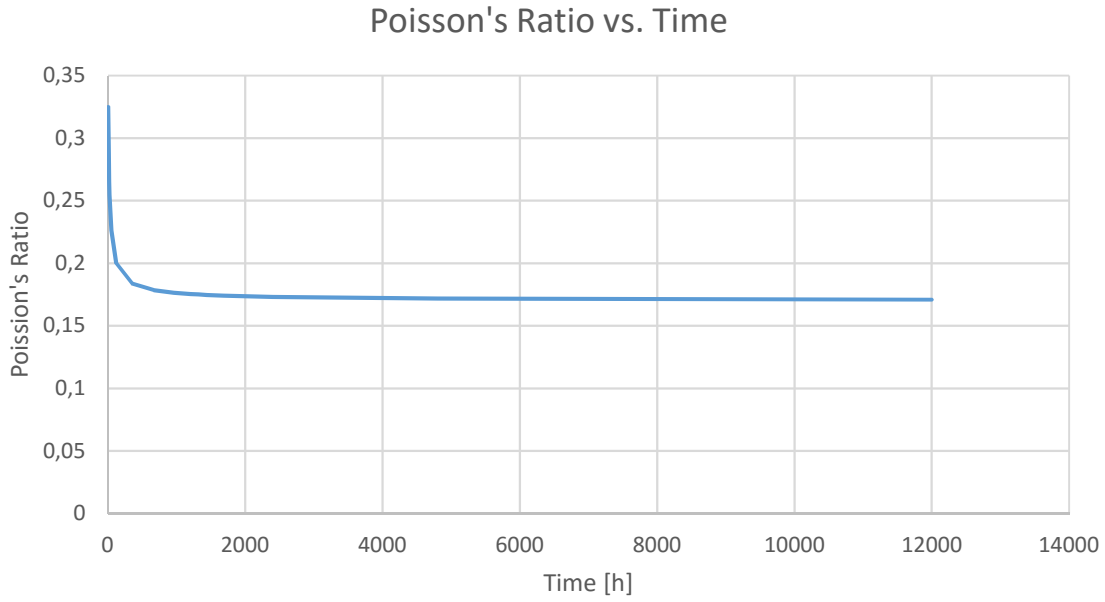

Shrinkage			
Hymostruc		Chu Kwong	
Time [h]	Strain [-]	Time [h]	Strain [-]
0,0	0,00E+00	0,0	1,09497E-05
0,3	1,96E-05	25,7	1,09497E-05
0,6	2,45E-05	32,1	2,03352E-05
1,0	3,06E-05	64,3	2,89385E-05
1,5	3,80E-05	96,4	3,87151E-05
2,2	4,71E-05	173,6	4,65363E-05
3,0	5,81E-05	270,0	4,84916E-05
4,0	7,14E-05	366,4	4,96648E-05
5,3	8,73E-05	495,0	5,0838E-05
6,9	1,06E-04	610,7	5,0838E-05
9,0	1,28E-04	726,4	5,0838E-05
11,6	1,52E-04	861,4	5,04469E-05
14,8	1,80E-04	996,4	5,12291E-05
19,0	2,11E-04	1131,4	5,16201E-05
24,1	2,44E-04	1266,4	5,20112E-05
30,6	2,80E-04	1407,9	5,20112E-05
38,8	3,17E-04		
49,1	3,55E-04		
62,1	3,93E-04		
78,4	4,30E-04		
99,0	4,63E-04		
124,9	4,92E-04		
157,5	5,17E-04		
198,5	5,38E-04		
250,2	5,57E-04		
1300,0	5,57E-04		

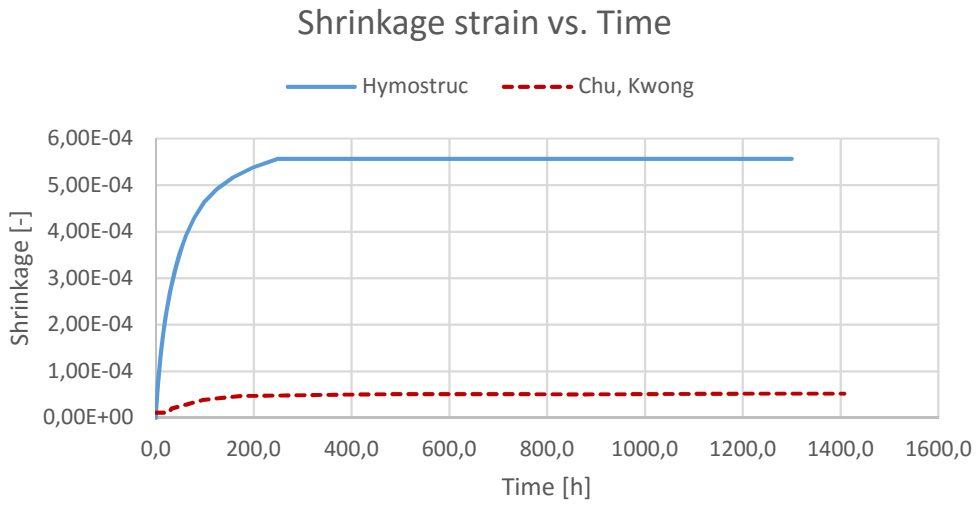

Appendix 3 - User supplied model

Appendix 3: Dat files

Material Models

```
'MATERI'
  2 NAME   "Soil Coarse Grained"
    MCNAME SOLROC
    MATMDL ELASTI
    ASPECT HEATFL
    POISON   4.00000E-01
    YOUNG    1.20000E+08
    DENSIT   2.20000E+03
    CAPACI   3.08000E+06
    CONDUC   2.10000E+00
  3 NAME   "CEM I(Bound)"
    MCNAME INTERF
    MATMDL FLBOUN
    ASPECT
    FLUXTY CONVEC
    CONPOW   1.00000E+00
    CONVEC   5.00000E+02
  4 NAME   "Timber(Bound)"
    MCNAME INTERF
    MATMDL FLBOUN
    ASPECT THERMA
    FLUXTY CONVEC
    CONPOW   1.00000E+00
    CONVEC   3.75000E+00
    TIMCNV   0.00000E+00   3.75000E+00   4.32000E+05   3.75000E+00
          4.32001E+05   5.00000E+02   8.64000E+05   5.00000E+02
  5 NAME   "Tarpaulin(Bound)"
    MCNAME INTERF
```

```
 MATMDL FLBOUN
 ASPECT THERMA
 FLUXTY CONVEC
 CONPOW   1.00000E+00
 CONVEC   9.80000E+00
 TIMCNV   0.00000E+00   9.80000E+00   4.32000E+05   9.80000E+00
             4.32001E+05   5.00000E+02   8.64000E+05   5.00000E+02
6 NAME   "Soil(Bound)"
 MCNAME INTERF
 MATMDL FLBOUN
 ASPECT THERMA
 FLUXTY CONVEC
 CONPOW   1.00000E+00
 CONVEC   8.00000E+01
7 NAME   "Interface with top"
 MCNAME INTERF
 MATMDL ELASTI
 ASPECT HEATFL
 IFTYP  SUR3D
 DSNZ     3.31196E+10
 DSSX     3.31196E+10
 DFLUX    5.00000E+02
8 NAME   "OwnMatModel"
 YOUNG    3.40000E+10
 POISON   2.00000E-01
 DENSIT   2.41100E+03
 THERMX   1.00000E-06
 EQUAGE ARRTYP
 ARRHEN   6.00000E+03
 ADIAB    0.00000E+00   2.93000E+02   1.80000E+03   2.93000E+02
       3.60000E+03   2.93000E+02   5.40000E+03   2.93000E+02
       7.20000E+03   2.93000E+02   9.00000E+03   2.93007E+02
       1.08000E+04   2.93047E+02   1.26000E+04   2.93168E+02
```

1.44000E+04	2.93412E+02	1.62000E+04	2.93803E+02
1.80000E+04	2.94347E+02	1.98000E+04	2.95037E+02
2.16000E+04	2.95859E+02	2.34000E+04	2.96793E+02
2.52000E+04	2.97820E+02	2.70000E+04	2.98921E+02
2.88000E+04	3.00076E+02	3.06000E+04	3.01268E+02
3.24000E+04	3.02481E+02	3.42000E+04	3.03699E+02
3.60000E+04	3.04912E+02	3.78000E+04	3.06107E+02
3.96000E+04	3.07279E+02	4.14000E+04	3.08418E+02
4.32000E+04	3.09522E+02	4.50000E+04	3.10585E+02
4.68000E+04	3.11605E+02	4.86000E+04	3.12583E+02
5.04000E+04	3.13518E+02	5.22000E+04	3.14411E+02
5.40000E+04	3.15261E+02	5.58000E+04	3.16071E+02
5.76000E+04	3.16841E+02	5.94000E+04	3.17574E+02
6.12000E+04	3.18271E+02	6.30000E+04	3.18934E+02
6.48000E+04	3.19565E+02	6.66000E+04	3.20165E+02
6.84000E+04	3.20736E+02	7.02000E+04	3.21281E+02
7.20000E+04	3.21799E+02	7.38000E+04	3.22294E+02
7.56000E+04	3.22766E+02	7.74000E+04	3.23216E+02
7.92000E+04	3.23647E+02	8.10000E+04	3.24058E+02
8.28000E+04	3.24452E+02	8.46000E+04	3.24829E+02
8.64000E+04	3.25190E+02	8.82000E+04	3.25536E+02
9.00000E+04	3.25867E+02	9.18000E+04	3.26185E+02
9.36000E+04	3.26491E+02	9.54000E+04	3.26785E+02
9.72000E+04	3.27068E+02	9.90000E+04	3.27340E+02
1.00800E+05	3.27603E+02	1.02600E+05	3.27856E+02
1.04400E+05	3.28100E+02	1.06200E+05	3.28336E+02
1.08000E+05	3.28563E+02	1.09800E+05	3.28783E+02
1.11600E+05	3.28996E+02	1.13400E+05	3.29202E+02
1.15200E+05	3.29401E+02	1.17000E+05	3.29595E+02
1.18800E+05	3.29782E+02	1.20600E+05	3.29963E+02
1.22400E+05	3.30139E+02	1.24200E+05	3.30310E+02
1.26000E+05	3.30476E+02	1.27800E+05	3.30637E+02
1.29600E+05	3.30794E+02	1.31400E+05	3.30946E+02

1.33200E+05 3.31094E+02 1.35000E+05 3.31238E+02

1.36800E+05 3.31379E+02 1.38600E+05 3.31515E+02

1.40400E+05 3.31648E+02 1.42200E+05 3.31778E+02

1.44000E+05 3.31905E+02 1.45800E+05 3.32028E+02

1.47600E+05 3.32148E+02 1.49400E+05 3.32266E+02

1.51200E+05 3.32381E+02 1.53000E+05 3.32493E+02

1.54800E+05 3.32602E+02 1.56600E+05 3.32709E+02

1.58400E+05 3.32814E+02 1.60200E+05 3.32916E+02

1.62000E+05 3.33016E+02 1.63800E+05 3.33114E+02

1.65600E+05 3.33209E+02 1.67400E+05 3.33303E+02

1.69200E+05 3.33395E+02 1.71000E+05 3.33485E+02

1.72800E+05 3.33573E+02 1.76400E+05 3.33743E+02

1.80000E+05 3.33907E+02 1.83600E+05 3.34064E+02

1.87200E+05 3.34216E+02 1.90800E+05 3.34362E+02

1.94400E+05 3.34503E+02 1.98000E+05 3.34639E+02

2.01600E+05 3.34771E+02 2.05200E+05 3.34898E+02

2.08800E+05 3.35021E+02 2.12400E+05 3.35139E+02

2.16000E+05 3.35255E+02 2.19600E+05 3.35366E+02

2.23200E+05 3.35474E+02 2.26800E+05 3.35580E+02

2.30400E+05 3.35681E+02 2.34000E+05 3.35781E+02

2.37600E+05 3.35877E+02 2.41200E+05 3.35970E+02

2.44800E+05 3.36061E+02 2.48400E+05 3.36150E+02

2.52000E+05 3.36236E+02 2.55600E+05 3.36320E+02

2.59200E+05 3.36402E+02 2.66400E+05 3.36559E+02

2.73600E+05 3.36709E+02 2.80800E+05 3.36851E+02

2.88000E+05 3.36988E+02 2.95200E+05 3.37118E+02

3.02400E+05 3.37242E+02 3.09600E+05 3.37362E+02

3.16800E+05 3.37477E+02 3.24000E+05 3.37587E+02

3.31200E+05 3.37693E+02 3.38400E+05 3.37794E+02

3.45600E+05 3.37893E+02 3.52800E+05 3.37987E+02

3.60000E+05 3.38079E+02 3.67200E+05 3.38167E+02

3.74400E+05 3.38252E+02 3.81600E+05 3.38335E+02

3.88800E+05 3.38415E+02 3.96000E+05 3.38492E+02

4.03200E+05	3.38567E+02	4.10400E+05	3.38640E+02
4.17600E+05	3.38710E+02	4.24800E+05	3.38779E+02
4.32000E+05	3.38845E+02	4.46400E+05	3.38972E+02
4.60800E+05	3.39093E+02	4.75200E+05	3.39207E+02
4.89600E+05	3.39316E+02	5.04000E+05	3.39419E+02
5.18400E+05	3.39518E+02	5.32800E+05	3.39612E+02
5.47200E+05	3.39702E+02	5.61600E+05	3.39789E+02
5.76000E+05	3.39871E+02	5.90400E+05	3.39951E+02
6.04800E+05	3.40027E+02	6.19200E+05	3.40101E+02
6.33600E+05	3.40171E+02	6.48000E+05	3.40240E+02
6.62400E+05	3.40305E+02	6.76800E+05	3.40369E+02
6.91200E+05	3.40430E+02	7.05600E+05	3.40490E+02
7.20000E+05	3.40547E+02	7.34400E+05	3.40603E+02
7.48800E+05	3.40657E+02	7.63200E+05	3.40709E+02
7.77600E+05	3.40760E+02	8.06400E+05	3.40857E+02
8.35200E+05	3.40948E+02	8.64000E+05	3.41035E+02
8.92800E+05	3.41118E+02	9.21600E+05	3.41196E+02
9.50400E+05	3.41271E+02	9.79200E+05	3.41342E+02
1.00800E+06	3.41410E+02	1.03680E+06	3.41475E+02
1.06560E+06	3.41537E+02	1.09440E+06	3.41597E+02
1.12320E+06	3.41655E+02	1.15200E+06	3.41710E+02
1.18080E+06	3.41763E+02	1.20960E+06	3.41815E+02
1.23840E+06	3.41864E+02	1.26720E+06	3.41912E+02
1.29600E+06	3.41958E+02	1.32480E+06	3.42003E+02
1.35360E+06	3.42046E+02	1.38240E+06	3.42088E+02
1.41120E+06	3.42129E+02	1.44000E+06	3.42168E+02
1.46880E+06	3.42206E+02	1.52640E+06	3.42279E+02
1.58400E+06	3.42348E+02	1.64160E+06	3.42413E+02
1.69920E+06	3.42475E+02	1.75680E+06	3.42534E+02
1.81440E+06	3.42590E+02	1.87200E+06	3.42644E+02
1.92960E+06	3.42695E+02	1.98720E+06	3.42744E+02
2.04480E+06	3.42791E+02	2.10240E+06	3.42836E+02
2.16000E+06	3.42880E+02	2.21760E+06	3.42921E+02

2.27520E+06 3.42961E+02 2.33280E+06 3.43000E+02

2.39040E+06 3.43038E+02 2.44800E+06 3.43074E+02

2.50560E+06 3.43109E+02 2.56320E+06 3.43142E+02

2.62080E+06 3.43175E+02 2.67840E+06 3.43207E+02

2.73600E+06 3.43238E+02 2.79360E+06 3.43267E+02

2.85120E+06 3.43296E+02 2.96640E+06 3.43352E+02

3.08160E+06 3.43404E+02 3.19680E+06 3.43453E+02

3.31200E+06 3.43501E+02 3.42720E+06 3.43545E+02

3.54240E+06 3.43588E+02 3.65760E+06 3.43629E+02

3.77280E+06 3.43668E+02 3.88800E+06 3.43706E+02

4.00320E+06 3.43742E+02 4.11840E+06 3.43776E+02

4.23360E+06 3.43809E+02 4.34880E+06 3.43841E+02

4.46400E+06 3.43872E+02 4.57920E+06 3.43902E+02

4.69440E+06 3.43931E+02 4.80960E+06 3.43958E+02

4.92480E+06 3.43985E+02 5.04000E+06 3.44011E+02

5.15520E+06 3.44036E+02 5.27040E+06 3.44061E+02

5.38560E+06 3.44084E+02 5.50080E+06 3.44107E+02

5.61600E+06 3.44130E+02 5.73120E+06 3.44152E+02

5.84640E+06 3.44173E+02 5.96160E+06 3.44193E+02

CONDUC 2.00000E+00

CAPACI 2.41100E+06

AGECND 0.00000E+00 2.10000E+00 4.32000E+04 2.10000E+00

8.64000E+04 1.70000E+00 7.20000E+06 1.70000E+00

MATSHR 0.00000e+00 1.09497E-05

9.25714E+04 1.09497E-05

1.15714E+05 2.03352E-05

2.31429E+05 2.89385E-05

3.47143E+05 3.87151E-05

6.24857E+05 4.65363E-05

9.72000E+05 4.84916E-05

1.31914E+06 4.96648E-05

1.78200E+06 5.08380E-05

2.19857E+06 5.08380E-05

2.61514E+06 5.08380E-05

3.10114E+06 5.04469E-05

3.58714E+06 5.12291E-05

4.07314E+06 5.16201E-05

4.55914E+06 5.20112E-05

5.06829E+06 5.20112E-05

5.00000E+13 5.20112E-05

MATYOU 0.00000E+00 8.77881E+08 4.32000E+04 1.51189E+09

6.91200E+04 1.83908E+09 8.64000E+04 1.98841E+09

1.72800E+05 2.41348E+09 4.32000E+05 2.86616E+09

1.29600E+06 3.24785E+09 2.41920E+06 3.40000E+09

3.45600E+06 3.47013E+09 3.88800E+06 3.49095E+09

4.32000E+06 3.50866E+09 4.75200E+06 3.52397E+09

5.18400E+06 3.53737E+09 5.61600E+06 3.54924E+09

6.04800E+06 3.55985E+09 8.64000E+06 3.60612E+09

1.72800E+07 3.67666E+09 4.32000E+07 3.74041E+09

8.64000E+07 3.77296E+09 4.32000E+08 3.81683E+09

8.64000E+08 3.82731E+09 8.64000E+13 3.82731E+09

MATPOI 0.00000E+00 3.24875E-01 1.72800E+04 3.24875E-01

4.32000E+04 2.87967E-01 6.91200E+04 2.65169E-01

8.64000E+04 2.54688E-01 1.72800E+05 2.26220E-01

4.32000E+05 2.00325E-01 1.29600E+06 1.83603E-01

2.41920E+06 1.78494E-01 3.45600E+06 1.76471E-01

3.88800E+06 1.75913E-01 4.32000E+06 1.75454E-01

4.75200E+06 1.75069E-01 5.18400E+06 1.74741E-01

5.61600E+06 1.74458E-01 6.04800E+06 1.74211E-01

8.64000E+06 1.73198E-01 1.72800E+07 1.71870E-01

4.32000E+07 1.70917E-01 8.64000E+07 1.70535E-01

4.32000E+08 1.70153E-01 8.64000E+08 1.70089E-01

1.29600E+09 1.70065E-01 1.29600E+14 1.70065E-01

MATALP 0.00000E+00 3.67480E-05 1.56522E+04 3.67480E-05

1.95652E+04 2.86179E-05 2.73913E+04 2.14634E-05

3.52174E+04 1.56098E-05 4.69565E+04 1.23577E-05

8.21739E+04 1.49594E-05 1.25217E+05 1.65854E-05

1.87826E+05 1.62602E-05 2.50435E+05 1.46341E-05

3.13043E+05 1.30081E-05 3.71739E+05 1.10569E-05

4.61739E+05 1.04065E-05 5.67391E+05 1.04065E-05

6.22174E+14 1.04065E-05

CREEP COMPLI

TRCRP 3.50000E+07 2.35000E+00

9 NAME "Ground Interface"

MCNAME INTERF

MATMDL ELASTI

ASPECT

IFTYP SUR3D

DSNZ 1.00000E+09

DSSX 0.00000E+00

DSSY 0.00000E+00

Appendix 4 - Analysis file

Analysis File

```
*PHASE LABEL="Phased"
 BEGIN ACTIVE
  ELEMEN "Low Slab" "Low Slab plane interface" \
       "Low Slab plane interface set 3" "Low Slab plane interface set 4" \
       "Low Slab plane interface set 5" "Soil" "Soil plane interface" \
       "Soil plane interface set 12" /
  SUPPOR "Soil Support" "Symmetry Soil" "Symm Bslab"
  FIXHEA ALL
  FIXPOT ALL
  FIXTEM ALL
  TYINGS ALL
 END ACTIVE
*HEATTR LABEL="Transient heat transfer"
 BEGIN INITIA
  BEGIN NONLIN
   HYDRAT DGRINI 0.01
   EQUAGE
  END NONLIN
  TEMPER INPUT FIELD 1
  SOLVE PARDIS
 END INITIA
 BEGIN EXECUT
  SIZES 360.000(35)
  NONLIN HYDRAT
  SOLVE PARDIS
  SAVE STEPS ALL /
 END EXECUT
 BEGIN OUTPUT
  TEXT "Analysis output"
  BINARY
  SELECT STEPS ALL /
```

```
 END OUTPUT
*NONLIN LABEL="Structural nonlinear"
 BEGIN TYPE
  BEGIN PHYSIC
   CORROS OFF
   TOTCRK OFF
   INTERF OFF
  END PHYSIC
 END TYPE
 BEGIN EXECUT
  BEGIN LOAD
   LOADNR 1
   STEPS EXPLIC
  END LOAD
  BEGIN ITERAT
   MAXITE 100
   METHOD NEWTON
   LINESE
  END ITERAT
 END EXECUT
 BEGIN EXECUT
  TEXT "new execute block 2"
  TIME STEPS EXPLIC SIZES 360.000(35)
  BEGIN ITERAT
   MAXITE 100
   METHOD NEWTON
   LINESE
  END ITERAT
 END EXECUT
 SOLVE PARDIS
 BEGIN OUTPUT
  TEXT "Output"
  BINARY
```

```
SELECT STEPS ALL /
STRAIN TOTAL GREEN GLOBAL XX YY ZZ XY YZ ZX
STRAIN TEMPER GREEN GLOBAL XX YY ZZ XY YZ ZX
STRAIN SHRINK GREEN VOLUME
BEGIN STRAIN
  BEGIN TOTAL
    BEGIN GREEN
      BEGIN PRINCI
        "1" "2" "3"
        NODES
      END PRINCI
    END GREEN
  END TOTAL
END STRAIN
BEGIN STRAIN
  BEGIN CREEP
    BEGIN GREEN
      BEGIN PRINCI
        "1" "2" "3"
        NODES
      END PRINCI
    END GREEN
  END CREEP
END STRAIN
BEGIN STRESS
  BEGIN TOTAL
    BEGIN CAUCHY
      BEGIN PRINCI
        "1" "2" "3"
        NODES
      END PRINCI
    END CAUCHY
  END TOTAL
```

```
  END STRESS
  STRESS TOTAL CAUCHY GLOBAL XX YY ZZ XY YZ ZX
  TEMPER TOTAL
  MATURI TOTAL
 END OUTPUT
*PHASE LABEL="Phased 2"
 BEGIN ACTIVE
  ELEMEN "Low Slab" "Low Slab plane interface" \
       "Low Slab plane interface set 3" "Low Slab plane interface set 4" \
       "Low Slab plane interface set 5" "Mid Slab" \
       "Mid Slab plane interface" "Mid Slab plane interface set 8" \
       "Mid Slab plane interface set 9" "Soil" "Soil plane interface" \
       "Soil plane interface set 12" /
  SUPPOR "Soil Support" "Symmetry Soil" "Symm Bslab" "Symm ISlab"
  FIXHEA ALL
  FIXPOT ALL
  FIXTEM ALL
  TYINGS ALL
 END ACTIVE
*HEATTR LABEL="Transient heat transfer 2"
 BEGIN INITIA
  BEGIN NONLIN
   HYDRAT DGRINI 0.01
   EQUAGE
  END NONLIN
  TEMPER INPUT FIELD 3
  SOLVE PARDIS
 END INITIA
 BEGIN EXECUT
  SIZES 360.000(45)
  NONLIN HYDRAT
  SOLVE PARDIS
  SAVE STEPS ALL /
```

```
 END EXECUT
 BEGIN OUTPUT
  TEXT "Analysis output"
  BINARY
  SELECT STEPS ALL /
 END OUTPUT
*NONLIN LABEL="Structural nonlinear 2"
 BEGIN TYPE
  BEGIN PHYSIC
   CORROS OFF
   TOTCRK OFF
   INTERF OFF
  END PHYSIC
 END TYPE
 BEGIN EXECUT
  BEGIN LOAD
   LOADNR 2
   STEPS EXPLIC
  END LOAD
  ITERAT METHOD NEWTON
 END EXECUT
 BEGIN EXECUT
  TEXT "new execute block 2"
  TIME STEPS EXPLIC SIZES 360.000(45)
  BEGIN ITERAT
   MAXITE 100
   METHOD NEWTON
   LINESE
  END ITERAT
 END EXECUT
 SOLVE PARDIS
 BEGIN OUTPUT
  TEXT "Output"
```

```
BINARY
SELECT STEPS ALL /
STRAIN TOTAL GREEN GLOBAL XX YY ZZ XY YZ ZX
STRAIN TEMPER GREEN GLOBAL XX YY ZZ XY YZ ZX
STRAIN SHRINK GREEN VOLUME
BEGIN STRAIN
  BEGIN TOTAL
    BEGIN GREEN
      BEGIN PRINCI
        "1" "2" "3"
        NODES
      END PRINCI
    END GREEN
  END TOTAL
END STRAIN
BEGIN STRAIN
  BEGIN CREEP
    BEGIN GREEN
      BEGIN PRINCI
        "1" "2" "3"
        NODES
      END PRINCI
    END GREEN
  END CREEP
END STRAIN
BEGIN STRESS
  BEGIN TOTAL
    BEGIN CAUCHY
      BEGIN PRINCI
        "1" "2" "3"
        NODES
      END PRINCI
    END CAUCHY
```

```
    END TOTAL
  END STRESS
  STRESS TOTAL CAUCHY GLOBAL XX YY ZZ XY YZ ZX
  TEMPER TOTAL
  MATURI TOTAL
 END OUTPUT
```

***PHASE LABEL="Phased 3"**

```
 BEGIN ACTIVE
  ELEMEN "Low Slab" "Low Slab plane interface" \
       "Low Slab plane interface set 3" "Low Slab plane interface set 4" \
       "Low Slab plane interface set 5" "Mid Slab" \
       "Mid Slab plane interface" "Mid Slab plane interface set 8" \
       "Mid Slab plane interface set 9" "Soil" "Soil plane interface" \
       "Soil plane interface set 12" "Up Slab" "Up Slab plane interface" \
       "Up Slab plane interface set 15" "Up Slab plane interface set 16" \
       "Up Slab plane interface set 17" "Up Slab plane interface set 18" /
  SUPPOR "Soil Support" "Symmetry Soil" "Symm Bslab" "Symm ISlab" \
"Symm USlab"
  FIXHEA ALL
  FIXPOT ALL
  FIXTEM ALL
  TYINGS ALL
 END ACTIVE
```

**HEATTR LABEL=" Transient heat transfer 3"*

```
 BEGIN INITIA
  BEGIN NONLIN
   HYDRAT DGRINI 0.01
   EQUAGE
  END NONLIN
  TEMPER INPUT FIELD 4
  SOLVE PARDIS
 END INITIA
 BEGIN EXECUT
```

```
  SIZES 360.000(38)
  NONLIN HYDRAT
  SOLVE PARDIS
  SAVE STEPS ALL /
 END EXECUT
 BEGIN OUTPUT
  TEXT "Analysis output"
  BINARY
  SELECT STEPS ALL /
 END OUTPUT
*NONLIN LABEL="Structural nonlinear 3"
 BEGIN TYPE
  BEGIN PHYSIC
   CORROS OFF
   TOTCRK OFF
   INTERF OFF
  END PHYSIC
 END TYPE
 BEGIN EXECUT
  BEGIN LOAD
   LOADNR 3
   STEPS EXPLIC
  END LOAD
  ITERAT METHOD NEWTON
 END EXECUT
 BEGIN EXECUT
  TEXT "new execute block 2"
  TIME STEPS EXPLIC SIZES 360.000(38)
  BEGIN ITERAT
   MAXITE 100
   METHOD NEWTON
   LINESE
  END ITERAT
```

```
END EXECUT
SOLVE PARDIS
BEGIN OUTPUT
 TEXT "Output"
 BINARY
 SELECT STEPS ALL /
 STRAIN TOTAL GREEN GLOBAL XX YY ZZ XY YZ ZX
 STRAIN TEMPER GREEN GLOBAL XX YY ZZ XY YZ ZX
 STRAIN SHRINK GREEN VOLUME
 BEGIN STRAIN
  BEGIN TOTAL
   BEGIN GREEN
    BEGIN PRINCI
     "1" "2" "3"
     NODES
    END PRINCI
   END GREEN
  END TOTAL
 END STRAIN
 BEGIN STRAIN
  BEGIN CREEP
   BEGIN GREEN
    BEGIN PRINCI
     "1" "2" "3"
     NODES
    END PRINCI
   END GREEN
  END CREEP
 END STRAIN
 BEGIN STRESS
  BEGIN TOTAL
   BEGIN CAUCHY
    BEGIN PRINCI
```

```
        "1" "2" "3"
        NODES
      END PRINCI
    END CAUCHY
  END TOTAL
 END STRESS
 STRESS TOTAL CAUCHY GLOBAL XX YY ZZ XY YZ ZX
 TEMPER TOTAL
 MATURI TOTAL
END OUTPUT
```

***PHASE LABEL="Phased 4"**

```
BEGIN ACTIVE
 ELEMEN "Low Slab" "Low Slab plane interface" \
      "Low Slab plane interface set 3" "Low Slab plane interface set 4" \
      "Low Slab plane interface set 5" "Mid Slab" \
      "Mid Slab plane interface" "Mid Slab plane interface set 8" \
      "Mid Slab plane interface set 9" "Soil" "Soil plane interface" \
      "Soil plane interface set 12" "Up Slab" "Up Slab plane interface" \
      "Up Slab plane interface set 15" "Up Slab plane interface set 16" \
      "Up Slab plane interface set 17" "Up Slab plane interface set 18" \
      "Low Wall" "Low Wall plane interface" \
      "Low Wall plane interface set 21" \
      "Low Wall plane interface set 22" /
 SUPPOR "Soil Support" "Symmetry Soil" "Symm Bslab" "Symm ISlab" \
"Symm USlab" "Symm BWall"
 FIXHEA ALL
 FIXPOT ALL
 FIXTEM ALL
 TYINGS ALL
END ACTIVE
```

**HEATTR LABEL="Transient heat transfer 4"*

```
BEGIN INITIA
 BEGIN NONLIN
```

```
    HYDRAT DGRINI 0.01
    EQUAGE
  END NONLIN
  TEMPER INPUT FIELD 5
  SOLVE PARDIS
 END INITIA
 BEGIN EXECUT
  SIZES 540.000(25)
  NONLIN HYDRAT
  SOLVE PARDIS
  SAVE STEPS ALL /
 END EXECUT
 BEGIN OUTPUT
  TEXT "Analysis output"
  BINARY
  SELECT STEPS ALL /
 END OUTPUT
*NONLIN LABEL="Structural nonlinear 4"
 BEGIN TYPE
  BEGIN PHYSIC
   CORROS OFF
   TOTCRK OFF
   INTERF OFF
  END PHYSIC
 END TYPE
 BEGIN EXECUT
  BEGIN LOAD
   LOADNR 4
   STEPS EXPLIC
  END LOAD
  ITERAT METHOD NEWTON
 END EXECUT
 BEGIN EXECUT
```

```
 TEXT "new execute block 2"
 TIME STEPS EXPLIC SIZES 540.000(25)
 BEGIN ITERAT
  MAXITE 100
  METHOD NEWTON
  LINESE
 END ITERAT
END EXECUT
SOLVE PARDIS
BEGIN OUTPUT
 TEXT "Output"
 BINARY
 SELECT STEPS ALL /
 STRAIN TOTAL GREEN GLOBAL XX YY ZZ XY YZ ZX
 STRAIN TEMPER GREEN GLOBAL XX YY ZZ XY YZ ZX
 STRAIN SHRINK GREEN VOLUME
 BEGIN STRAIN
  BEGIN TOTAL
   BEGIN GREEN
    BEGIN PRINCI
     "1" "2" "3"
     NODES
    END PRINCI
   END GREEN
  END TOTAL
 END STRAIN
 BEGIN STRAIN
  BEGIN CREEP
   BEGIN GREEN
    BEGIN PRINCI
     "1" "2" "3"
     NODES
    END PRINCI
```

```
    END GREEN
   END CREEP
  END STRAIN
  BEGIN STRESS
   BEGIN TOTAL
    BEGIN CAUCHY
     BEGIN PRINCI
      "1" "2" "3"
      NODES
     END PRINCI
    END CAUCHY
   END TOTAL
  END STRESS
  STRESS TOTAL CAUCHY GLOBAL XX YY ZZ XY YZ ZX
  TEMPER TOTAL
  MATURI TOTAL
 END OUTPUT
```

***PHASE LABEL="Phased 5"**

```
 BEGIN ACTIVE
  ELEMEN "Low Slab" "Low Slab plane interface" \
       "Low Slab plane interface set 3" "Low Slab plane interface set 4" \
       "Low Slab plane interface set 5" "Mid Slab" \
       "Mid Slab plane interface" "Mid Slab plane interface set 8" \
       "Mid Slab plane interface set 9" "Soil" "Soil plane interface" \
       "Soil plane interface set 12" "Up Slab" "Up Slab plane interface" \
       "Up Slab plane interface set 15" "Up Slab plane interface set 16" \
       "Up Slab plane interface set 17" "Up Slab plane interface set 18" \
       "Low Wall" "Low Wall plane interface" \
       "Low Wall plane interface set 21" \
       "Low Wall plane interface set 22" "Up Wall" \
       "Up Wall plane interface" "Up Wall plane interface set 25" \
       "Up Wall plane interface set 26" "Up Wall plane interface set 27" /
  SUPPOR "Soil Support" "Symmetry Soil" "Symm Bslab" "Symm ISlab" \
```

```
 "Symm USlab" "Symm BWall" "Symm UWall"
   FIXHEA ALL
   FIXPOT ALL
   FIXTEM ALL
   TYINGS ALL
 END ACTIVE
*HEATTR LABEL="Transient heat transfer 5"
 BEGIN INITIA
   BEGIN NONLIN
     HYDRAT DGRINI 0.01
     EQUAGE
   END NONLIN
   TEMPER INPUT FIELD 6
   SOLVE PARDIS
 END INITIA
 BEGIN EXECUT
   SIZES 3600.00(104)
   NONLIN HYDRAT
   SOLVE PARDIS
   SAVE STEPS ALL /
 END EXECUT
 BEGIN OUTPUT
   TEXT "Analysis output"
   BINARY
   SELECT STEPS ALL /
 END OUTPUT
*NONLIN LABEL=" Structural nonlinear 5"
 BEGIN TYPE
   BEGIN PHYSIC
     CORROS OFF
     TOTCRK OFF
     INTERF OFF
   END PHYSIC
```

```
END TYPE
BEGIN EXECUT
 BEGIN LOAD
  LOADNR 5
  STEPS EXPLIC
 END LOAD
 ITERAT METHOD NEWTON
END EXECUT
BEGIN EXECUT
 TEXT "new execute block 2"
 TIME STEPS EXPLIC SIZES 3600.00(104)
 BEGIN ITERAT
  MAXITE 100
  METHOD NEWTON
  LINESE
 END ITERAT
END EXECUT
SOLVE PARDIS
BEGIN OUTPUT
 TEXT "Output"
 BINARY
 SELECT STEPS ALL /
 STRAIN TOTAL GREEN GLOBAL XX YY ZZ XY YZ ZX
 STRAIN TEMPER GREEN GLOBAL XX YY ZZ XY YZ ZX
 STRAIN SHRINK GREEN VOLUME
 BEGIN STRAIN
  BEGIN TOTAL
   BEGIN GREEN
    BEGIN PRINCI
     "1" "2" "3"
     NODES
    END PRINCI
   END GREEN
```

```
    END TOTAL
  END STRAIN
  BEGIN STRAIN
    BEGIN CREEP
      BEGIN GREEN
        BEGIN PRINCI
          "1" "2" "3"
          NODES
        END PRINCI
      END GREEN
    END CREEP
  END STRAIN
  BEGIN STRESS
    BEGIN TOTAL
      BEGIN CAUCHY
        BEGIN PRINCI
          "1" "2" "3"
          NODES
        END PRINCI
      END CAUCHY
    END TOTAL
  END STRESS
  STRESS TOTAL CAUCHY GLOBAL XX YY ZZ XY YZ ZX
  TEMPER TOTAL
  MATURI TOTAL
 END OUTPUT
```

***PHASE LABEL="Phased 6"**

```
 BEGIN ACTIVE
   ELEMEN "Low Slab" "Low Slab plane interface" \
          "Low Slab plane interface set 3" "Low Slab plane interface set 4" \
          "Low Slab plane interface set 5" "Mid Slab" \
          "Mid Slab plane interface" "Mid Slab plane interface set 8" \
          "Mid Slab plane interface set 9" "Soil" "Soil plane interface" \
```

```
        "Soil plane interface set 12" "Up Slab" "Up Slab plane interface" \
        "Up Slab plane interface set 15" "Up Slab plane interface set 16" \
        "Up Slab plane interface set 17" "Up Slab plane interface set 18" \
        "Low Wall" "Low Wall plane interface" \
        "Low Wall plane interface set 21" \
        "Low Wall plane interface set 22" "Up Wall" \
        "Up Wall plane interface" "Up Wall plane interface set 25" \
        "Up Wall plane interface set 26" "Up Wall plane interface set 27" /
   SUPPOR "Soil Support" "Symmetry Soil" "Symm Bslab" "Symm ISlab" \
 "Symm USlab" "Symm BWall" "Symm UWall"
   FIXHEA ALL
   FIXPOT ALL
   FIXTEM ALL
   TYINGS ALL
 END ACTIVE
*HEATTR LABEL="Transient heat transfer 6"
 BEGIN INITIA
   BEGIN NONLIN
     HYDRAT DGRINI 0.01
     EQUAGE
   END NONLIN
   TEMPER OFF
   SOLVE PARDIS
 END INITIA
 BEGIN EXECUT
   SIZES 86400.0(11)
   NONLIN HYDRAT
   SOLVE PARDIS
   SAVE STEPS ALL /
 END EXECUT
 BEGIN OUTPUT
   TEXT "Analysis output"
   BINARY
```

```
  SELECT STEPS ALL /
 END OUTPUT
*NONLIN LABEL="Structural nonlinear 6"
 BEGIN TYPE
  BEGIN PHYSIC
   CORROS OFF
   TOTCRK OFF
   INTERF OFF
  END PHYSIC
 END TYPE
 BEGIN EXECUT
  TEXT "new execute block 2"
  TIME STEPS EXPLIC SIZES 86400.0(11)
  BEGIN ITERAT
   MAXITE 100
   METHOD NEWTON
   LINESE
  END ITERAT
 END EXECUT
 SOLVE PARDIS
 BEGIN OUTPUT
  TEXT "Output"
  BINARY
  SELECT STEPS ALL /
  STRAIN TOTAL GREEN GLOBAL XX YY ZZ XY YZ ZX
  STRAIN TEMPER GREEN GLOBAL XX YY ZZ XY YZ ZX
  STRAIN SHRINK GREEN VOLUME
  BEGIN STRAIN
   BEGIN TOTAL
    BEGIN GREEN
     BEGIN PRINCI
      "1" "2" "3"
      NODES
```

```
        END PRINCI
       END GREEN
      END TOTAL
    END STRAIN
    BEGIN STRAIN
     BEGIN CREEP
      BEGIN GREEN
       BEGIN PRINCI
        "1" "2" "3"
        NODES
       END PRINCI
      END GREEN
     END CREEP
    END STRAIN
    BEGIN STRESS
     BEGIN TOTAL
      BEGIN CAUCHY
       BEGIN PRINCI
        "1" "2" "3"
        NODES
       END PRINCI
      END CAUCHY
     END TOTAL
    END STRESS
    STRESS TOTAL CAUCHY GLOBAL XX YY ZZ XY YZ ZX
    TEMPER TOTAL
    MATURI TOTAL
  END OUTPUT
```

***PHASE LABEL="Phased 7"**

```
  BEGIN ACTIVE
    ELEMEN "Low Slab" "Low Slab plane interface" \
          "Low Slab plane interface set 3" "Low Slab plane interface set 4" \
          "Low Slab plane interface set 5" "Mid Slab" \
```

```
        "Mid Slab plane interface" "Mid Slab plane interface set 8" \
        "Mid Slab plane interface set 9" "Soil" "Soil plane interface" \
        "Soil plane interface set 12" "Up Slab" "Up Slab plane interface" \
        "Up Slab plane interface set 15" "Up Slab plane interface set 16" \
        "Up Slab plane interface set 17" "Up Slab plane interface set 18" \
        "Low Wall" "Low Wall plane interface" \
        "Low Wall plane interface set 21" \
        "Low Wall plane interface set 22" "Up Wall" \
        "Up Wall plane interface" "Up Wall plane interface set 25" \
        "Up Wall plane interface set 26" "Up Wall plane interface set 27" /
   SUPPOR "Soil Support" "Symmetry Soil" "Symm Bslab" "Symm ISlab" \
 "Symm USlab" "Symm BWall" "Symm UWall"
   FIXHEA ALL
   FIXPOT ALL
   FIXTEM ALL
   TYINGS ALL
 END ACTIVE
*HEATTR LABEL="Transient heat transfer 7"
 BEGIN INITIA
   BEGIN NONLIN
     HYDRAT DGRINI 0.01
     EQUAGE
   END NONLIN
   TEMPER OFF
   SOLVE PARDIS
 END INITIA
 BEGIN EXECUT
   SIZES 5.85882e+06
   NONLIN HYDRAT
   SOLVE PARDIS
   SAVE STEPS ALL /
 END EXECUT
 BEGIN OUTPUT
```

```
  TEXT "Analysis output"
  BINARY
  SELECT STEPS ALL /
 END OUTPUT
*NONLIN LABEL="Structural nonlinear 7"
 BEGIN TYPE
  BEGIN PHYSIC
   CORROS OFF
   TOTCRK OFF
   INTERF OFF
  END PHYSIC
 END TYPE
 BEGIN EXECUT
  TEXT "new execute block 2"
  TIME STEPS EXPLIC SIZES 5.85882e+06
  BEGIN ITERAT
   MAXITE 100
   METHOD NEWTON
   LINESE
  END ITERAT
 END EXECUT
 SOLVE PARDIS
 BEGIN OUTPUT
  TEXT "Output"
  BINARY
  SELECT STEPS ALL /
  STRAIN TOTAL GREEN GLOBAL XX YY ZZ XY YZ ZX
  STRAIN TEMPER GREEN GLOBAL XX YY ZZ XY YZ ZX
  STRAIN SHRINK GREEN VOLUME
  BEGIN STRAIN
   BEGIN TOTAL
    BEGIN GREEN
     BEGIN PRINCI
```

```
        "1" "2" "3"
        NODES
       END PRINCI
      END GREEN
     END TOTAL
    END STRAIN
    BEGIN STRAIN
     BEGIN CREEP
      BEGIN GREEN
       BEGIN PRINCI
        "1" "2" "3"
        NODES
       END PRINCI
      END GREEN
     END CREEP
    END STRAIN
    BEGIN STRESS
     BEGIN TOTAL
      BEGIN CAUCHY
       BEGIN PRINCI
        "1" "2" "3"
        NODES
       END PRINCI
      END CAUCHY
     END TOTAL
    END STRESS
    STRESS TOTAL CAUCHY GLOBAL XX YY ZZ XY YZ ZX
    TEMPER TOTAL
    MATURI TOTAL
   END OUTPUT
*PHASE LABEL="Phased 8"
   BEGIN ACTIVE
    ELEMEN "Low Slab" "Low Slab plane interface" \
```

```
        "Low Slab plane interface set 3" "Low Slab plane interface set 4" \
        "Low Slab plane interface set 5" "Mid Slab" \
        "Mid Slab plane interface" "Mid Slab plane interface set 8" \
        "Mid Slab plane interface set 9" "Soil" "Soil plane interface" \
        "Soil plane interface set 12" "Up Slab" "Up Slab plane interface" \
        "Up Slab plane interface set 15" "Up Slab plane interface set 16" \
        "Up Slab plane interface set 17" "Up Slab plane interface set 18" \
        "Low Wall" "Low Wall plane interface" \
        "Low Wall plane interface set 21" \
        "Low Wall plane interface set 22" "Up Wall" \
        "Up Wall plane interface set 25" "Up Wall plane interface set 26" \
        "Up Wall plane interface set 27" "Roof Slab" \
        "Roof Slab plane interface" "Roof Slab plane interface set 30" \
        "Roof Slab plane interface set 31" \
        "Roof Slab plane interface set 32" \
        "Roof Slab plane interface set 33" \
        "Roof Slab plane interface set 34" \
        "Roof Slab plane interface set 35" \
        "Roof Slab plane interface set 36" /
   SUPPOR "Soil Support" "Symmetry Soil" "Symm Bslab" "Symm ISlab" \
 "Symm USlab" "Symm BWall" "Symm UWall" "Top Slab"
   FIXHEA ALL
   FIXPOT ALL
   FIXTEM ALL
   TYINGS ALL
  END ACTIVE
*HEATTR LABEL="Transient heat transfer 8"
  BEGIN INITIA
   BEGIN NONLIN
    HYDRAT DGRINI 0.01
    EQUAGE
   END NONLIN
   TEMPER INPUT FIELD 7
```

```
  SOLVE PARDIS
 END INITIA
 BEGIN EXECUT
  SIZES 1800.00(96)
  NONLIN HYDRAT
  SOLVE PARDIS
  SAVE STEPS ALL /
 END EXECUT
 BEGIN OUTPUT
  TEXT "Analysis output"
  BINARY
  SELECT STEPS ALL /
 END OUTPUT
*NONLIN LABEL="Structural nonlinear 8"
 BEGIN TYPE
  BEGIN PHYSIC
   CORROS OFF
   TOTCRK OFF
   INTERF OFF
  END PHYSIC
 END TYPE
 BEGIN EXECUT
  BEGIN LOAD
   LOADNR 6
   STEPS EXPLIC
  END LOAD
  ITERAT METHOD NEWTON
 END EXECUT
 BEGIN EXECUT
  TEXT "new execute block 2"
  TIME STEPS EXPLIC SIZES 1800.00(96)
  BEGIN ITERAT
   MAXITE 100
```

```
  METHOD NEWTON
  LINESE
 END ITERAT
END EXECUT
SOLVE PARDIS
BEGIN OUTPUT
 TEXT "Output"
 BINARY
 SELECT STEPS ALL /
 STRAIN TOTAL GREEN GLOBAL XX YY ZZ XY YZ ZX
 STRAIN TEMPER GREEN GLOBAL XX YY ZZ XY YZ ZX
 STRAIN SHRINK GREEN VOLUME
 BEGIN STRAIN
  BEGIN TOTAL
   BEGIN GREEN
    BEGIN PRINCI
     "1" "2" "3"
     NODES
    END PRINCI
   END GREEN
  END TOTAL
 END STRAIN
 BEGIN STRAIN
  BEGIN CREEP
   BEGIN GREEN
    BEGIN PRINCI
     "1" "2" "3"
     NODES
    END PRINCI
   END GREEN
  END CREEP
 END STRAIN
 BEGIN STRESS
```

```
    BEGIN TOTAL
      BEGIN CAUCHY
        BEGIN PRINCI
          "1" "2" "3"
          NODES
        END PRINCI
      END CAUCHY
    END TOTAL
  END STRESS
  STRESS TOTAL CAUCHY GLOBAL XX YY ZZ XY YZ ZX
  TEMPER TOTAL
  MATURI TOTAL
 END OUTPUT
```

***PHASE LABEL="Phased 9"**

```
 BEGIN ACTIVE
  ELEMEN "Low Slab" "Low Slab plane interface" \
       "Low Slab plane interface set 3" "Low Slab plane interface set 4" \
       "Low Slab plane interface set 5" "Mid Slab" \
       "Mid Slab plane interface" "Mid Slab plane interface set 8" \
       "Mid Slab plane interface set 9" "Soil" "Soil plane interface" \
       "Soil plane interface set 12" "Up Slab" "Up Slab plane interface" \
       "Up Slab plane interface set 15" "Up Slab plane interface set 16" \
       "Up Slab plane interface set 17" "Up Slab plane interface set 18" \
       "Low Wall" "Low Wall plane interface" \
       "Low Wall plane interface set 21" \
       "Low Wall plane interface set 22" "Up Wall" \
       "Up Wall plane interface set 25" "Up Wall plane interface set 26" \
       "Up Wall plane interface set 27" "Roof Slab" \
       "Roof Slab plane interface" "Roof Slab plane interface set 30" \
       "Roof Slab plane interface set 31" \
       "Roof Slab plane interface set 32" \
       "Roof Slab plane interface set 33" \
       "Roof Slab plane interface set 34" \
```

```
        "Roof Slab plane interface set 35" \
        "Roof Slab plane interface set 36" /
   SUPPOR "Soil Support" "Symmetry Soil" "Symm Bslab" "Symm ISlab" \
 "Symm USlab" "Symm BWall" "Symm UWall" "Top Slab"
   FIXHEA ALL
   FIXPOT ALL
   FIXTEM ALL
   TYINGS ALL
 END ACTIVE
*HEATTR LABEL="Transient heat transfer 9"
 BEGIN INITIA
   BEGIN NONLIN
     HYDRAT DGRINI 0.01
     EQUAGE
   END NONLIN
   TEMPER INPUT FIELD 7
   SOLVE PARDIS
 END INITIA
 BEGIN EXECUT
   SIZES 7200.00(120)
   NONLIN HYDRAT
   SOLVE PARDIS
   SAVE STEPS ALL /
 END EXECUT
 BEGIN OUTPUT
   TEXT "Analysis output"
   BINARY
   SELECT STEPS ALL /
 END OUTPUT
*NONLIN LABEL="Structural nonlinear 9"
 BEGIN TYPE
   BEGIN PHYSIC
     CORROS OFF
```

```
    TOTCRK OFF
    INTERF OFF
  END PHYSIC
END TYPE
BEGIN EXECUT
  TEXT "new execute block 2"
  TIME STEPS EXPLIC SIZES 7200.00(120)
  BEGIN ITERAT
    MAXITE 100
    METHOD NEWTON
    LINESE
  END ITERAT
END EXECUT
SOLVE PARDIS
BEGIN OUTPUT
  TEXT "Output"
  BINARY
  SELECT STEPS ALL /
  STRAIN TOTAL GREEN GLOBAL XX YY ZZ XY YZ ZX
  STRAIN TEMPER GREEN GLOBAL XX YY ZZ XY YZ ZX
  STRAIN SHRINK GREEN VOLUME
  BEGIN STRAIN
    BEGIN TOTAL
      BEGIN GREEN
        BEGIN PRINCI
          "1" "2" "3"
          NODES
        END PRINCI
      END GREEN
    END TOTAL
  END STRAIN
  BEGIN STRAIN
    BEGIN CREEP
```

```
      BEGIN GREEN
       BEGIN PRINCI
        "1" "2" "3"
        NODES
       END PRINCI
      END GREEN
    END CREEP
  END STRAIN
  BEGIN STRESS
   BEGIN TOTAL
    BEGIN CAUCHY
     BEGIN PRINCI
      "1" "2" "3"
      NODES
     END PRINCI
    END CAUCHY
   END TOTAL
  END STRESS
  STRESS TOTAL CAUCHY GLOBAL XX YY ZZ XY YZ ZX
  TEMPER TOTAL
  MATURI TOTAL
 END OUTPUT
*END
```

Appendix 5 - Contest report

C:MockUpMarieholm3.CPR

Report

Contents

1 Software & Project Information

1.1 Software

System name: ConTeSt
System version: 1.0
Developed by: JEJMS Concrete AB

1.2 Project

Original filename: C:\Users\SEALEMAT\Desktop\Contest Mock Up\NoNameProject1.CPR
Created: 2016.05.02 09.46.02
Created by: SEALEMAT on SELCND5411Z44
Current filename: C:\Users\SEALEMAT\Desktop\Contest Mock Up\MockUpMarieholm3.CPR
Last change: 2016.05.13 13.16.55
Last change by: SEALEMAT on SELCND5411Z44

2 Geometry & Time

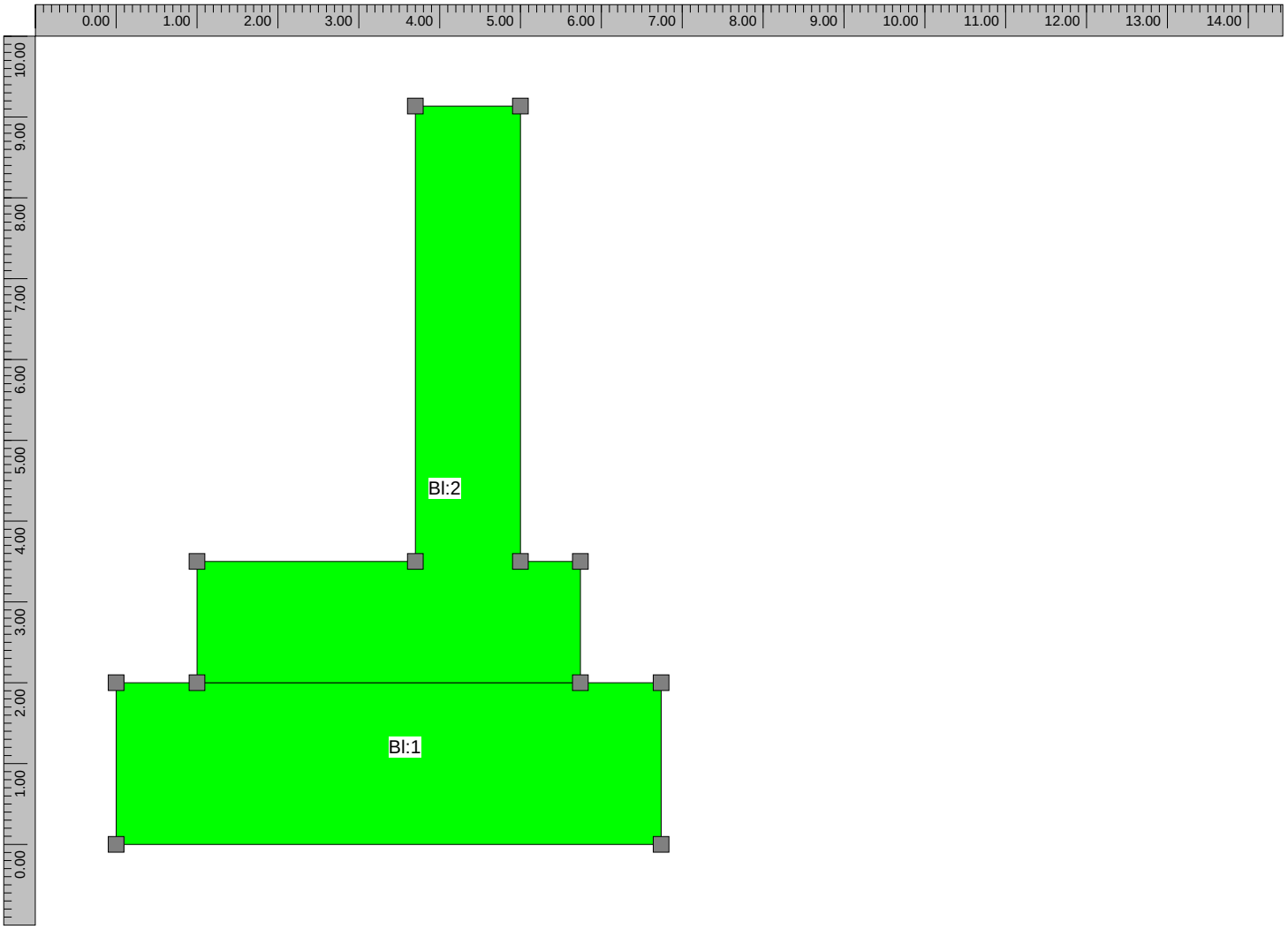

2.1 Description

2.1.1 Blocks

Block 1: (0.000;0.000) - (6.740;0.000) - (6.740;2.000) - (5.740;2.000) - (1.000;2.000) - (0.000;2.000)
Block 2: (5.740;2.000) - (5.740;3.500) - (5.000;3.500) - (5.000;9.135) - (3.700;9.135) - (3.700;3.500) - (1.000;3.500) - (1.000;2.000)

2.1.2 Computation time

Total time length: 1636 (h)

3 Element Size

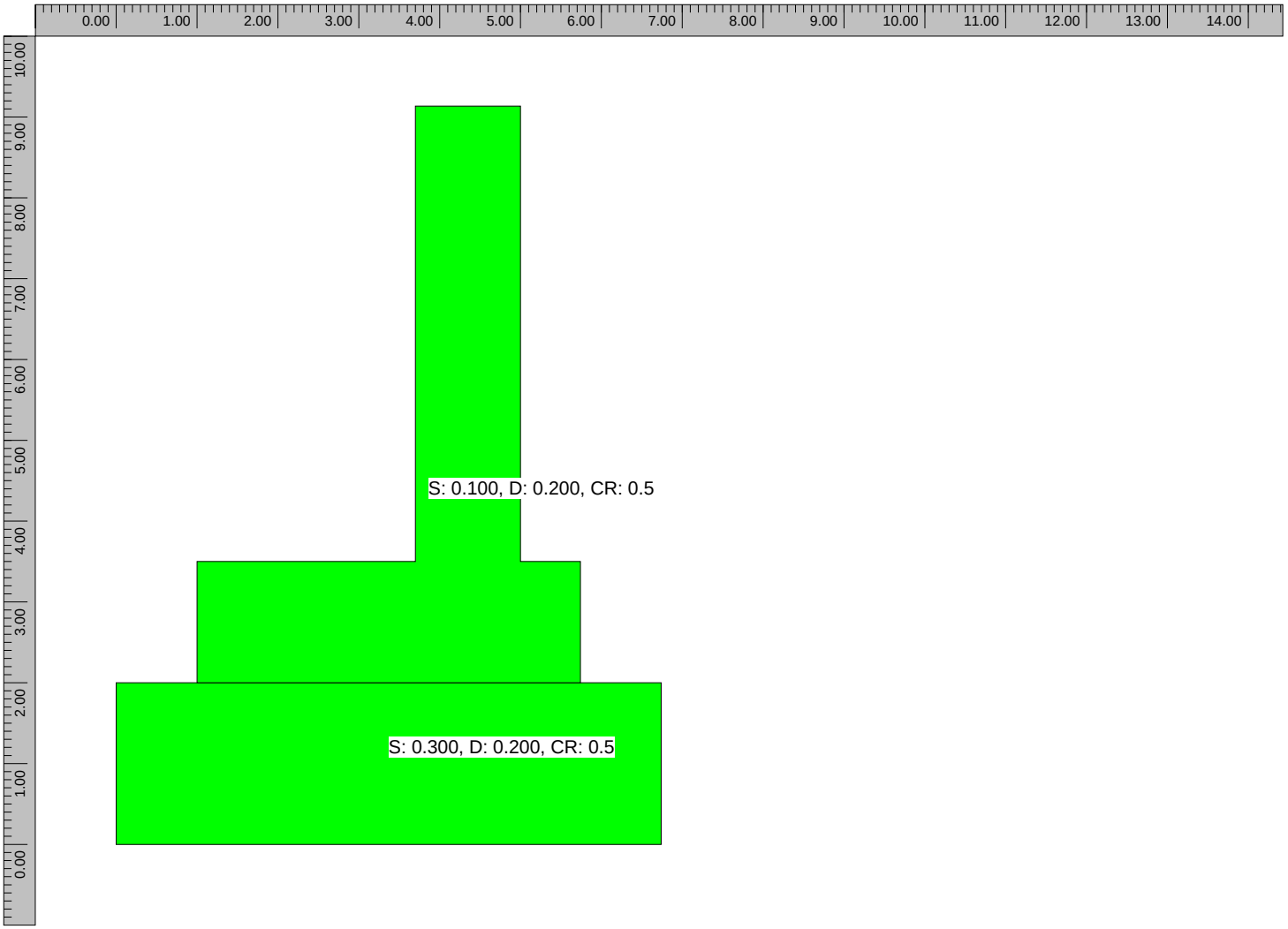

4 Computation Mesh

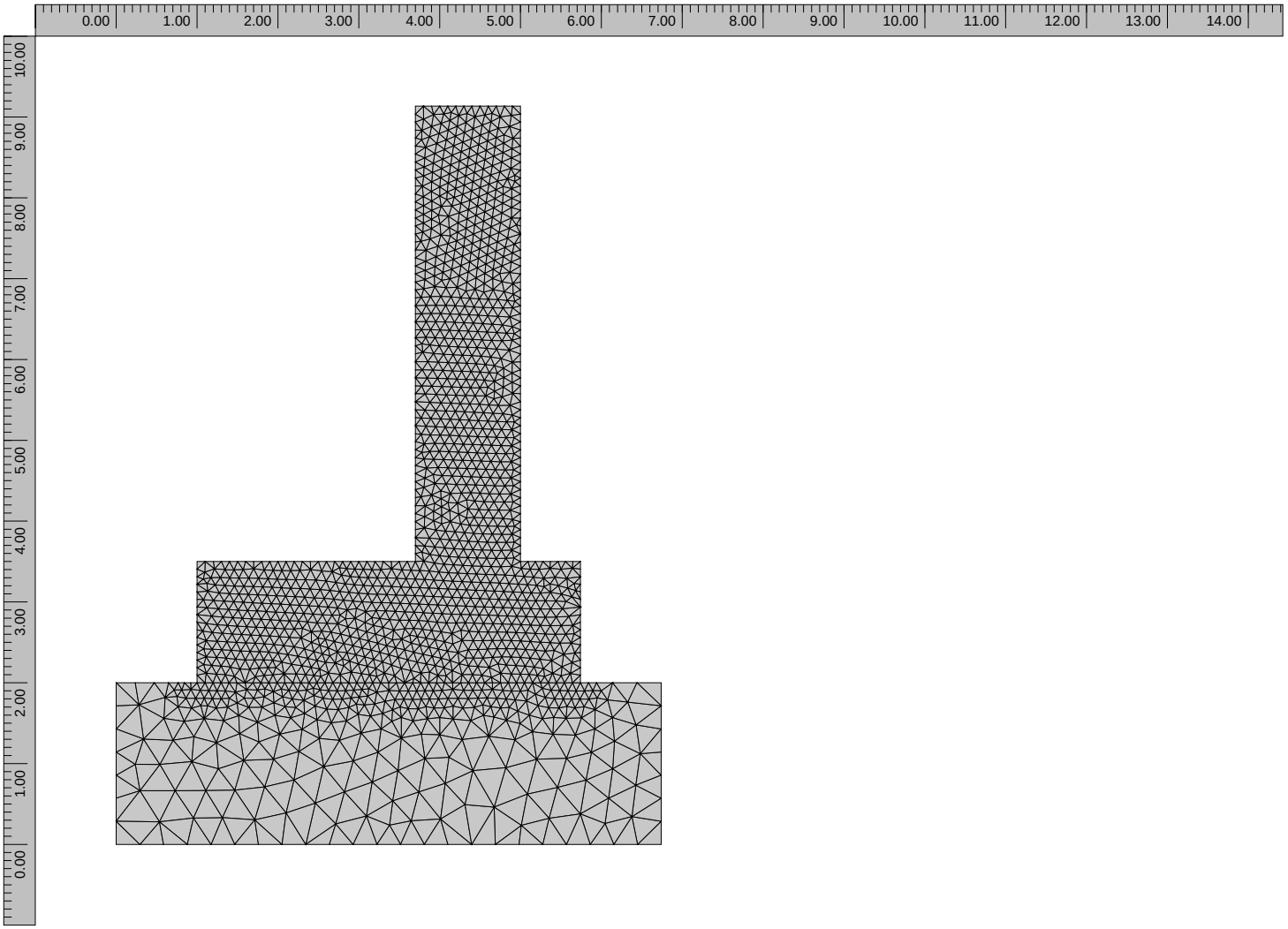

5 Heat Properties

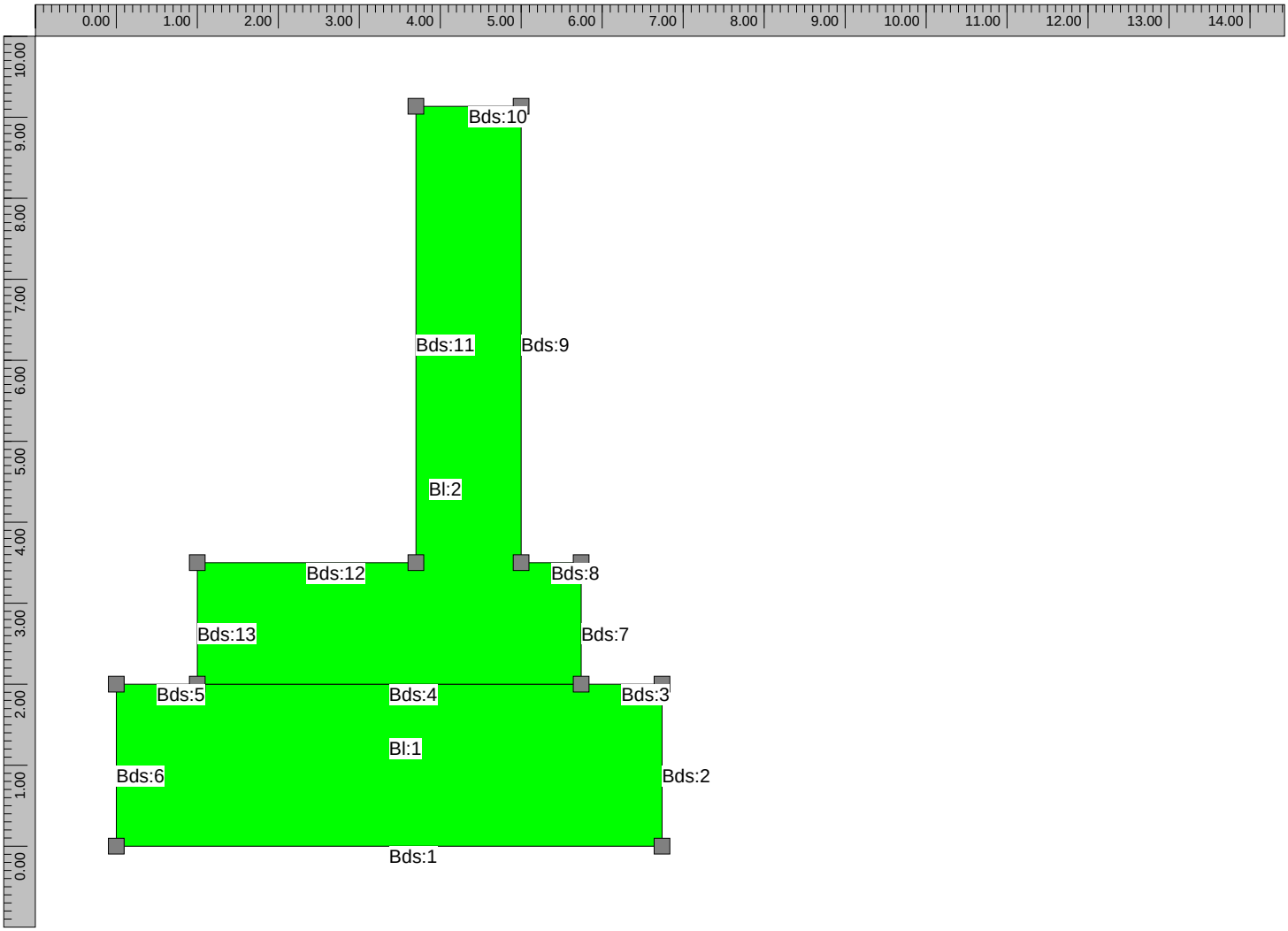

5.1 Description

5.1.3 Block type list

Soil: Other material
- Start temperature:
  - Constant: 20.0
- Material definition: Coarse grained soil
- Source
  - Luleå University of Technology 1997
- Description
  - e.g. till, moraine and gravel
- Original material parameters
  - Density: 2200 (kg/m³), Heat cap. 1400 (J/(kg·K))
  - Heat cond. 2.1 (W/m²K)

CEM I 42.5: Young concrete
- Start temperature:
  - Constant: 20.0
- Material definition: C35/45 w0/C = 0.40 Air entrainment (str)
- Source
  - Luleå University of Technology, Sweden
  - Tests during 1995 to 2004
  - Adjustment to a "general" data base 2006
- Description
  - Moderate heat cement (Degerhamn OPC) from Cementa AB in Sweden.

  - Primarily aimed for use in civil engineering structures.

Original material parameters
Density: 2350 (kg/m³), Heat cap. 1000 (J/(kg·K))
Heat cond. (W/m²K) as piece-wise linear function of equivalent time of maturity (h), (equ. time; heat cond.): (0;2.1), (12;2.1), (24;1.7), (10000;1.7),
C 425 (kg/m³), Wc 325000 (J/kg), Lambda1 2.2 (-), t1 4.75 (h), Kappa1 1.65 (-)
te0 0 (h), BetaD 1 (-), ThetaRef 4200 (K), Kappa3 0.5 (-)
s 0.331 (-), tS 5.556 (h), tA 8.334 (h), nA 1.148 (-)
Lambda2 0 (-), Tr2 1 (°C), Kappa2 0 (-)
Fcc28 53 (MPa)
Following material parameters are changed by the user
Density: 2411 (kg/m³)
C 415 (kg/m³)
Fcc28 54.5 (MPa)

5.1.4 Block connection list

Block 1: Soil
Block 2: CEM I 42.5, simulate filling

5.1.5 Boundary type list

Soil Bott
Temperature
Constant 5 (°C)
Heat transfer coefficient
Constant 30 (W/m²K)
Supplied heat
Constant 0 (W/m²)
Free Surface(Ext Temp)
Temperature
Constant 0 (°C)
Wind velocity
Constant 2 (m/s)
Heat transfer coefficient
Constant 500 (W/m²K)
Supplied heat
Constant 0 (W/m²)
Timber Form
Temperature
Constant 0 (°C)
Wind velocity
Constant 2 (m/s)
Heat transfer coefficient
Piece-wise constant (time (h);htc (W/m²K))
(0:7.77778)
Wood 0.018 (m)
(120:500)
Free Surface
Supplied heat
Constant 0 (W/m²)
Tarpaulin
Temperature
Constant 0 (°C)
Wind velocity
Constant 2 (m/s)
Heat transfer coefficient
Piece-wise constant (time (h);htc (W/m²K))
(0:18)
Expanded polyethylene 0.002 (m)
(120:500)
Free Surface
Supplied heat
Constant 0 (W/m²)
Moving Boundary: Moving boundary
Temperature
Constant 0 (°C)
Wind velocity
Constant 2 (m/s)

Heat transfer coefficient
Constant 500 (W/m²K)
Free Surface
Supplied heat
Constant 0 (W/m²)

5.1.6 Boundary connection list

Boundary segment 1: Soil Bott
Boundary segment 2: adiabatic (no heat flow)
Boundary segment 3: Free Surface(Ext Temp)
Boundary segment 4: inner segment (full thermal contact)
Boundary segment 5: Free Surface(Ext Temp)
Boundary segment 6: adiabatic (no heat flow)
Boundary segment 7: Timber Form
Boundary segment 8: Timber Form
Boundary segment 9: Timber Form
Boundary segment 10: Tarpaulin
Boundary segment 11: Timber Form
Boundary segment 12: Tarpaulin
Boundary segment 13: Timber Form

5.1.7 Inner point type list

5.1.8 Simulation of filling process for young concrete

Surface position as a piece-wise linear func. of time (time (h); y-coord. (m))
(0;2), (8.3;3.5), (15.8;9.135),

6 Plane-Surface Analysis

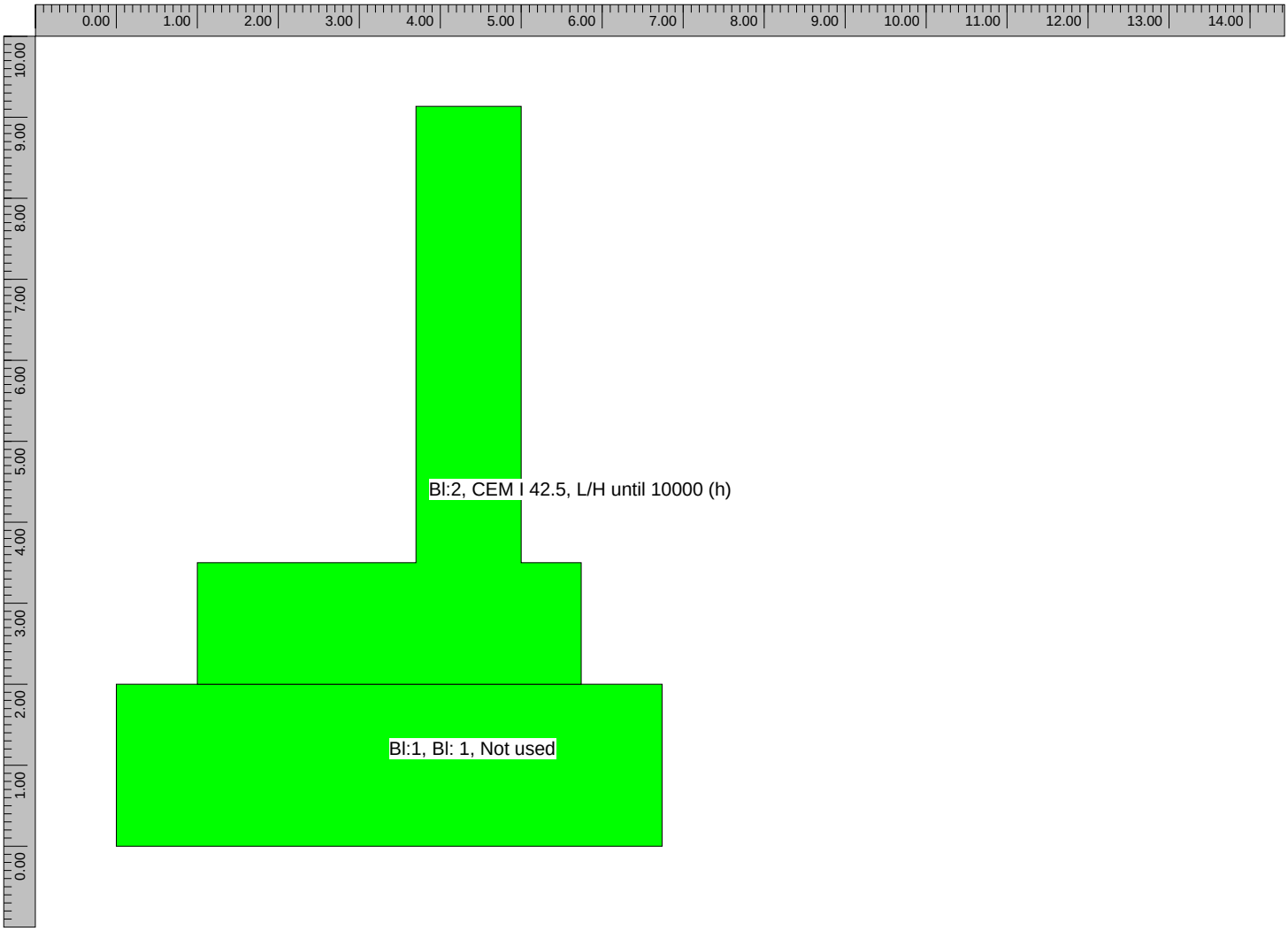

6.1 Description

6.1.9 Stress case

Default time stepping
- Translation
  - Free (0.000)
- Rotation around X-axis
  - Free (0.000)
- Rotation around Y-axis
  - Constant = 0.000
- Resilience: LH-based
  - Structure length: 7.000 (m)
  - Data source: Standard

6.1.10 Block data list

Block 2: CEM I 42.5, L/H until 10000 (h)

6.1.11 Block type list

CEM I 42.5: Young concrete
- Material definition: C35/45 w0/C = 0.40 Air entrainment (str)
- Source
  - Luleå University of Technology, Sweden
  - Tests during 1995 to 2004
  - Adjustment to a "general" data base 2006
- Description

Moderate heat cement (Degerhamn OPC) from Cementa AB in Sweden.

Primarily aimed for use in civil engineering structures.

Original material parameters
Po-ratio 0.18 (-), AlfaHeat 1.1e-05 (1/K), AlfaCool 9e-06 (1/K)
ThetaT 5000 (K), RelaxTime1 0.005 (d), TimeZero 0.25 (d)
Fcc28 53 (MPa), Fcref 53 (MPa), Ftref 3.68 (MPa)
Beta1 0.667 (-), Alfact 0.9 (-), RaaT 0 (-), RaaFi 0.9 (-)
KFi 2 (-), Eps1 0 (-), TimeS1 6 (h)
Eps2 -0.0001368 (-), TimeS2 24 (h), ThetaSH 120 (h), EthaSH 0.3 (-)
Relax: Age 0.249 (d), Units (GPa) 0.01 0.01 0.01 0.01 0.01 0.01 0.01 0.01
Relax: Age 0.5 (d), Units (GPa) 0.857221 0.256405 3.50511 1.16388 0.786528 0.439177 0.122558 0.101706
Relax: Age 1.077 (d), Units (GPa) 2.67304 4.80813 9.03774 3.7919 4.01799 2.19963 0.705556 0.754292
Relax: Age 2.321 (d), Units (GPa) 2.11587 4.25012 8.20966 7.23161 6.34904 3.5086 1.10078 0.684051
Relax: Age 5 (d), Units (GPa) 1.26691 2.75358 5.95473 8.32677 7.27362 3.96807 1.25504 3.14366
Relax: Age 10.772 (d), Units (GPa) 0.801966 1.78874 4.18532 7.43422 7.50287 4.12974 1.31843 7.05465
Relax: Age 23.208 (d), Units (GPa) 0.539145 1.25091 2.9427 6.22062 7.65742 4.43895 1.40975 9.90401
Relax: Age 50 (d), Units (GPa) 0.399024 0.941339 2.22694 5.08507 7.71281 5.01355 1.56935 11.4966
Relax: Age 107.722 (d), Units (GPa) 0.327423 0.75879 1.85384 4.2392 7.64612 5.8679 1.86341 11.9331
Relax: Age 232.079 (d), Units (GPa) 0.290016 0.655347 1.65703 3.71388 7.45375 6.88487 2.37315 11.4866
Following material parameters are changed by the user

7 Heat Computation Results

7.1 48 HOURS

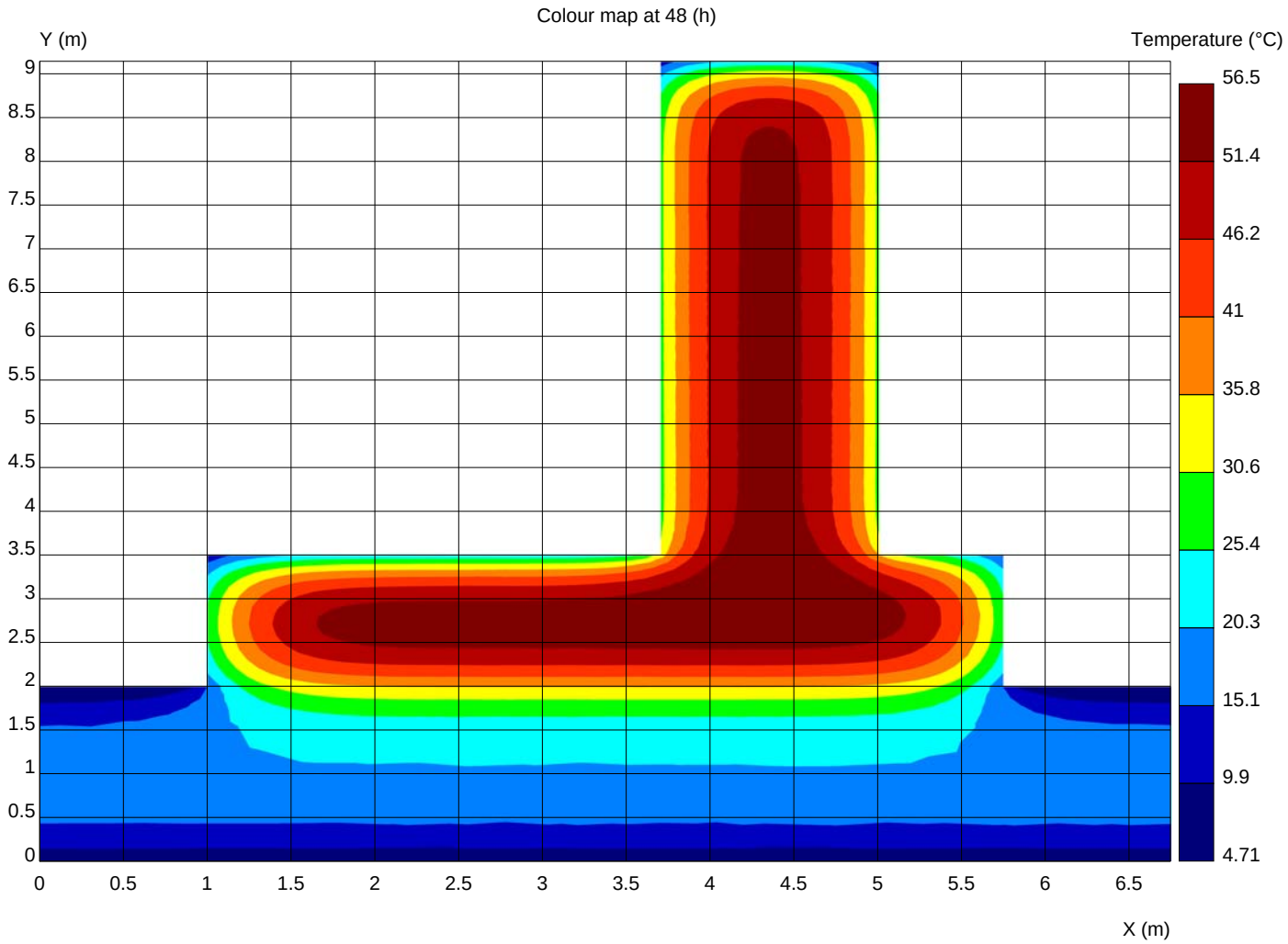

7.2 Max Temp

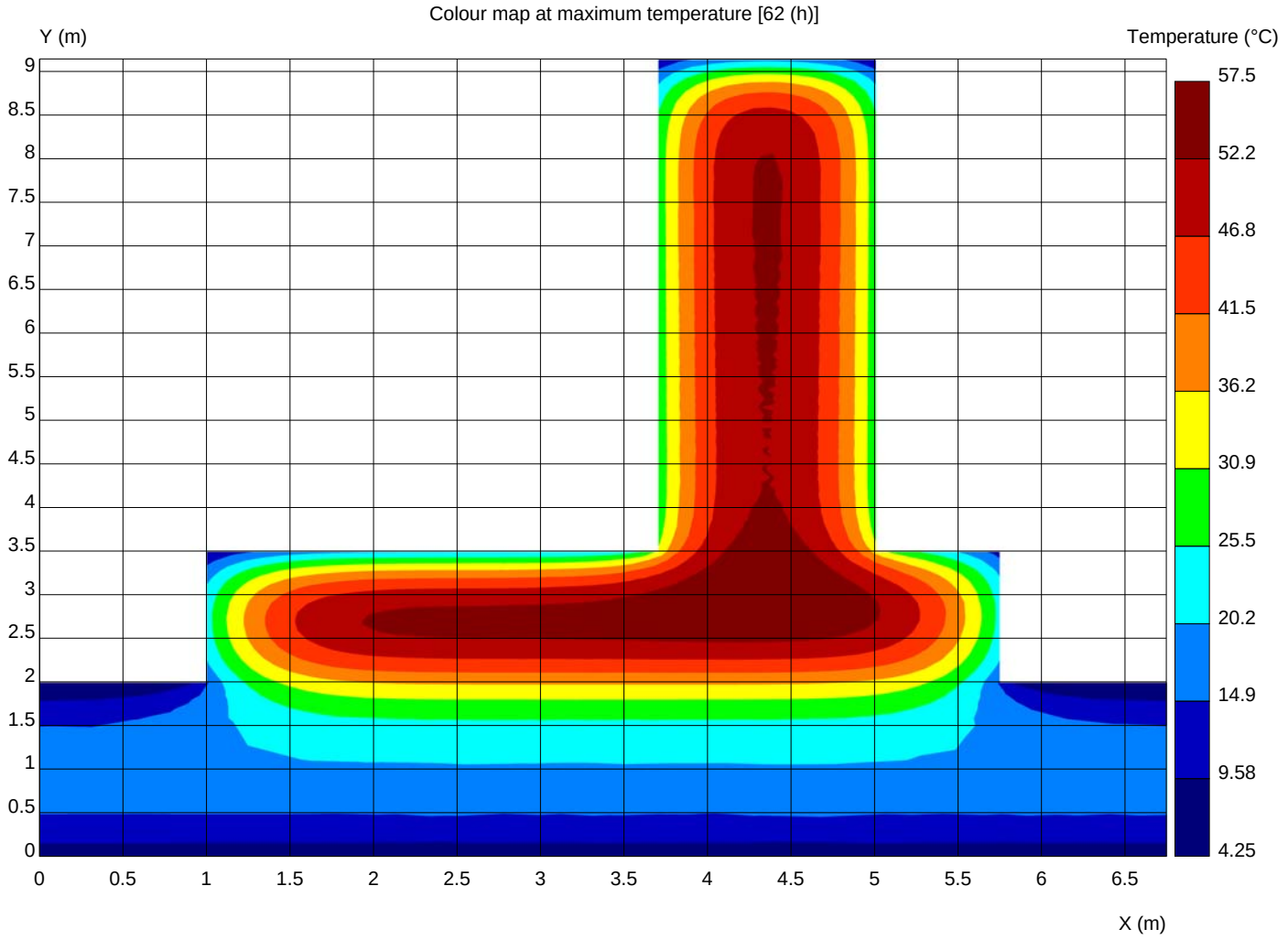
Colour map at maximum temperature [62 (h)]
Y (m)
Temperature (°C)
9
8.5
8
7.5
7
6.5
6
5.5
5
4.5
4
3.5
3
2.5
2
1.5
1
0.5
0
0
0.5
1
1.5
2
2.5
3
3.5
4
4.5
5
5.5
6
6.5
X (m)
57.5
52.2
46.8
41.5
36.2
30.9
25.5
20.2
14.9
9.58
4.25

7.3 Curve

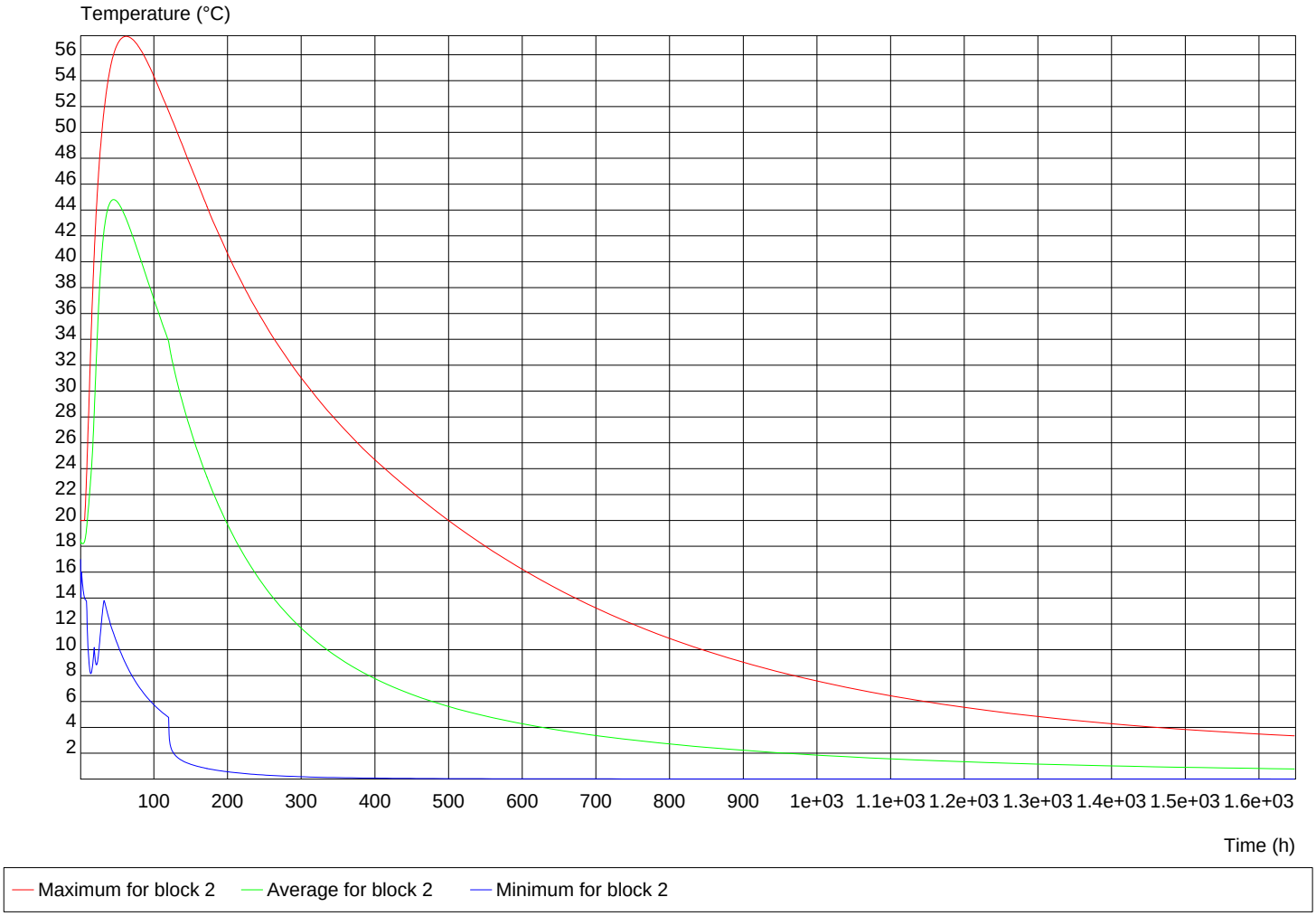
Temperature (°C)
56
54
52
50
48
46
44
42
40
38
36
34
32
30
28
26
24
22
20
18
16
14
12
10
8
6
4
2
100
200
300
400
500
600
700
800
900
1e+03
1.1e+03
1.2e+03
1.3e+03
1.4e+03
1.5e+03
1.6e+03
Time (h)
Maximum for block 2
Average for block 2
Minimum for block 2

7.4 Half Wall

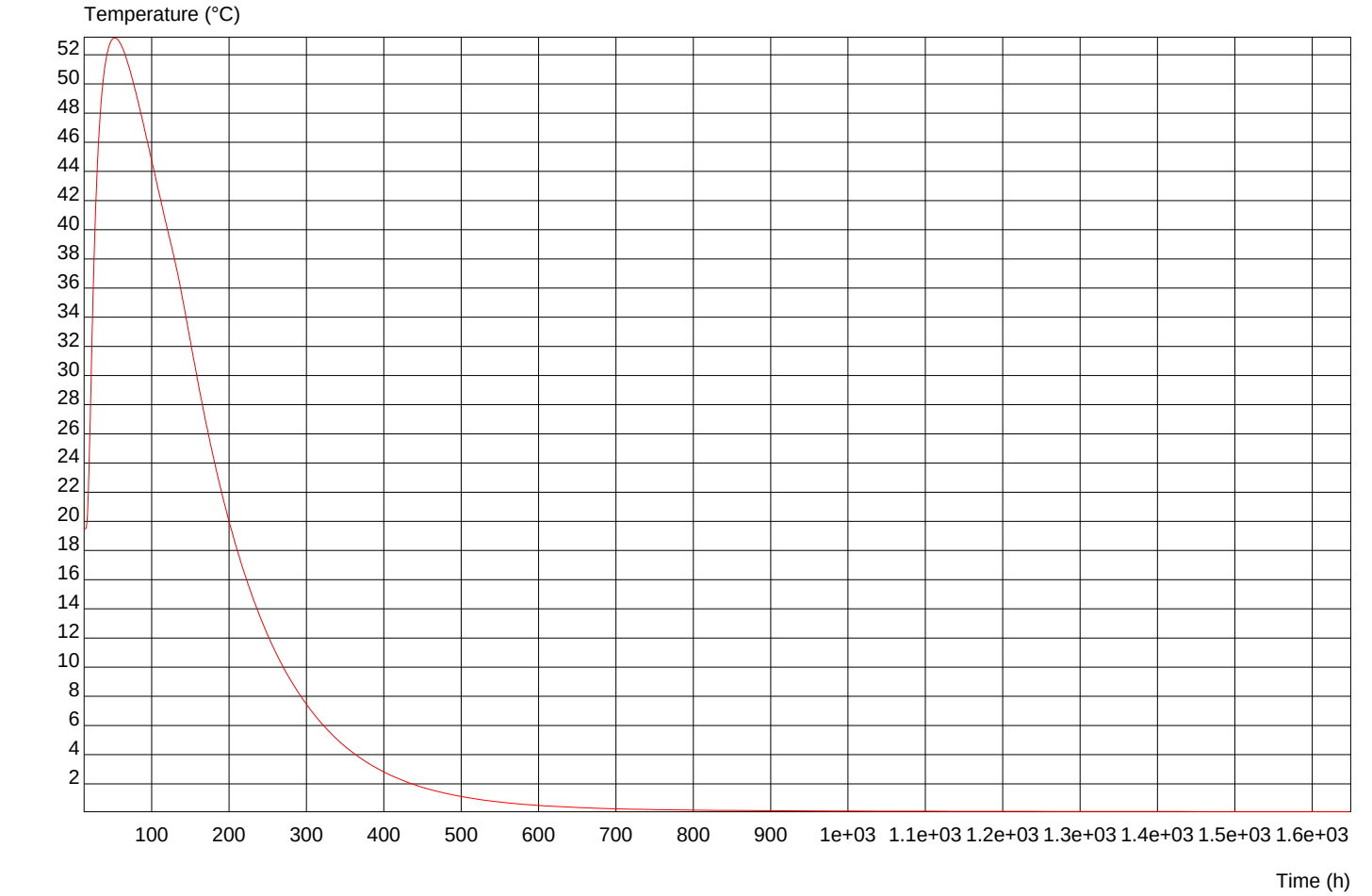
Temperature (°C)
52
50
48
46
44
42
40
38
36
34
32
30
28
26
24
22
20
18
16
14
12
10
8
6
4
2
100
200
300
400
500
600
700
800
900
1e+03
1.1e+03
1.2e+03
1.3e+03
1.4e+03
1.5e+03
1.6e+03
Time (h)
Point (4.350;6.315)

8 Plane-Surface Computation Results

8.1 48h

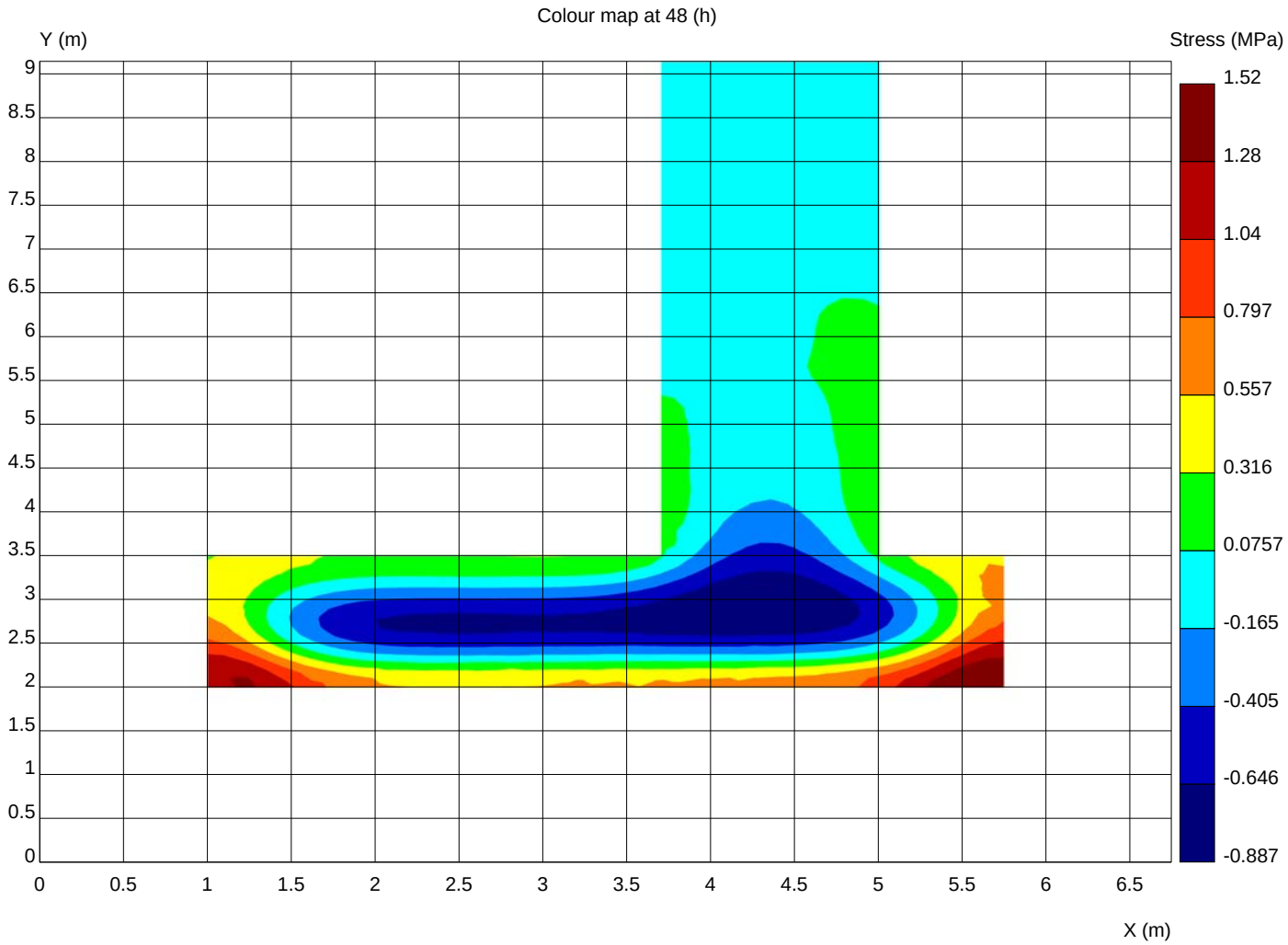

8.2 Max

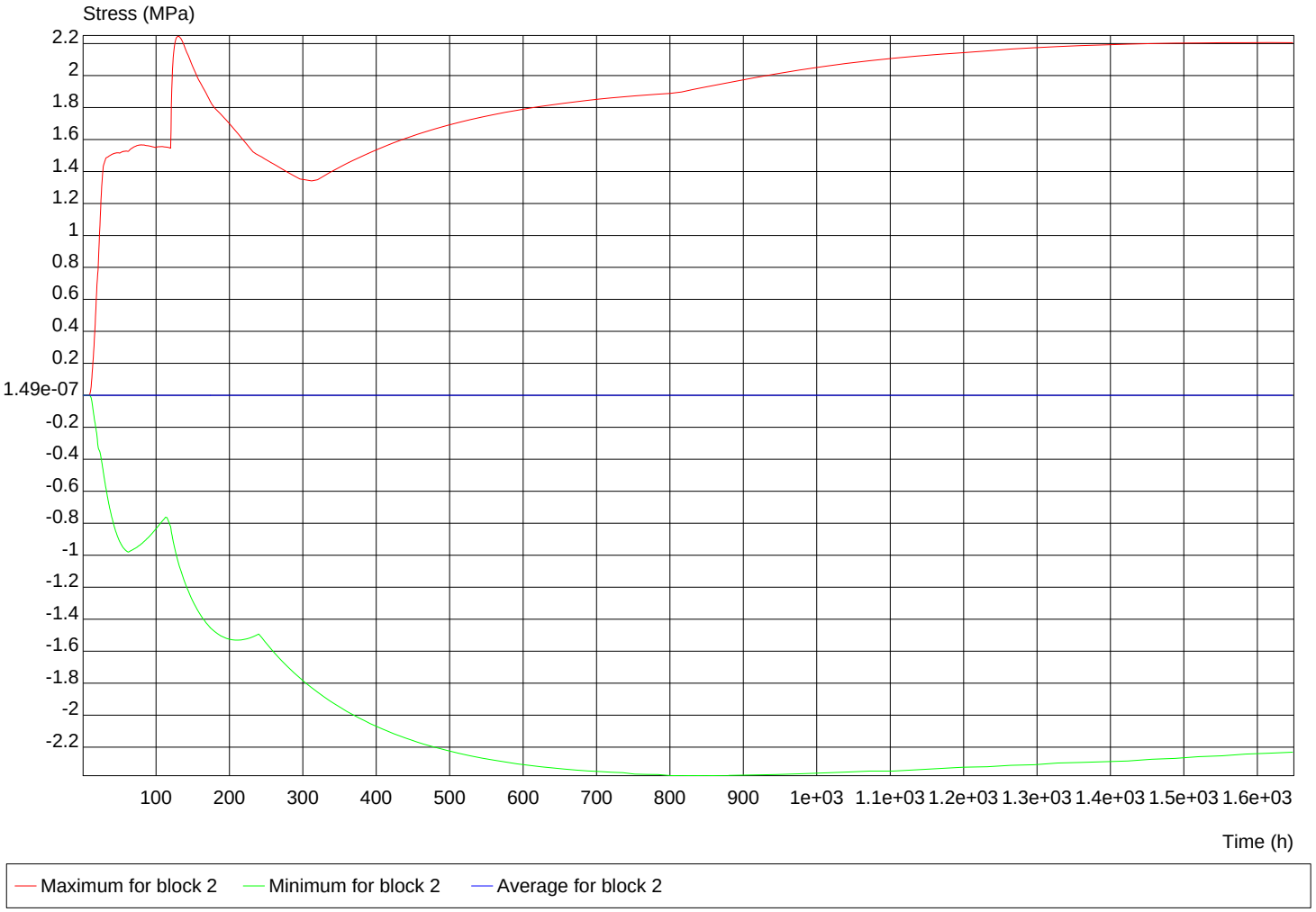

8.3 48h stress/strength

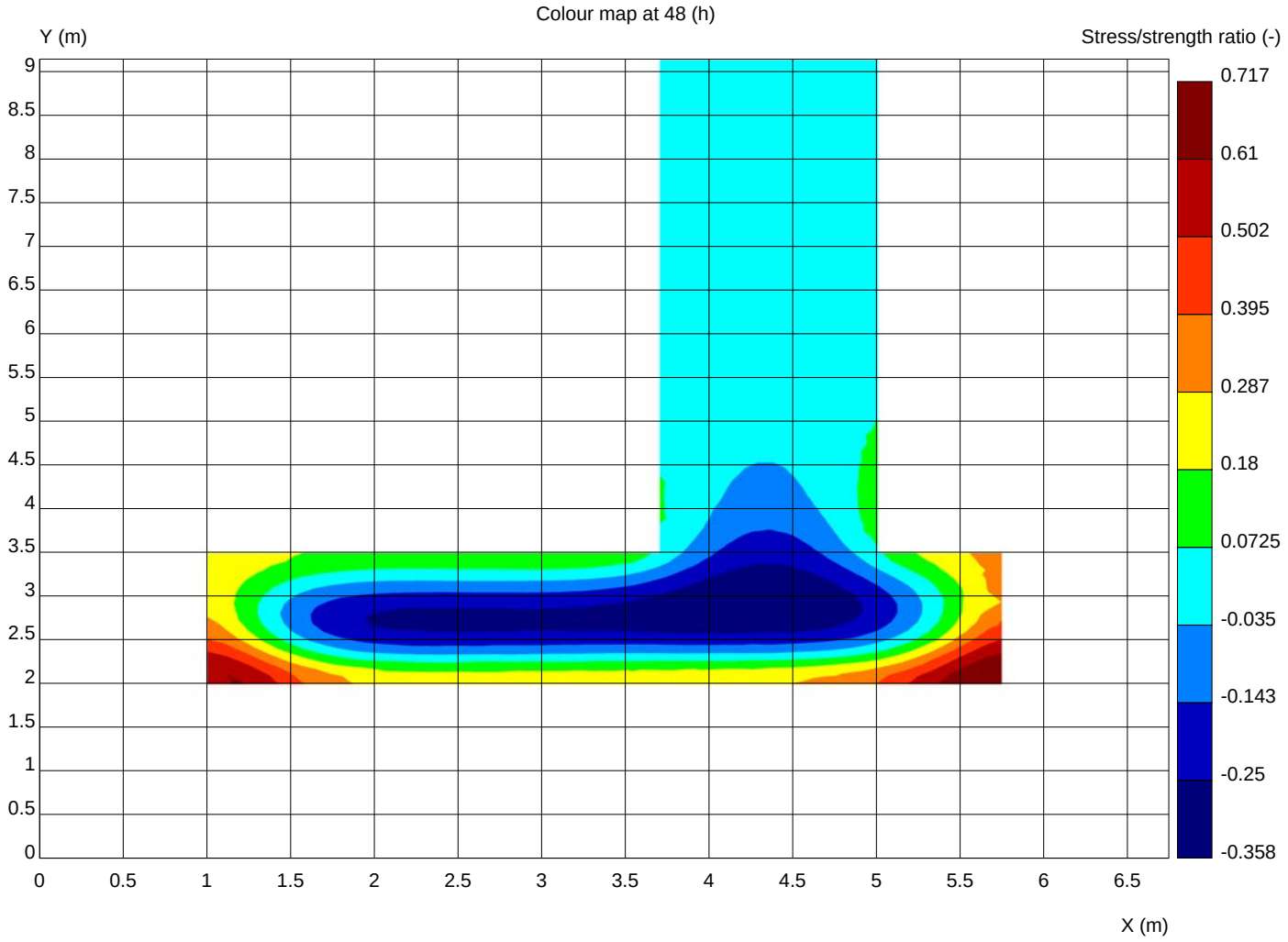

8.4 Max stress/strength

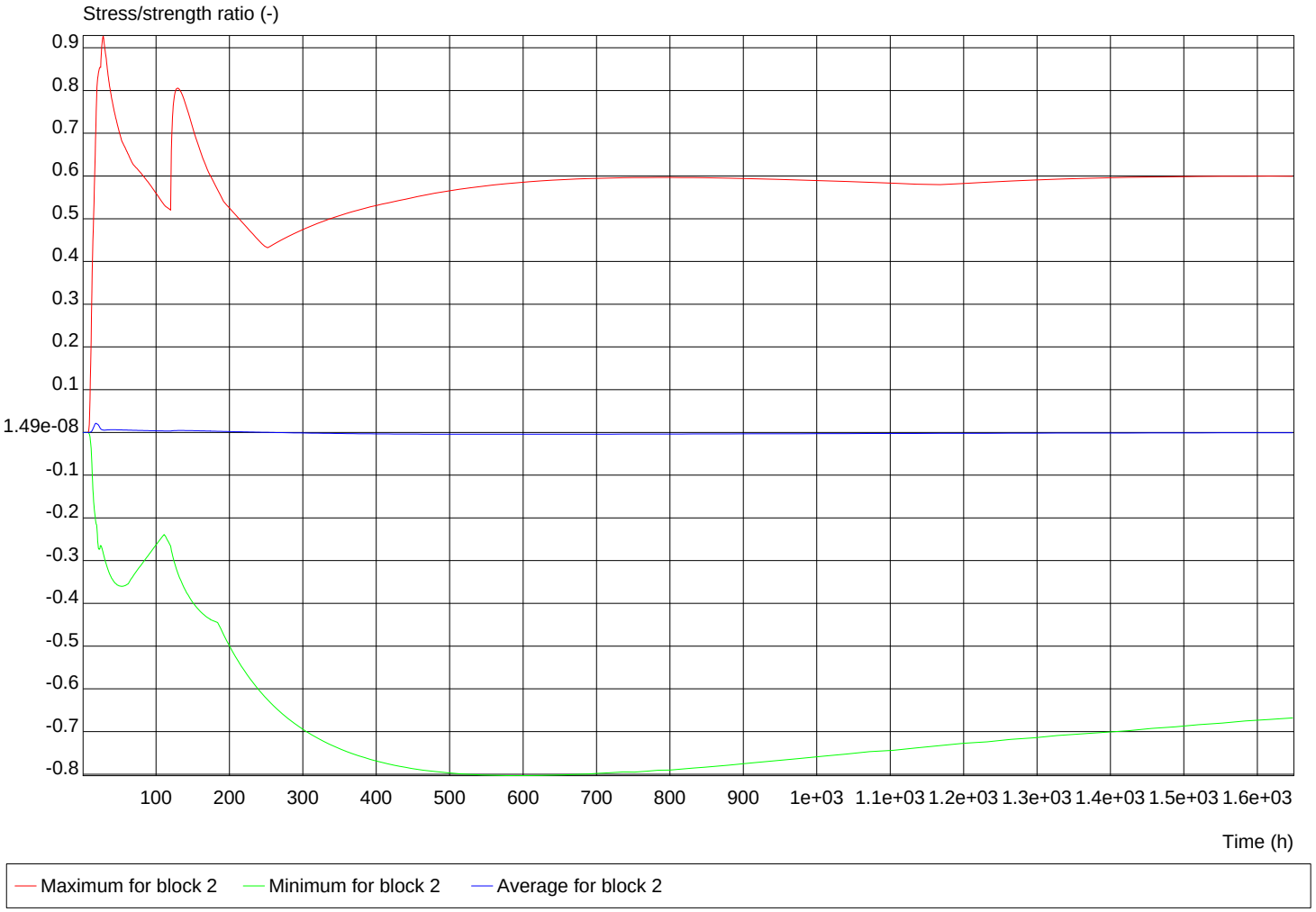
Stress/strength ratio (-)
0.9
0.8
0.7
0.6
0.5
0.4
0.3
0.2
0.1
1.49e-08
-0.1
-0.2
-0.3
-0.4
-0.5
-0.6
-0.7
-0.8
100
200
300
400
500
600
700
800
900
1e+03
1.1e+03
1.2e+03
1.3e+03
1.4e+03
1.5e+03
1.6e+03
Time (h)
Maximum for block 2
Minimum for block 2
Average for block 2

8.5 strstr

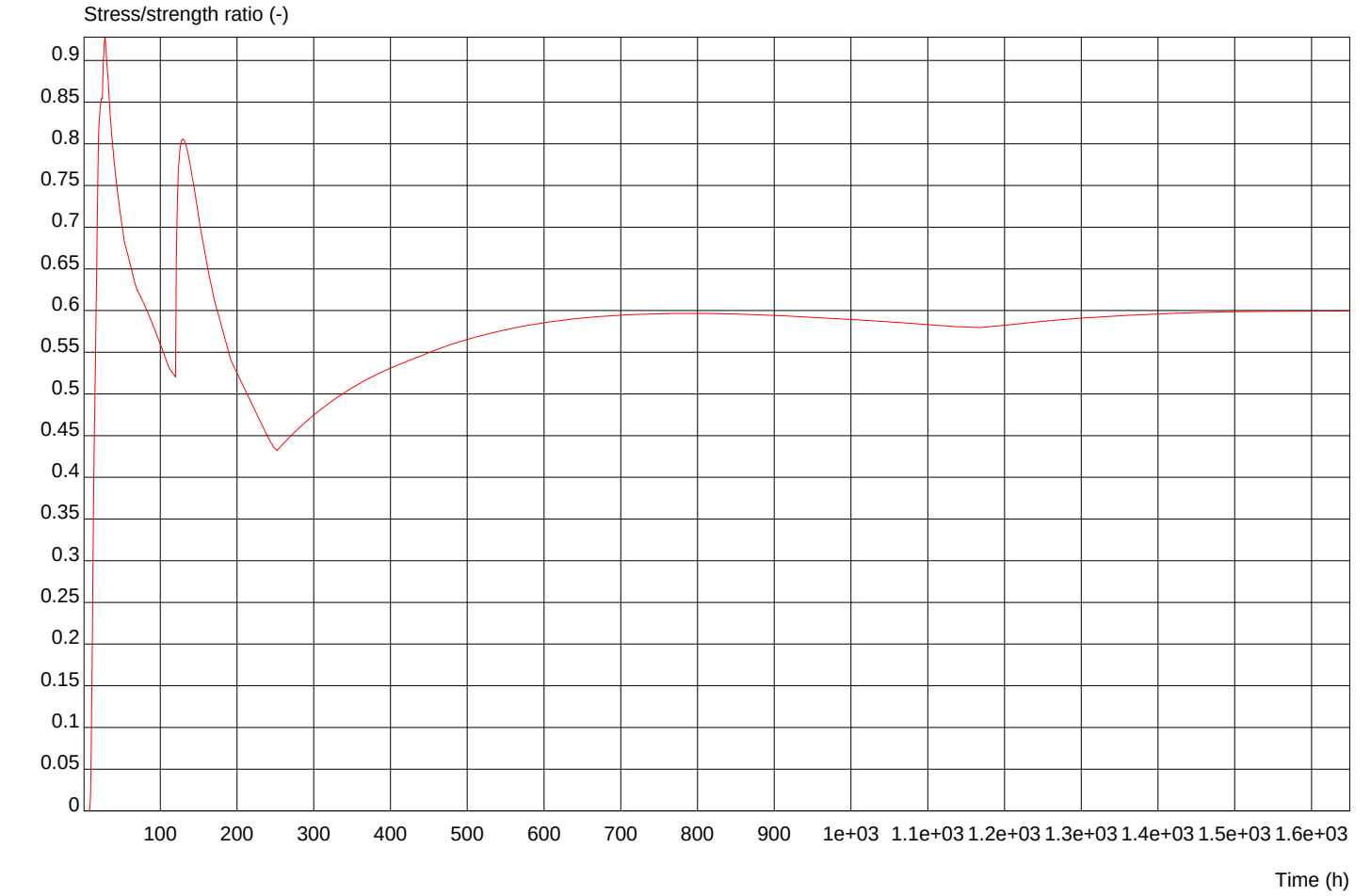

8.6 Strainratio

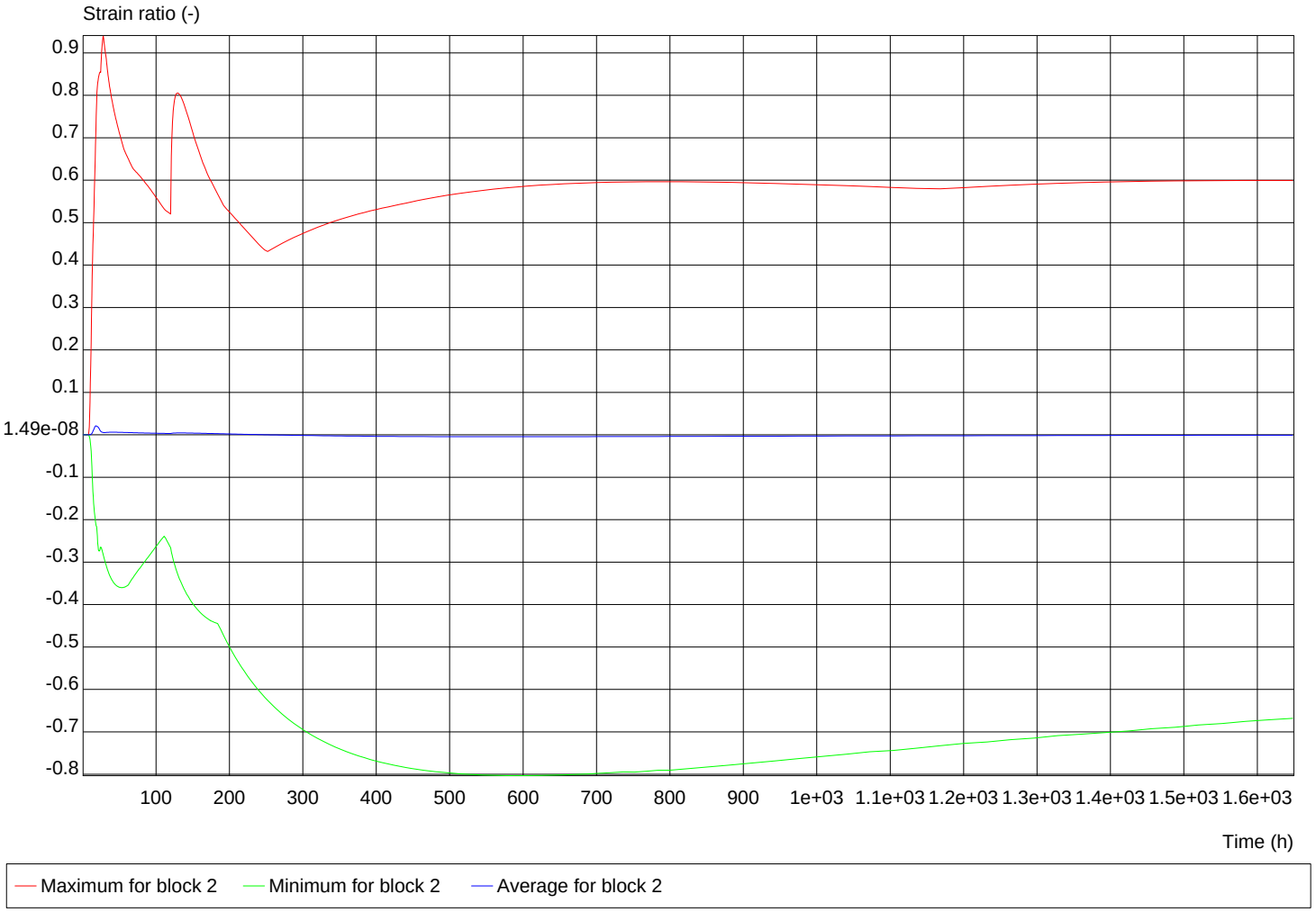
Strain ratio (-)
0.9
0.8
0.7
0.6
0.5
0.4
0.3
0.2
0.1
1.49e-08
-0.1
-0.2
-0.3
-0.4
-0.5
-0.6
-0.7
-0.8
100
200
300
400
500
600
700
800
900
1e+03
1.1e+03
1.2e+03
1.3e+03
1.4e+03
1.5e+03
1.6e+03
Time (h)
Maximum for block 2
Minimum for block 2
Average for block 2

12 References

Atrushi, D.S., 2003. *Tensile and Compressive Creep of Early Age Concrete : Testing and Modelling*.

Bamford, P., 2007. *Early-Age thermal crack control in concrete*, London: CIRIA.

Benboudjema, F. & Torrenti, J.M., 2008. Early-age behaviour of concrete nuclear containments. *Nuclear Engineering and Design*, 238(10), pp.2495–2506.

Bernarder, S., 1973. Cooling by means of Embedded Cooling Pipes.Applications in Connection with the construction of the Tingstad Tunnel. *Nordisk Betong*.

Bernarder, S. & Emborg, M., 1994. Risk of cracking in Massive Concrete Structures - New development andexperiences. *RILEM International Symposium*, pp.385–392.

Bissonnette, B., Pigeon, M. & Vaysburd, A.M., 2007. Tensile creep of concrete: Study of its sensitivity to basic parameters. *ACI Materials Journal*, 104(4), pp.360–368.

Bjøntegaard, Ø., 2011. *Basis for and practical approaches to stress calculations and crack risk estimation in hardening concrete structures – State of the art*,

Bottoni, M., 2012. Modelization of thermohydration , the drying and the shrinking of the concrete Code _ Aster. *Code Aster*.

Briffaut, M. et al., 2012. Concrete early age basic creep: Experiments and test of rheological modelling approaches. *Construction and Building Materials*, 36, pp.373–380. Available at: http://www.sciencedirect.com/science/article/pii/S0950061812003030 [Accessed February 16, 2016].

Brown, T., Lemay, H.E. & Bursten, B.E., 1988. *Chemistry:The central Science*, Prentice Hall.

CEN, 2004. *BS EN 1992-1-1:2004 - Eurocode 2: Design of concrete structures - Part 1-1: General rules and rules for buildings*,

Cervenka, J.A.N., Jendele, L. & Smilauer, V.I.T., Modelling of Crack Development in Young Concrete. *VIII International Conference on Fracture Mechanics of Concrete and Concrete Structures*, p.11.

Chu, I. et al., 2012. Estimation of temperature effects on autogenous shrinkage of concrete by a new prediction model. *Construction and Building Materials*, 35, pp.171–182. Available at: http://dx.doi.org/10.1016/j.conbuildmat.2012.03.005.

Dahlblom, L. & Lindemann, J., 2000. *Hacon: a Program for Simulation of Temperature and Stress in Hardening Concrete*, Available at: www.byggmek.lth.se.

Diana, T.N.O., 2014. Tno diana. Available at: http://tnodiana.com/.

Eierle, B., 1999. Computational modelling of concrete at early ages using DIANA. *Diana World*, pp.1–8. Available at: http://www.bst.bv.tum.de/pdf/diana.pdf.

Emborg, M., 1989. Thermal streses in concrete at early ages. *PhD Dissertation, Lulea University of Technology*, p.pp.289.

Engström, B., 2014. *Restraint cracking of reinforced concrete structures*, Göteborg.

Folliard, K.J. et al., 2008. *Prediction Model for Concrete Behavior.*, Austin.

Guenot, L. & Torrenti, J.M., 1994. Stresses in concrete at early ages: comparison of different creep models. *Proc. of international RILEM symposium on thermal cracking in concrete at early ages*, pp.pp.103–110.

Hattel, J.H. & Thorborg, J., 2003. A numerical model for predicting the thermomechanical conditions during hydration of early-age concrete. *Applied Mathematical Modelling*, 27(1), pp.1–26.

Hauggaard, A., Damkilde, L. & Hansen, F., 1999. Transitional Thermal Creep of Early

Age Concrete. *Engineering*, 125(April), pp.458–465.
Hilaire, A. et al., 2013. Some Issues on Prediction of Massive Structures Cracking. In *FraMCos-8*. p. 8.
Holt, E.E., 2001. *Early age autogenous shrinkage of concrete*, Available at: http://www.vtt.fi/inf/pdf/publications/2001/P446.pdf [Accessed February 16, 2016].
Ji, G., 2008. *Cracking risk of concrete structures in the hardening phase : Experiments , material modeling and finite element analysis Guomin Ji Doctoral Thesis Department of Structural Engineering The Norwegian University of Science and Technology Trondheim , Norway* . Norweigan university of science and techonology.
Knoppik-Wróbel, A. & Klemczak, B., 2015. Degree of restraint concept in analysis of early-age stresses in concrete walls. *Engineering Structures*, 102, pp.369–386. Available at: http://linkinghub.elsevier.com/retrieve/pii/S0141029615005246.
Lacarrière, L., 2007. *Prévision et évaluation de la fissuration précoce des ouvrages en béton*. Available at: http://scholar.google.com/scholar?hl=en&btnG=Search&q=intitle:Prevision+et+evaluation+de+la+fissuration+precode+des+ouvrages+en+beton#0\nhttp://eprint.insa-toulouse.fr/archive/00000165/.
Liu, X. et al., 2014. Early-age behaviour of precast concrete immersed tunnel based on degree of hydration concept. *Structural Concrete*, 15(1), pp.66–80.
Di Luzio, G. & Cusatis, G., 2013. Solidification-microprestress-microplane (SMM) theory for concrete at early age: Theory, validation and application. *International Journal of Solids and Structures*, 50(6), pp.957–975.
Lynam, C.G., 1934. Growth and Movement in Portland Cement Concrete. *Oxford University Press*, pp.25–45.
Mindess, S. & Young, J.F., 1981. *Concrete*,
Olofsson, J. & Uhlan, M., Round Robin Simulation. , p.48.
Patzák, B. & Bittnar, Z., 2004. OOFEM–An Object Oriented Framework for Finite Element Analysis. *Acta Polytechnica*, 44(5). Available at: http://ojs.cvut.cz/ojs/index.php/ap/article/view/618\nhttps://ojs.cvut.cz/ojs/index.php/ap/article/view/618.
Riding, K. a, 2007. Early Age Concrete Thermal Stress Measurement and Modeling. *PhD Dissertation*, (University of Texas, Austin).
Scherer, G.W., 2015. Drying, Shrinkage, and Cracking of Cementitious Materials. *Transport in Porous Media*, 110(2), pp.311–331. Available at: "http://dx.doi.org/10.1007/s11242-015-0518-5.
Schießl, P., Plannerer, M. & Brandes, C., 2000. Influence of binders and admixtures on autogenous shrinkage of high performance concrete. In *International RILEM Workshop on Shrinkage of Concrete*. pp. 179–190.
Schutter, G. De, 1999. Degree of hydration based Kelvin model for the basic creep of early age concrete. *Materials and Structures*, 32(May), pp.260–265. Available at: http://link.springer.com/article/10.1007/BF02479595.
Schutter, G. & Taerwe, L., 2000. Fictitious degree of hydration method for the basic creep of early age concrete. *Materials and Structures*, 33(6), pp.370–380.
Sellevold, E.J. & Bjøntegaard, Ø., 2006. Coefficient of thermal expansion of cement paste and concrete: Mechanisms of moisture interaction. *Materials and Structures*, 39(9), pp.809–815.
Singh, B.P., Yazdani, N. & Ramirez, G., 2013. Effect of a Time Dependent Concrete Modulus of Elasticity on Prestress Losses in Bridge Girders. *International Journal*

of Concrete Structures and Materials, 7(3), pp.183–191.
Tazawa, E., 1998. Autogenous Shrinkage of Concrete. *Japan Concrete Institute, Technical Committee on Autogenous Shrinkage of Concret "Committee Report"*, p.432. Available at: http://books.google.com/books?id=GB1ANbHorB8C.
TNO DIANA, 2008. User ' s Manual Material Library.
Trafikverket, 2015. Marieholmstunneln. Available at: http://www.trafikverket.se/marieholmstunneln/.
Ulm, F.-J. & Coussy, O., 1995. Modeling of thermochemomechanical couplings of concrete at early ages. , 121(July), pp.785–794.
Utsi, S. & Jonasson, J.-E., 2012. Estimation of the risk for early thermal cracking for SCC containing fly ash. *Materials and Structures*, 45(1-2), pp.153–169.
Yeon, J.H., Choi, S. & Won, M.C., 2009. Effect of Relative Humidity on Coefficient of Thermal Expansion of Hardened Cement Paste and Concrete. *Transportation Research Record: Journal of the Transportation Research Board*, 2113(09), pp.83–91.
Zhou, C., Shu, X. & Huang, B., 2014. Predicting concrete coefficient of thermal expansion with an improved micromechanical model. *Construction and Building Materials*, 68, pp.10–16. Available at: http://dx.doi.org/10.1016/j.conbuildmat.2014.06.039.